Microtubule Supported Trafficking of Synaptic Vesicle Precursors and Recycling Synaptic Vesicles

by

Mason Parkes

A dissertation submitted to the Graduate Faculty of
Auburn University
in partial fulfillment of the
requirements for the Degree of
Doctor of Philosophy

Auburn, Alabama
May 10, 2025

Keywords: Axonal Transport, Synaptic Vesicle, Hippocampus, Actin, Microtubule, Presynapse

Approved by

Michael Gramlich, Chair, Assistant Professor of Physics
Allen Landers, Howard Earl and Carolyn Taylor Carr Professor and Chair of the Department of Physics
Marcelo Kuroda, Thomas and Jean Walter Associate Professor of Physics
Alexey Petrov, Associate Professor of Biology
Steven Brown, Morris Savage Endowed Chair, Professor, Law and Justice
Program Director, Department of Political Science

Abstract

Synaptic Vesicles are critical components for synaptic communication in the nervous system. The proteins associated with synaptic vesicles that enable their functionality must be continuously produced, transported to necessary locations, and then eventually removed for degradation to ensure healthy function throughout the lifetime of the neuron. The microtubule cytoskeleton has long been known to support motion of many components within the cell, and filamentary actin has been shown to support local motion of synaptic vesicles between presynapses in an activity dependent manner. However, questions remained as to the level of microtubule-based synaptic vesicle motion.

This dissertation presents results showing the mechanistic effects of the microtubule cytoskeleton on axonal cargo, as microtubule ends must be navigated by synaptic vesicle precursors delivering vital synaptic vesicle proteins to the presynapse. Further, our results show that synaptic vesicles also utilize the microtubule cytoskeleton. This microtubule supported motion allows for directional differences in motion due to the microtubule polarization within the axon. Directional differences are observed near functioning presynapses, as recently recycled vesicles are less likely to be captured by a presynapse when moving at higher speeds towards the cell body. A model of motion including differential capture probability among vesicles supported by different cytoskeletal networks is laid out and shown to support a net retrograde flux that supports healthy turnover of synaptic vesicle proteins.

Chapter 2 provides background information on the biological elements and concepts underlying my research. This presents essential topics needed to understand what was studied, the results of the experiments, and the context of the results within the larger landscape of research. Chapter 3 then sets the stage with open questions in the field upon which my research sheds new light. Chapter 4 explains the methods and materials used to experimentally study synaptic vesicles and synaptic vesicle precursors. This chapter will build on the background information provided with specific information about how these elements are studied. Chapter 5 contains the experimental results and computational models based on those results. Finally, Chapter 6 contains discussion of the results, as well as an extended discussion of their meaning within the larger context of the field, along with further questions yet to be answered.

Acknowledgements

I'd like to thank the many members of the physics department who guided me on my path to this thesis. Dr. Michael Gramlich provided essential training in experimental techniques as well as the deeper more subtle process of performing scientific research that I hope will stick with me throughout my life. Many other members of the department also made their mark on me through instruction and example and while there are too many to name them all I'd like to make specific mention of Dr. Eric Burkholder, Dr. Stuart Loch, and Dr. Daniel Merrill, who provided excellent examples as scholars and educators that I hope to emulate in my career as well.

I'd also like to thank the other graduate students I had the pleasure of studying with. Especially those who started alongside me, Andrew, Brandon, Dakotah, Isaac, Jared, Michael, Roger, Shawn, Thomas, and Tomie, who I really got to know and have lots of fun with and try to relax with as things got difficult. Special thanks have to go to Tomie, who ran a multi-year DnD game for us that was a huge highlight of so many stressful weeks. It was also great to work alongside other great graduate students like Paxton Wilson and Jeremiah Pfitzer, and the many dedicated undergraduate students who helped in our research group.

Thank you to the Auburn Public library for providing such nice study spaces. I don't think I could have ever gotten this written without them.

Finally, and most importantly of all, I'd like to thank my family. First, my parents, Lane and Michelle Parkes, and my grandparents Stephen and Shirley Brown and Patricia and Richard Swapp, who taught me the value of education and supported me in getting as much as I could. I wouldn't have been able to make it to this point without them. Grandpa Swapp passed away in 2022, and I think he was the only person I knew who had a Ph.D. before I started college, that example helped me see that I could do something like that too. I'd also like to thank Camden Henderson for his help during difficult times on this journey and for the whole Mingledorff clan for their love and support.

My family, my wonderful wife Brianna, and my two lovely daughters, Abby and Calliope, also deserve more thanks than I can possibly provide on this page. I'm so grateful to them for the support and patience they provided that allowed me to pursue my Ph.D., as well as being the lights and sources of joy that made it all worth it. I know this wasn't always easy on them, but I'm so glad they were here with me and I'm so glad we get to move on to new things together!

Table of Contents

List of Figures

1 Introduction

Neurons are a specialized type of cell which make up the nervous system, a complex network within an organism that supports sensation and cognition. A key feature of neurons is their ability to communicate with other neurons across chemical synapses. At a chemical synapse, neurotransmitter is released from one neuron, the presynaptic neuron, and that chemical signal is received at another, postsynaptic, neuron. Successful synaptic transmission relies on myriad proteins on both the presynaptic and postsynaptic sides.

Proteins are complex molecules produced within each cell. The makeup of the protein determines structures they fold into and thereby the function that they perform. Many of the proteins required for synaptic transmission are associated with synaptic vesicles themselves. Synaptic vesicles are protein-studded spheres within the presynaptic neuron that are crucial to synaptic transmission. Proteins on their surface fill them with neurotransmitter and facilitate their docking at and fusing with the presynaptic cell membrane where a pore opens and allows the neurotransmitter to make its way to the postsynaptic cell. These synaptic vesicles are then recycled, the whole process taking only milliseconds, and prepared for repeated use.

By their nature as cells specializing in communication, neurons have long protrusions called axons that stretch to other cells with which they need to communicate. The presynaptic areas from which a chemical synaptic transmission is initiated are located along this axon. These axons can often be millimeters and sometimes even meters long. Despite this length, proteins supporting presynaptic function must be transported from the cell body to each presynaptic location and back to enable continued healthy function.

In addition to maintaining healthy function, the phenomenon of learning is supported by physical changes in neurons. Synaptic plasticity is the term used to describe changes in the cellular machinery around a synapse that changes the strength and reliability with which signals are sent and received. Any change at that level that results in learning is some activity sensitive regulation of proteins around the presynapse.

In order to maintain synaptic protein homeostasis within neurons and to allow changes that provide the microscopic basis for learning, complicated systems of intracellular transport are required. A cytoskeleton (“cyto” meaning “cell”, “skeleton” meaning, well, “skeleton”) is present within the cell to provide structure but also to act as scaffolding for specialized motor proteins to walk along.

The following dissertation introduces more about this cytoskeleton, details of its makeup within the axon and then introduces how it supports cargo-bearing motor proteins through the axon in a specialized process called axonal transport. The

background will conclude with a closer look at synaptic vesicles and what is known of their life cycle.

Results will then be presented that investigate the role of microtubule structure in axonal transport and how that structure impacts the synaptic vesicle life cycle. Another set of studies then look closer at the role that microtubules play in the motion of synaptic vesicles themselves and the potential importance their unique organization within the axon may play in the synaptic vesicle lifecycle.

2 Background

This chapter will summarize the fundamental biological concepts needed to understand the results presented of this dissertation. This begins with an introduction of the major cytoskeletal networks present within the axon, then a deeper look at axonal traffic in general, including the motor proteins that propel cargo through the cell. The final section within this chapter focuses on synaptic vesicles, the principle cellular element observed in my experiments and a key player in the healthy function of the nervous system.

2.1 Cytoskeleton

The cytoskeleton is a key component of cells that support a variety of functions, including providing structural support and facilitating transport of material. Because the axon is morphologically unique, being incredibly long compared to the other dimensions of the cell, the structure and function of the cytoskeleton is especially important. The cytoskeleton needs to be able to support axonal lengths that are extremely long for the cellular scale. This extended axonal length also necessitates efficient transport across those distances, up to meters for some neurons, and on the order of millimeters in hippocampal rat neurons used for the studies in this dissertation (Fletcher and Theriot, 2004; Muzio et al., 2025; Ropireddy et al., 2011). The axonal cytoskeleton is crucial for both of these roles (Guedes-Dias and Holzbaur, 2019; Hirokawa et al., 2009; Kapitein and Hoogenraad, 2015, 2011). The major cytoskeletal elements of import in this dissertation are the actin network and the microtubule network (See figure 2.1).

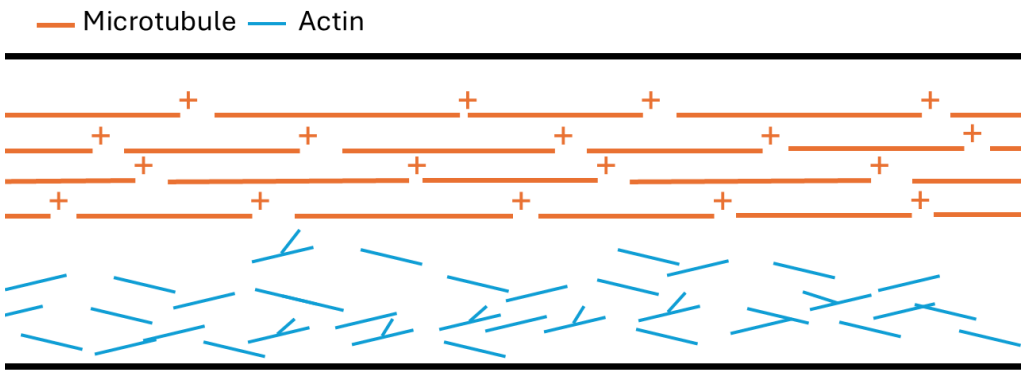

Figure 2.1: Drawing of Axonal Cytoskeleton. Actin within the axon is shown in blue, both longitudinal actin filaments running the length of the axon (light blue, drawn in lower portion). The microtubule cytoskeleton with unique polarized organization within the axon is also shown (orange, upper portion of drawing).

2.1.1 Actin

Actin filaments are structurally polarized polymers (6 nm diameter) composed of individual globular actin (G-Actin) protein monomers (Cooper, 2000; Ulferts et al., 2021). These small spherical proteins form together into longer actin filaments (F-

actin) (Cooper, 2000; Ulferts et al., 2021). Multiple actin filaments form complex actin structures that can in turn form various shapes within cells (See figure 2.1) and provide a substrate for molecular motors to walk on (Bingham et al., 2023; Chenouard et al., 2020; Goo et al., 2017; Gramlich and Klyachko, 2017). F-actin organizes in a polarized manner with a "barbed" (or plus) end on one side and a "pointed" (or minus) end on the other (Korn et al., 1987; Wegner, 1976).

Within the axon, F-actin can organize in varied directions, with barbed and pointed ends aligned, anti-aligned or at other angles to each other (Gangulay et al., 2015). Because of this varied orientation, actin-based motion within the axon moving towards the pointed end of an actin filaments can be towards the cell body or away from the cell body. Motors on neighboring actin filaments both moving towards the barbed end may not be moving in the same direction relative to the cell. This will contrast with the organization of MTs within the axon that will be discussed in the next section.

Various proteins support the formation of these actin structures. One such protein which will be modified and discussed in this study is the ARP2/3 protein complex (Mullins et al., 1998). These proteins allow actin to branch at characteristic 123-degree angles from existing actin filaments and form branched structures. These daughter branches grow with a 123-degree angle formed between the pointed end (-) side and the new branch, or a 57-degree angle between the two barbed (+) ends (Mullins et al., 1998). ARP2/3 has been shown to be important in actin structures within the presynapse. (Bingham et al., 2023).

2.1.2 Microtubules

Another cytoskeletal element that plays multiple roles in the neuron is the microtubule (MT) network. MTs are formed by two small globular proteins: α-tubulin and β-tubulin (Cooper, 2000). These form together sequentially and, along with many others of their species, form into long hollow tubes with a 25 nm outer diameter (Cooper, 2000). The orientation of the tubulin proteins creates a polarity in the MT, where one end (+) has all β -ends exposed, and the other end (-) has all α -subunits exposed (Fan et al., 1996; Nogales et al., 1995) (See figure 2.1).

Individual MT filaments commonly grow to lengths around 2 μm, though they can grow up to 20 μm in length (Juene-Smith and Hess, 2010). However, they form in bundles that allow the network to span much larger distances (Brandt and Lee, 1994). MTs are not generally of static length, but grow and shrink as more tubulin dimers from the environment are added to the plus or minus ends (Cooper, 2000). This means that the filament is rarely static, but instead relies on dynamic stability and treadmilling to provide a substrate that is important for motion and structure within the cell. Notably, however, MTs within the axon are more stable than those in other cell types (Conde and Cáceres, 2009; Kapitein and Hoogenraad, 2015; Stepanova et al., 2003).

In most cells, MT networks can be oriented in many different directions (Conde and Cáceres, 2009), however, within the long narrow geometry of the axon, MTs orient along the axis of the axon, and even more specifically, the plus ends all point

away from the cell body, with the negative ends pointing towards the cell body (Conde and Cáceres, 2009; Kapitein and Hoogenraad, 2015; Stepanova et al., 2003). (see Figure 2.1). This anisotropy in the axonal MT network allows for potential differences in retrograde (moving towards the cell body) and anterograde (moving away from the cell body) motion because different motors drive motion in different directions and there are different proteins creating distinct environments at the opposite ends of the MTs (Gennerich and Vale, 2009; Guedes-Dias and Holzbaur, 2019; Reck-Peterson et al., 2018; Yogev et al., 2016).

2.1.2.1 End-Binding Proteins

A variety of microtubule associated proteins (MAPs) are present near MTs and are important for maintaining their structure, as well as assembly and disassembly (Akhmanova and Steinmetz, 2015; Conde and Cáceres, 2009; Stepanova et al., 2003). Some MAPs are present at the primarily at the MT end, some of which assist in the characteristic dynamic treadmilling observed in MTs (Akhmanova and Steinmetz, 2015; Conde and Cáceres, 2009; Stepanova et al., 2003). Certain proteins are performing essential functions at the growing and shrinking ends of the MT. They allow for the construction of MT out of tubulin in the surrounding cellular environment, as well as disassembling the MT.

These end-binding (EB) proteins are crucial for understanding the behavior of MTs and make up an important part of their structure (Komarova et al., 2009). These EB proteins create distinctive differences at each end of the MT, distinct from the directionality observed throughout the MT created by the ordering of α- and β-tubulin subunits (Akhmanova and Steinmetz, 2015). These distinct end environments are important to understand because as cargo uses MTs for transport they must interact with MT ends in order to progress past the finite MT length in their larger journeys (Juene-Smith and Hess, 2010; Brandt and Lee, 1994)

2.2 Axonal Transport

Due to the length of the axon, maintaining a functional population of proteins is challenging. Cellular mechanisms for trafficking cargo through the axon are critical. This collective specialized motion is called axonal transport. MT-based axonal transport is supported in different directions by different proteins (See figure 2.2). On the trip from the cell body to the distal end of the axon, this means that the kinesin family of motors are the driving factor. These are the motors that specialize in delivering the cargo from the cell body to where it needs to be in the cell.

Anterograde axonal transport is complex and supports overall function of the cell in many ways. For example, the delivery of proteins to a presynapse is crucial in controlling the function of that presynapse, causing its signal to grow, shrink, or remain constant in proportion to the quantity of delivered components (Cai, et al, 2007). Anterograde axonal transport relies on the MT cytoskeleton and is driven by motor proteins from the kinesin superfamily (see Figure 2.2) (Niwa et al., 2008; Okada et al., 1995; Seog et al., 2004) that will be elaborated on below.

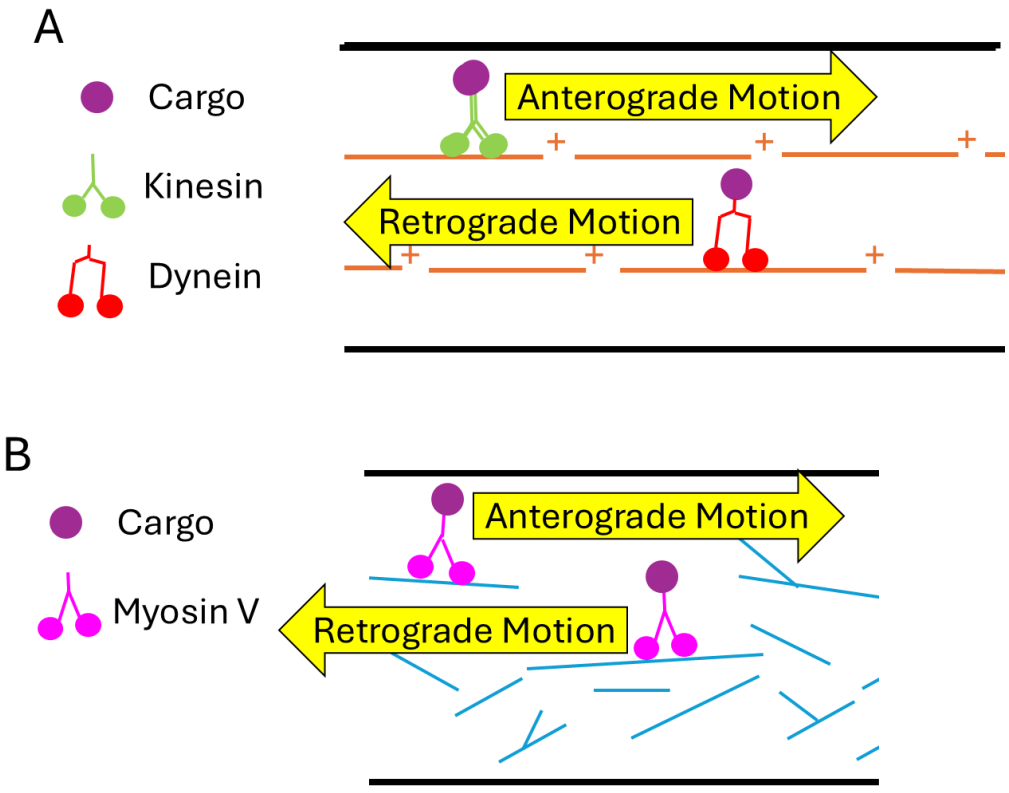

Figure 2.2: Sketch Showing axonal transport along the axonal cytoskeleton driven by motor proteins. (A) Microtubule supported motion moving in Anterograde and Retrograde directions supported by Kinesin and Dynein motors, respectively. (B) Actin supported motion driven by Myosin V motors. These motors drive both anterograde and retrograde motion due to the bi-directional organization of actin within the axon.

Axonal transport in the retrograde direction (moving back towards the cell body) is also critical. Retrograde transport is important for recycling cellular components (Burkhardt et al., 1997, Ravikumar et al., 2005) and retrograde signaling via neurotrophic factors (Delcroix et al., 2003; Yano, et al., 2004). This retrograde transport also relies largely upon the MT cytoskeleton, but this time upon the dynein family of motor proteins (Gennerich and Vale, 2009; Guedes-Diaz and Holzbaur, 2019).

Long range motion on the MT cytoskeleton, however, is not the only axonal transport that has been observed. Recycling synaptic vesicles (SVs) have been observed to move short distances between presynapses in a process known as inter-synaptic vesicle exchange (ISVE) (Darcy, et al., 2006; Staras, et al., 2010). This ISVE is known to make use of the actin cytoskeleton via myosin motors (Gramlich and Klyachko, 2017, Chenouard et al., 2020).

2.2.1 Cytoskeletal Motor Proteins

Proteins are long chains of amino acids that fold into intricate shapes and work together to perform innumerable tasks within the cell. Among these tasks is the

transport of cargo that happens in many cells and which we are focusing on in the axon of neurons (Gennerich and Vale, 2009; Guedes-Dias and Holzbaur, 2019). Motor proteins are responsible for directed motion in living cells. They use a mechanochemical cycle in which they bind an ATP molecule, the common source of energy within cells, and use the energy released via ATP hydrolysis to propel themselves and their cargo forward along cytoskeletal substrates (Alberts, 2002; Gennerich and Vale, 2009; Goodman, et al., 2012; Hancock, 2016). We will dive into the families in the following sections with a particular view in understanding how they support neuronal function.

2.2.1.1 Kinesins

The kinesin superfamily proteins are a group of motor proteins that transport cargo along MTs (Niwa et al., 2008; Okada et al., 1995; Seog et al., 2004). There are many motors within this family, but the studies in this dissertation focus on the kinesin-3 family, specifically kinesins known to be present in within neurons and involved in active transport, namely, the mammalian KIF1A motor, and its homolog within *C. elegans* Unc-104 (hereafter referred to as kinesin) (Yogev, et al., 2016; Gong et al, 1999; Okada et al., 1995; Hall and Hedgecock, 1991).

Kinesin motors walk along MT tracks, taking one 8.1 nm step per ATP that it uses (Coy et al., 1999). Kinesins move towards the plus ends of MTs (see figure 2.2). Kinesin functions as a dimer made up of two connected proteins, each with a motor domain or head that connects to the MT cytoskeleton at specific MT binding site (also spaced 8.1nm apart) (Huang et al., 1994; Ray et al., 1993) and a longer stalk that intertwines (forming a coiled coil) with the other leading up to a cargo binding domain where the various cellular components that can be moved by kinesins attach (Benoit et al., 2024; Gennerich and Vale, 2009; Hancock, 2016; Hirokawa et al., 2009). Kinesins walk in a hand-over-hand method, where the back "foot" lifts off the MT, moves over the front "foot" and reattaches, moving the center of the motor 8.1 nm (Gennerich and Vale, 2009; Hirokawa et al., 2009).

2.2.1.2 Dynein

Dyneins make up another family of MT based motor proteins that move in the opposite direction of the kinesins (see figure 2.2) (Vale, 2003; Vallee et al., 2004). Within axons, cytoplasmic dynein (hereafter dynein) is observed to drive cargo in retrograde motion (Gennerich and Vale, 2009; Guedes-Diaz and Holzbaur, 2019). Dyenein is structured differently than kinesin, instead made of 6 polypeptides and requiring various other activator or linker complexes to function (Reck-Peterson et al., 2018). The step size of dynein is also influenced by the repetitive nature of the MT, however due to the flexibility and longer stalk length of dynein, the steps can be more variable than observed in kinesin (Asai and Koonce, 2001; Reck-Peterson et al., 2006).

2.2.1.3 Myosin

The myosin superfamily of motor proteins is capable of walking on polymerized actin filaments (see figure 2.2). Myosin V motors are a member of this family that have been observed to contribute to processive motion in neurons in general (Rose

et al., 2003; Bridgman 2004) and of SVs specifically (Gramlich and Klyachko, 2017; Takamori et al., 2006). F-actin is structured differently from MTs, and myosin V motors are not as constrained to the same step size, instead exhibiting a step size of 36 nm per ATP hydrolyzed (Sakamoto et al., 2000; Yildiz et al., 2003). Myosin V motors move in a hand over hand motion similar to the previously discussed motors (Kodera et al., 2010).

2.2.2 Dysfunction in Neurodegenerative Diseases

Disfunction of axonal traffic has been observed in many neurodegenerative diseases, including Alzheimer's disease, Parkinson's disease, Huntington's disease, hereditary spastic paraplegia, amyotrophic lateral sclerosis, and Charcot-Marie-Tooth disease (see Berth and Lloyd 2023 for Review). Mutation of a KIF1A homologue in humans is observed to cause Charcot-Marie-Tooth Disease.(Zhao et al., 2001) Because of the extensive role that axonal transport plays in providing new cellular components to support neuronal function, removing old cellular components to prevent buildup of defective proteins, and moving essential components such as SVs and mitochondria to support effective synaptic activity, it is no surprise that disruptions to these systems are often far reaching.

2.3 Synaptic Vesicles

Synaptic Vesicles (SVs) are key to the functioning of chemical synapses, where communication occurs between neurons. They are used at the presynaptic site where they fuse into the cell membrane and release the neurotransmitter they contain into the synaptic cleft so that it can be sensed by the postsynaptic cell (Cotman and McGaugh, 1980). The studies in this dissertation focus on tracking SVs and describing their behavior, so it is important to understand these structures in greater detail. The following section gives a more detailed look at SVs, first through an outline of their structure, then looking at how they come to be, a deeper look at their role in neuronal activity, and finally how they reach the end of their usefulness within the cell.

SVs are spherical compartments that exist within a cell (See figure 2.3). They are enclosed by a lipid membrane similar to lipids that compose the cell membrane as a whole (Takamori et al., 2006). This lipid membrane is interspersed with proteins that help the SV fulfill all the roles necessary for synaptic communication (Takamori et al., 2006). SVs are 40-50 nm in diameter, with a relatively conserved size across locations within an organism and between organisms. These spheres are covered with proteins, with hundreds of proteins on each SV (Takamori et al., 2006). These proteins can be found on the surface of the lipid membrane or passing all the way through the membrane. Some of these proteins will be discussed below in the section outlining the SVs role in synaptic transmission.

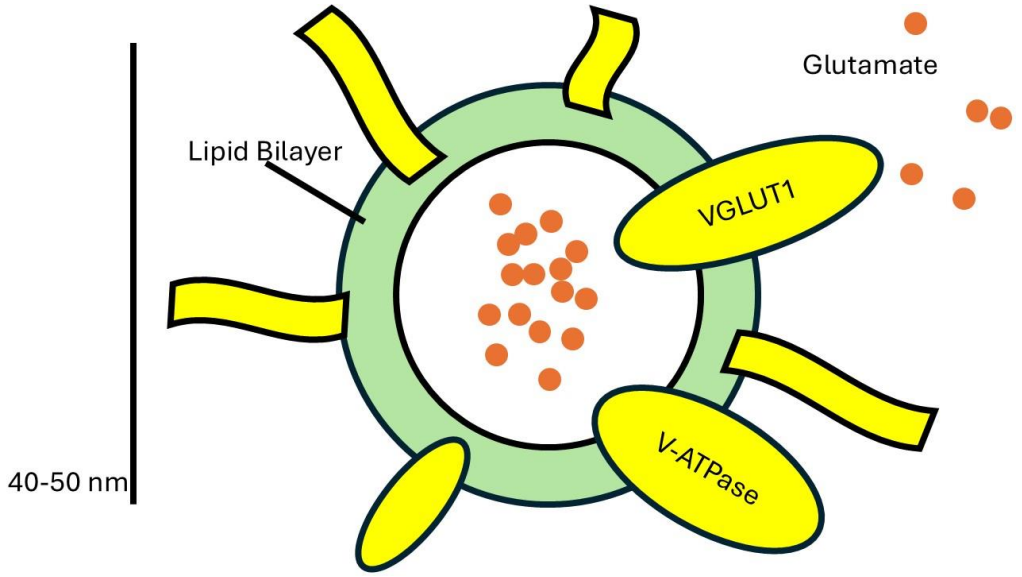

Figure 2.3: Cartoon of Synaptic Vesicle. Synaptic Vesicles are lipid-membrane-enclosed, protein-studded compartments within neurons. Some key proteins are labeled that allow for the filling of the vesicle with neurotransmitter, glutamate shown here in orange.

2.3.1 Synaptic Vesicle Precursors

In order for SVs to perform their vital function they need a wide variety of proteins to work properly. These proteins, and all others needed for proper cellular functions, are made within the cell body each neuron (Alberts, 2002; Cooper, 2000; Watson et al., 2023). They must then be packaged with other SV proteins into synaptic vesicle precursors (SVPs) and transported down the axon to the presynapse where they can assist in synaptic transmission (Fornasiero et al., 2018; Okada et al., 1995; Watson et al., 2023). This section takes a deeper look at that process.

2.3.1.1 Protein Production

Proteins are made within our bodies when genetic codes stored in DNA are transcribed into RNA messages and transported to ribosomes where RNA is used as a blueprint for what proteins should be assembled in a process called translation. This process occurs within the cell body, or soma, of neurons (Alberts, 2002; Cooper, 2000; Watson et al., 2023) (see Figure 2.4B). The proteins created in this process are needed throughout the neuron. Due to the specialized geometry of neurons, transporting proteins needed for synaptic transmission to locations that can be millimeters or even meters from the cell body (see figure 2.4) presents a challenge.

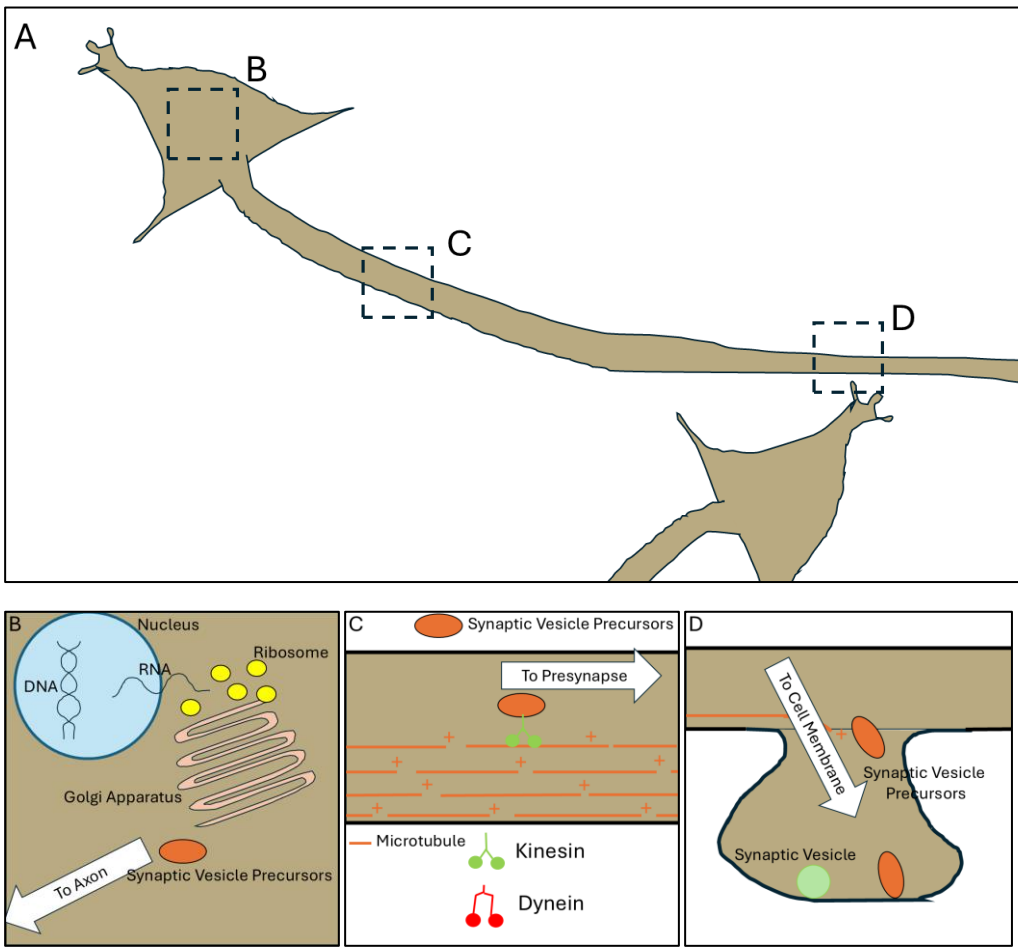

Figure 2.4: Sketch of Neurons and the progress of Synaptic Vesicle Precursors. (A) Two neurons in close contact. Sections labeled to indicate key parts of SVP transport to presynapses, corresponding to respective panels. (B) Protein production and packaging into SVPs. (C) SVP trafficking within the axon. (D) SVP delivery to the presynapse.

Some of these proteins are the specialized SV proteins essential for the healthy function of SVs. SV proteins are the proteins embedded into the surface of SVs that allow them to perform their biologically essential function of filling with neurotransmitter, docking to the cell membrane, releasing neurotransmitter into the synaptic cleft, and reforming within the cell to begin the cycle again, all on millisecond time scales (See Sudhof, 2004 for review). SV proteins reach the presynaptic regions where they will be used by being transported in special organelles called SVPs (De Pace et al., 2020; Guedes-Dias and Holzbaur, 2019; Okada et al., 1995; Watson et al., 2023).

SVPs are created in the cell body (Boncompain et al., 2012; Farías et al., 2016; Watson et al., 2023). They are also made up of lipid membranes, like SVs, and packed with the essential SV proteins needed at the presynapse (Watson et al., 2023; De Pace et al., 2020). SV proteins are packed into SVPs within the cell body in preparation for axonal transport (Nakata et al., 1998). After being trafficked to the presynapse, SVPs are delivered to the presynaptic cell membrane where they

exocytose, and new SVs can be endocytosed including the delivered SV proteins (Bonanomi et al., 2006).

SVP axonal transport is known to depend on kinesin-3 family motors, specifically KIF1A and KIF1Bβ (Okada et al., 1995; Niwa, et al., 2008). The MT cytoskeleton that supports this Kinesin-based motility is important to the motion of SVPs, limiting the run lengths observed as SVPs must navigate MT ends after pausing (Yogev et al., 2016) Microtubule (MT)-based motion is prevalent in the axon, and, as stated previously, MT-based cargo is propelled by Kinesin and Dynein motors along the MT network. Studies manipulating MT-based motors have shown effects on SVP delivery to the presynapse (Guedes-Diaz, et al., 2019), and SVP motion has been shown to be impacted by the location of MT ends (Yogev et al., 2016), leading to the conclusion that SVPs are one of many MT-based cargos in the axon (Yogev et al., 2016; Guedes-Diaz et al., 2019).

2.3.2 Synaptic Vesicles in Synaptic Transmission

2.3.2.1 Overview of Synaptic Transmission

Neurons are specialized in communicating information to other cells. Generally, a signal starts at the cell body. The signal is an excitatory electric potential, raising the potential from a resting potential to a higher value due to the influx of positive ions from outside the cell. This influx can be caused by a signal from another cell or via other specialized proteins structures that allow the sensation of mechanical, chemical, optical, or thermal stimuli.

Once this signal starts at the cell body or soma of one neuron, it propagates down the axon of that neuron as an action potential. When the action potential reaches a specialized presynaptic region, it triggers the release of SVs filled with neurotransmitter. SVs fuse with the cell membrane and release their payload to the extra-cellular environment where it can be received by waiting cells, for example, other neurons to pass the signal further or combine signals for cognitive tasks, or to skeletal muscles to contract and generate motion within the larger organism.

2.3.2.2 Synaptic Vesicle Cycle

As the action potential propagates down the axon, it causes its characteristic spiking of potential in specialized presynaptic region (Bear et al., 2020). Within these regions, there are voltage gated channels that allow calcium ions into the cell when the action potential reaches the presynapse (Emperador-Melero and Kaeser, 2020; Südhof, 2012). These calcium ions play a key role in synaptic vesicle release (Emperador-Melero and Kaeser, 2020; Südhof, 2012; Sudhof, 2004; Sakaba, 2008).

Synaptic vesicles are present throughout the presynaptic region (and indeed, throughout the axon as we will later see). Some are kept docked near the active zone (Maschi and Klyachko, 2017; Sakamoto et al., 2018; Südhof, 2012). When calcium flows into the presynapse because the voltage gated calcium channels open, the calcium ions cause the SVs to move towards the cell membrane and fuse with it in preparation to release neurotransmitter (Sudhof, 2004). The fused SV then opens a fusion pore, connecting the inside of the SV with the extracellular medium so that the neurotransmitter within the SV can exit the cell.

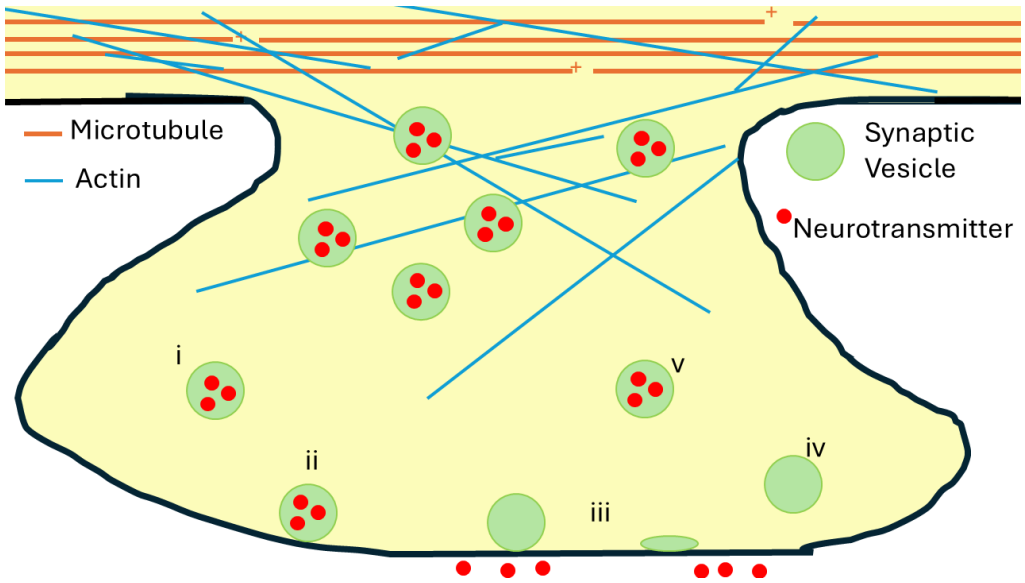

Figure 2.5: Synaptic Vesicles undergoing exocytosis within the presynapse. The microtubules within the axon are shown, as well as the actin, which is particularly enriched in the presynapse. Synaptic vesicles are shown, generally filled with neurotransmitter. Important steps in the synaptic vesicle cycle are labeled. (i) The SV filled with neurotransmitter moves into position at the active zone of the presynapse to be released. (ii) The SV docks with the cell membrane in preparation of release. (iii) the SV fuses with the cell membrane and releases neurotransmitter into the synaptic cleft. Two types of fusion are shown, the SV on the left is undergoing kiss-and-run fusion, where a fusion pore opens, and neurotransmitter can leave. The SV on the right is undergoing full collapse where the SV collapses into the cell membrane. (iv) The SV is retrieved from the cell membrane and re-enters the cell. (v) The SV refills with neurotransmitter and is ready for another round of release.

SVs are filled with neurotransmitter by specialized membrane proteins on the SVs that pump hydrogen ions (protons) from within the SV and replace it with a neurotransmitter molecule (Forgac, 2007; Martineau et al., 2017). Once the SV has been refilled with neurotransmitter, it is capable of being used again to send another signal to a waiting cell.

The neurotransmitters are released into a synaptic cleft, a region between the presynapse on one neuron, and the postsynaptic area of another neuron. Postsynapses are specialized cellular regions on dendrites where there are special proteins that respond to neurotransmitters, allowing positive ions to flow in and raising the potential within the postsynaptic cell (Bear et al., 2020). A single neuron can have many postsynaptic areas on a dendrite, and many dendrites that all lead back to the cell body. It is the combined signal of many postsynaptic areas responding to many presynaptic SV release events that determines if a signal is carried on (Mason et al., 1991; Olmi et al., 2017; Teramae et al., 2012). This complex output mechanism from the presynapses and input mechanism to the postsynapses allows great variability in the strength and frequency of synaptic transmission (Mason et al., 1991; Olmi et al., 2017; Teramae et al., 2012). SVs play a key role in this and their motion between various presynapses is important to understanding how this process works.

2.3.3 Degradation of SV Proteins

As time passes, proteins become damaged or otherwise modified in ways that can impede their use (Goldberg, 2003; Labbadia and Morimoto, 2015; Yerbury et al., 2016). Older proteins must be degraded and removed from functional service and replaced by new proteins so that function is not disrupted. SV proteins are replaced at variable rates that depend on use (Sheehan et al., 2016; Jähne, et al., 2021). Though precisely how these SVs are recycled remains unclear. There are multiple well-established routes to protein degradation seen in many cell types that are also present in neurons and active in presynaptic processes (Dikic, 2017; Ivanova and Cousin, 2022; Turegano-Lopez et al., 2020; Yerbury et al., 2016; Zhao et al., 2022).

The ubiquitin-proteasome system (UPS) is a degradative pathway in which a small protein called ubiquitin is added to proteins that are then targeted for degradation by a proteasome that breaks them down (Zhao et al., 2022). The UPS is active in neurons and dysfunction of this system has been implicated in neurodegenerative diseases (Yerbury et al., 2016). This system primarily targets and controls short lived proteins (Kawahata and Fukunaga, 2020; Pohl and Dikic, 2019) and has been suggested to play a role in regulating SV turnover (Ding and Shen, 2011)

The endolysosomal pathway is another way for proteins to be recycled. In this pathway, a proteins group called the endosomal sorting complex required for transport (ESCRT) accumulates ubiquitinated membrane cargo (Hurley, 2008). This cargo targeted for degradation is accumulated in multi-vesicular bodies (MVBs). MVBs are then trafficked towards the cell body where the relevant proteins can be broken down by lysosomes (Piper and Luzio, 2007). MVBs are observed in axons, however, they are predominantly located within the soma and dendrites of neurons (Turegano-Lopez et al., 2020). Axonal MVBs are also observed to be smaller than MVBs located within the dendrites (Turegano-Lopez et al., 2020) but there is some evidence that these may play a role in SV turnover (Sheehan et al., 2016).

Macroautophagy is another process that can degrade proteins within cells (Zhao et al., 2022). Autophagosomes within the cell transport material ready to be degraded to lysosomes (Ballabio and Bonifacino, 2020). Within neurons specifically, axonal autophagosomes are observed to form at the distal end of axons and proceed towards the cell body utilizing dynein-based motion (Cheng et al., 2015). Several SV proteins have been observed to interact with autophagosomal processes (Okerlund et al., 2017; tom Dieck et al., 1998; Verstreken et al., 2003) but it is unknown the full extent of this relationship (Decet and Verstreken, 2021).

While all of these processes are present within the axon, playing a key role in removing old and damaged proteins involved in many cellular processes, and they may be involved in the breakdown of SV proteins as well. However, measurement of SV protein lifetimes show differences from other proteins in neurons (Fornasiero et al., 2018), and SVs are capable of moving independent of the endolysosomal or autophagy systems (Chenouard et al., 2020; Gramlich and Klyachko, 2017; Herzog et al., 2011; Staras et al., 2010), so there may be additional ways they can return to the soma for degradation besides these pathways.

3 Motivation and Open Questions

Neurons are among the most structurally complex and spatially extended cells in the human body, placing extraordinary demands on the intracellular systems that maintain synaptic health. Of particular interest are synaptic vesicles (SVs), which mediate neurotransmission and must be produced, transported, used, and ultimately degraded, all within an environment where synaptic distances from the soma can span millimeters or more. The results presented in this dissertation are motivated by key gaps in our understanding of the intracellular transport mechanisms that support synaptic vesicle lifecycle, and how these processes intersect with cytoskeletal architecture and proteostatic maintenance.

3.1 Neuronal Transport and Proteostasis

Due to their extreme polarity, neurons rely on precise regulation of protein transport and degradation. Synaptic vesicle proteins undergo hundreds of cycles of use and recycling (Truckenbrodt et al., 2018), yet the mechanisms underlying their long-term maintenance and eventual turnover remain poorly understood (Soykan et al., 2021). Maintaining a balance between delivery of new SV components and degradation of damaged or aged proteins, proteostasis, is essential to preserving synaptic function and plasticity.

Impairments in vesicle trafficking and proteostasis have been implicated as early features in a variety of neurodegenerative disorders, including Alzheimer's disease, Parkinson's disease, and Charcot-Marie-Tooth disease (Berth and Lloyd, 2023; Zhao et al., 2001). The earliest signs of pathology often appear in axons and presynaptic terminals (Burke and O'Malley, 2014), underscoring the importance of local transport dynamics in disease onset. Understanding how these systems fail, and how they are sustained under healthy conditions, offers a promising avenue for developing therapies aimed at prolonging synaptic health.

3.2 Transport on the Microtubule Cytoskeleton

A key focus of this dissertation is microtubule-supported transport in the axon. Though microtubules are structurally polar and uniformly oriented within the axon, their individual lengths are short relative to the axon's span, only spanning distances of several microns (Pampaloni et al., 2006; Bray, 2021). As such, cargo such as SVPs must navigate discontinuous tracks, frequently encountering microtubule ends. The behaviors of motor proteins at these ends, whether they pause, detach, switch tracks, or respond to regulatory cues, remain incompletely understood.

3.3 Dual Cytoskeletal Support and Vesicle Capture

The MT cytoskeleton, known to support axonal trafficking of other cargo, was previously unobserved to support SV motion. Early thought was that, like much

axonal traffic, this motion was supported by MTs (Darcy et al., 2006, Kamin et al., 2010, Staras et al., 2010, Westphal et al., 2008). Later work showed that actin filaments and myosin V motors drove this motion (Gramlich and Klyachko, 2017) and indeed later work even claimed that this was the sole network responsible for this motion (Chenouard et al., 2020). However, if MT based motor proteins are found associated with SVs (Takamori et al., 2006) and drive so much other axonal traffic, are there also parts of ISVE that are supported by MTs and MT-based motor proteins?

Investigating MT-based SV motion is also important because the anisotropy of MTs within the axon provides possibilities for directional biases in motion, as observed in other MT-based cargo (Gennerich and Vale, 2009; Hendricks et al., 2010; Hancock, 2014). The possible directional biases could play an important role in regulating SV populations and SV homeostasis.

3.4 Vesicle Degradation Pathways

Once removed from synaptic cycles, SVs must be degraded, but the routes by which this occurs remain uncertain. While canonical degradation pathways such as the ubiquitin-proteasome system, the endolysosomal pathway, and macroautophagy are present in neurons, their roles in SV turnover are incompletely characterized. Notably, many SVs are observed to move independently of these systems, raising questions about alternate or auxiliary degradation routes.

The observed retrograde bias in SV motion may represent a dedicated transport mechanism that delivers aging vesicles to regions better equipped for degradation, such as the soma. In this framework, intracellular transport becomes a gatekeeper of protein quality control, selecting which vesicles are retained for reuse and which are earmarked for removal.

3.5 Key Questions Addressed in this Dissertation

The following key questions frame the contributions of this dissertation:

- How do synaptic vesicle precursors and recycling SVs interact with microtubule ends in the axon?
- What determines whether a synaptic vesicle is recaptured by a presynapse versus continuing its journey?
- Can the cytoskeleton coordinate not just motion but vesicle lifespan, through biased retrograde transport?
- How might these dynamics contribute to synaptic resilience or vulnerability in the context of aging and disease?

4 Approach

4.1 Sample Preparation

To learn more about how SVs move within neurons, it is critical to study them inside of neurons. *In vitro* studies and *in silico* simulations can help us learn a great deal about complex situations. There are always concerns about what happens differently inside of cells. Running fluorescent microscopy experiments on living neurons presents interesting challenges because sensitive cells must be removed from a living animal, separated from non-neuronal cells, cultured and allowed to grow, and then transferred to the experimental set-up where they must be further maintained until imaging is done. Further, there are extra steps that allow enhanced imaging, viewing otherwise inaccessible cellular elements.

The methods and materials used to conduct the experiments and achieve the results in the present dissertation are outlined in this section. Further details and step-by-step instructions are found in the appendices.

4.1.1 Dissection

Neurons we use in experiments are harvested from prenatal rat pups. Rat gestational periods are around 3 weeks in length, and as rats approach day 19 of gestation, we euthanize the dam via CO_2 asphyxiation and decapitation before removing the pups and placing them on ice for euthanasia. All animal euthanasia was carried out with permission and oversight from the Auburn University Institutional Animal Care and Use Committee (IACUC).

Euthanized rat pups are then transferred to a biosafety level 2 (BSL-2) cabinet to keep samples free from contamination during the rest of the dissection. Additionally, protective equipment including hairnets, clothes-covering gowns, and surgical masks must be worn to prevent contamination of the samples.

One by one, the euthanized pups are decapitated and picked up using a pair of forceps. Using surgical scissors, an incision is made from the base of the skull towards the top of the head. The skull and skin can then be moved to the side, the brain removed and placed into ice cold Earle's Balanced Salt Solution (EBSS). Once all brains have been removed, they are separated into distinct hemispheres. Left and right hemispheres are then placed in separate ice cold EBSS containers, leaving the brain stem and cerebellum behind. Transferring the pieces to smaller dishes also allows excess materials from previous steps to be left out of the final preparation.

From the isolated hemispheres, the hippocampus is located and removed, again being transferred to a clean EBSS dish. Finally, when only hippocampi remain, they are cut into pieces roughly 1-2mm in length. Using a glass pipette, the pieces of hippocampus are added to a specially prepared digestion media (Appendix 1.4) and incubated for 30 min, agitating occasionally to ensure uniform chemical digestion. This step breaks down intracellular connections so that cells can come apart more easily.

Once the incubation in digestion media is complete, cells, are transferred to culturing medium and are further separated via mechanical action as the pieces of hippocampus are pipetted up and down through a flame narrowed glass pipette until no large pieces remain.

Cells are now able to be counted. Using a Neubauer hemocytometer, a small amount of the cell-containing media is added to specially constructed chamber of known volume on the glass slide. When counted under a microscope, this allows a calculation of the number of cells per unit volume. Optimal cell distribution for imaging occurs when 10,000 cells are placed onto prepared glass coverslips with a thin layer of astrocytes. Based on the cell density counted previously, a volume is added to each well to achieve the desired cell density. Cells added to the plates are placed in Neuronal growth media that supports the settling and growth of neurons.

Remaining cells are added to a cell culture flask that allows air flow. These are placed into a separate media that does not allow neurons to grow, instead astrocytes among these cells will grow for two weeks until they are added to glass coverslips which will be used to plate neurons from future dissections.

4.1.2 Cell Culturing

In order to learn how SVs move within functioning neurons, neurons must grow *in vitro* to make functional synapses. This process takes several days, during which the cell health must be monitored and maintained to ensure reliable data can be obtained.

4.1.2.1 Astrocytes

Astrocytes and other glial cells are critical for neuronal health and play an important role in neuronal communication as well by clearing excess neurotransmitter. As such, we culture and plate astrocytes to obtain a more reliable image of what happens to SVs within cells.

Beginning directly after dissection, a mixture of astrocytes and neurons is added to cell culture flasks in Fetal Calf Serum (FCS) media (see Appendix 1.1). This media allows astrocytes to grow, but is not suitable for neurons. Astrocytes grow within flasks for 2 weeks, media fully replaced every 2-3 days, until they are ready to be plated. For plating, FCS is removed via aspiration and trypsin, an enzyme that digests connections between astrocytes and the cell flask, is added. Astrocytes incubate in the trypsin media for 5 minutes. The trypsin is then removed from the flask after additional mechanical perturbation is used to ensure removal of all astrocytes, and transferred to a conical tube. The conical tube is inserted into a centrifuge and spun at high speed to condense cells out of the media into a single pellet. The trypsin media is then aspirated away and fresh FCS media added and mixed until the pellet is resuspended in media. The mixture is then added to specially prepared glass coverslips. After allowing three days for cells to settle on the coverslips, media changes with fresh FCS then occur at 2-day intervals until the day before dissection, when Neuronal growth media (See Appendix 1.2) is added to prepare the cells and provide suitable media for neurons the following day.

4.1.2.2 Neurons

Neurons are added to the prepared glass coverslips coated with astrocytes. After 24 hours, Neuronal growth media is removed and replaced with enriched neurobasal media (See Appendix 1.3). 1 ml of neurobasal media is removed and replaced with fresh neurobasal media every 2-3 days until samples are ready for experimentation, 12-18 days after plating. Media changes and other relevant details can be tracked for each set of sample plates using a cell log tracker (Appendix 2.2.3)

4.1.3 Lentiviral Transfection

In order to image certain cellular components, fluorescent proteins can be added. Sometimes these fluorescent elements are added as a dye during the experiment, but they can also be added to specific proteins within the cells by adding a virus that changes cellular instructions on how to make proteins, adding instructions to add a fluorescent protein. This can be done in a variety of ways.

To perform the experiments in this dissertation, we used lentiviral transfection. Briefly, a specially designed virus is added to the cells after plating. This virus modifies the genetic code within the cells to produce a fluorescent protein attached to the desired protein. The precise quantity of virus, measured as a multiplicity of infection (MOI) the ratio of viruses to cells, depends on the quantity of cells present and takes fine tuning depending on the quality of measured images. Virus is added after 24-72 hours, and then removed after a similar incubation period. Cells are then cultured as usual until ready to be imaged.

4.2 Fluorescence Microscopy

A key tool used in these studies to measure motion of SV, SVP, and cytoskeletal elements that support their motion within living systems is fluorescence microscopy (FM). Neurons are transparent to visible wavelengths. Additionally, if you were able to see everything within a cell, there would be too much information to make any sense of it. FM proves a valuable tool in this area by allowing selection of key elements to be made visible relative to everything else within the cell.

FM requires an excitation light source. A fluorescent marker that can be excited by that light source, and a way to capture emitted light. Certain molecules, by nature of the spacing of the energetic states, can absorb light and then emit a lower energy photon afterwards. Some such molecules occur in nature and can be adapted to many different biological situations. The fluorescent marker must be carefully selected to match the application and equipment used. Once the marker is attached to the cellular element to be identified or tracked, a light source is shone on the sample. In our setup, which will be explored in more depth later, a filtering cube then serves its first purpose of cutting down the white light from the light source. Light of a narrow band of wavelengths near the excitation wavelength of the selected fluorescent marker then shines on the fluorescent markers to excite them. The fluorescent markers then emit light at a slightly lower energy (higher wavelength) as the molecules return to their other states. The dichroic cube now serves its second purpose, allowing only the emitted light though to be detected by the camera.

In this way, what was initially just the outline of a cell, hard to make out against a low contrast background, becomes an image of carefully selected cellular elements that allows for more careful study and analysis.

4.2.1 High Resolution FM

A third challenge in using light microscopy to study cells is that many of the cellular elements and the processes they undergo occur on scales smaller than the diffraction limit of light. There are various ways to use FM to go past this limit and see what is happening at the nanometer scale. These studies specifically take advantage of the fact that light is emitted from a small area, the fluorescent marker, so that even though when detected, the light is a diffraction induced point spread function the order of hundreds of nanometers, a mathematical fit of the recorded light intensity allows specification of the light emitting area to a much smaller area. We accomplish this using the uTrack software package, the precise nature of this fitting will be described below.

4.2.2 Fluorescent Markers

4.2.2.1 SGC5

The primary method of marking recycling SV used in these studies was the lipophilic dye SGC5. SCC5 sticks to lipid membranes that enclose the neurons and SVs. When a sample is transferred to the microscope on its glass coverslip, imaging media with added dye can be added and fully surrounds the cell. At this point, the cell membranes are brightly visible, but the SVs within are not, as they are not exposed to the dye outside the cell in large quantities.

When the cells are stimulated to induce exocytosis, however, the SV membranes come in contact with the extracellular media containing the dye. SVs are then dyed. However, the large amount of dye on the membranes of the surrounding cells makes the dye present on any one SV impossible to discern. An essential second step is to wash away excess dye, after allowing time to ensure SVs return to the intracellular environment, taking their fluorescent dye with them. Once the excess dye is washed away from the outside of the cells, the only dye remaining that will show up as bright spots in the fluorescent images is the dye attached to recycled SVs.

4.2.2.2 EB3-RFP

End Binding Protein 3 (EB3) is a microtubule associated protein (MAP) that is present at the growing plus-tips of microtubules. The EB3-RFP lentiviral vector adds a red fluorescent protein to the EB3. This allows imaging of EB3 within the cells. EB3 proved more difficult to image than other elements mentioned herein.

4.2.3 Experimental Setup

While the more fundamental aspects that support collection of FM images of trafficking SVs are described above, the following section will focus on the specifics of the setup used in our lab to collect this data.

4.2.3.1 Coverslip Preparation

Glass coverslips are specially prepared via acid etching and coating with an adhesive layer to ensure optimal cell culturing that withstands the stresses of experimentation (see Appendix 2.1). 14 mm diameter glass coverslips are purchased in bulk and added to a flask. Nitric acid is added on top of the coverslips, which are carefully swirled to ensure that acid is able to surround each plate. The flask is then covered and placed into a sonicator where small vibrations agitate the flask and ensure the acid is interacting with each glass slip. The coverslips undergo this nitric acid treatment for one hour, interrupted briefly by manual agitation of the flask to ensure even coverage.

The nitric acid is then diluted and safely disposed of, and coverslips are washed several times in distilled-deionized water. Hydrochloric acid is then added and the treatment is repeated again. Following the second hour of acid etching, the hydrochloric acid is also diluted and disposed of and plates washed until all acid has been removed. Plates are further cleaned by rinsing in pure ethanol before being stored in pure ethanol in refrigeration until they are ready to be coated.

Plate coating involves transferring an individual acid etched cover slip to a well of a 12-well cell culturing plate and then applying a special mixture that will allow cells to attach effectively. All of this is performed in a BSL-2 certified cabinet to ensure that the sample is not contaminated with external agents. First, ethanol must be removed from the plates, so plates are placed upright in wells and allowed to dry until all ethanol has evaporated. Plates are then laid flat and 180 μL, just enough to cover the entire plate with coating solution (see appendix 2.1) is added to each plate. After allowing an hour for the coating solution to sit on the plates and the necessary proteins to settle on the surface, the excess coating solution is carefully removed via aspiration with a vacuum line within the hood. Each plate is then washed three times with distilled-deionized water to further remove excess coating.

4.2.3.2 Sample Holder

The sample holder is a set of custom machined plastic pieces designed to hold the glass coverslip in place and provide access for the electrical stimulation probes as well as inflow and outflow lines of essential media to sustain the sample during imaging.

The bottom piece is a rectangle with a depression in the center to hold the glass coverslip. A rubber O-ring is then placed around the coverslip to further prevent leaking onto the optics of the microscope. The top piece is then placed above the bottom piece and fastened with 4 plastic screws that hold the pieces together and secure the plate and media for experimentation.

4.2.3.3 Electrical Stimulation

Neurons in vivo respond to a variety of stimuli to know when to send a signal. The axon itself responds to changes in potential between the inside and outside of the cell that allow ion currents to flow in and out of the cell. We simulate this action potential via electrical probes near the sample. By applying a voltage across the sample, we cause the cells to depolarize and engage the cellular machinery

responsible for responding to natural electrical signals in the brain. This results in exocytosis of SV, which may then be measured using a fluorescent probe like VGlute1-GFP or labeled for later movement using a marker like SGC5.

4.2.3.4 Chemical Stimulation

Chemical stimulation can also be used to cause exocytosis. Ion concentrations control the potential difference across the cell membrane, increasing the concentration of a certain ion, like potassium, enough may trigger a large release of synaptic vesicles. Ammonium hydroxide can have a similar effect, also able to slip through potassium channels (Bosoi and Rose, 2009) and can also be used for the same purpose.

4.2.3.5 Microscope

Imaging was performed using a Nikon Eclipse Ti2-E inverted microscope. The microscope is equipped with a 100x oil-immersion objective lens. Images are collected onto a Hamamatsu Flash v4 CMOS camera. The entirety of the microscope and sample holder is enclosed in an incubator and maintained at physiological temperatures for cell health and better representation of a living system.

4.2.3.6 Profusion System

In order to keep cells alive and ensure optimal imaging, media containing nutrients for the cells and the ions they need to function properly are fed in using a computer-controlled profusion system. The temperature of the inflowing media is controlled via a temperature controller getting feedback from a temperature probe just above the sample. Media is removed via a vacuum line to keep a relatively constant volume in the sample chamber.

4.2.3.7 External Timing Control

Timing and triggering of the various experimental apparatus was handled using a Master-9 pulse stimulator. The Master-9 can be programmed either through the front interface or a computer application where “paradigms” can be stored and triggered that control each phase of the experiment (see Appendix 3.1)

4.3 Analysis Techniques

Various analysis techniques are used to obtain measurements and descriptive metrics that allow insights into how MTs support motion of necessary synaptic vesicles and their precursors within the cell. A few key methods will be described below.

4.3.1 Kymographs

Kymographs are obtained by taking a one-dimensional trace along an image and plotting the intensity along that trace through every frame of a movie. Doing this creates a two-dimensional image, where one dimension, the x-axis in the images in this dissertation, represents distance along the one-dimensional trace selected in the images, and the other dimension (y axis in images within this dissertation) showing how intensity along that trace changes in time. Because SV and SVP we analyzed

are moving within an axon, and therefore, on the order of μm, constrained to move in only one direction, kymographs provide a simple tool for more in-depth analysis of their motion.

4.3.2 uTrack

While kymographs can be useful for analyzing SV motion that occurs over distances of μm and seconds, smaller scale motion is lost. In order to understand what SV motion looks like more closely, super resolution tracking software is used that can pinpoint the source of fluorescent light on the SVs to within 10s of nanometers each 100 ms timestep. These measurements can then be used to understand smaller divisions within the large scale motion, and provide quantitative information on SV behavior that can be used for more detailed analysis.

4.3.3 Correlation Code

Using insights from the biological basis of the SV motion, we know that SVs and related endosomes can exhibit different types of motion. Directed motion is possible through their active transport via molecular motors. These motors can also pause, tethering the SV in place and preventing further motion. Finally, such cargo can diffuse through the crowded environment of the axon. Using quantified positions of SVs throughout a movie, the correlation code algorithm can analyze what an SV does during a single timestep in the context of what happened in previous or subsequent time steps, allowing categorization into different types of motion. Fast, directed motion corresponding to active transport using motor proteins, paused motion, with little displacement or consistent in direction, and intermediate motion, that falls outside of those more defined categories.

Further, by using the overall path of a measured SV, lab member Nathan Landers created an extension of this code that predicts the location and shape of the axon, allowing the correlation code to distinguish between motion parallel to and perpendicular to the axon.

Contribution Statement

SVP data discussed in section 5.1 was collected by S. Yogev and S. Balseiro Gomez from Yale University. Analysis was performed by Mason Parkes and Michael Gramlich. Modeling and fits presented in 5.1 were performed by Michael Gramlich.

SV data presented in sections 5.2 and 5.3 were collected by Mason Parkes and Michael Gramlich. Both also conducted the analysis, along with Nathan Landers. Modeling was done by Michael Gramlich.

5 Experimental Results

5.1 Synaptic Vesicle Precursor Pause Times at Microtubule Ends Determined by Proteins at Ends

The SVPs that deliver crucial SV proteins to the presynapse must traverse large distances from the cell body. The factors that limit that movement are important in understanding the biological limitations of that key process. SVPs have been previously observed to utilize the MT cytoskeleton from transport and to pause at MT ends. MT ends present an interesting challenge to the SVPs as they must somehow navigate from the terminal end of their current MT to another in order to continue their motion. Several possible methods for this traversal that depend on structural elements of the MT ends themselves, properties of the driving motors, or a combination of different motor effects could impact SVP's ability to traverse MT ends.

This subsection presents experimental measurements of SVP pause times measured within the axons of samples from the model organism C*aenorhabditis elegans* performed by Santiago Balseiro Gomez and Shaul Yogev of the Departments of Neuroscience and Cell Biology at Yale School of Medicine. Pause times at MT ends are quantified and modeled with a single rate constant model in which a single parameter controls the likelihood that a SVP detaches from its current MT, reaches another, and continues its motion. Differences in the pause time distributions of anterograde and retrograde SVPs indicate that different proteins at the MT ends affect SVP navigation of these obstacles.

5.1.1 Quantification of SVP Pause Times at MT Ends

We set out to further quantify SVP behavior near MT ends. SVP motion was recorded by Yogev et al. and analyzed in kymographs, composite images showing distance along a single axis in one dimension and time in another (See figure 5.1 panel B). SVPs move at relatively constant velocities during the experiments, which show up as diagonal lines in the kymographs. When SVPs pause, they leave vertical lines for the duration of the pause before continuing motion at the same speed as before (Figure 4.1 panel C) Pause time is quantified by measuring the difference in intercept of the two diagonal lines that indicate SVP motion.

This analysis allowed measurement of pause times as low as 1 frame (300 ms). Measurement included some locations that indicate SVPs or other fluorescent material stuck for the entire duration of the images (strong vertical lines Figure 4.1b) These pauses were not counted and other pauses at those locations were also discarded to reduce the impact that possible complications induced by paused cargo at those locations.

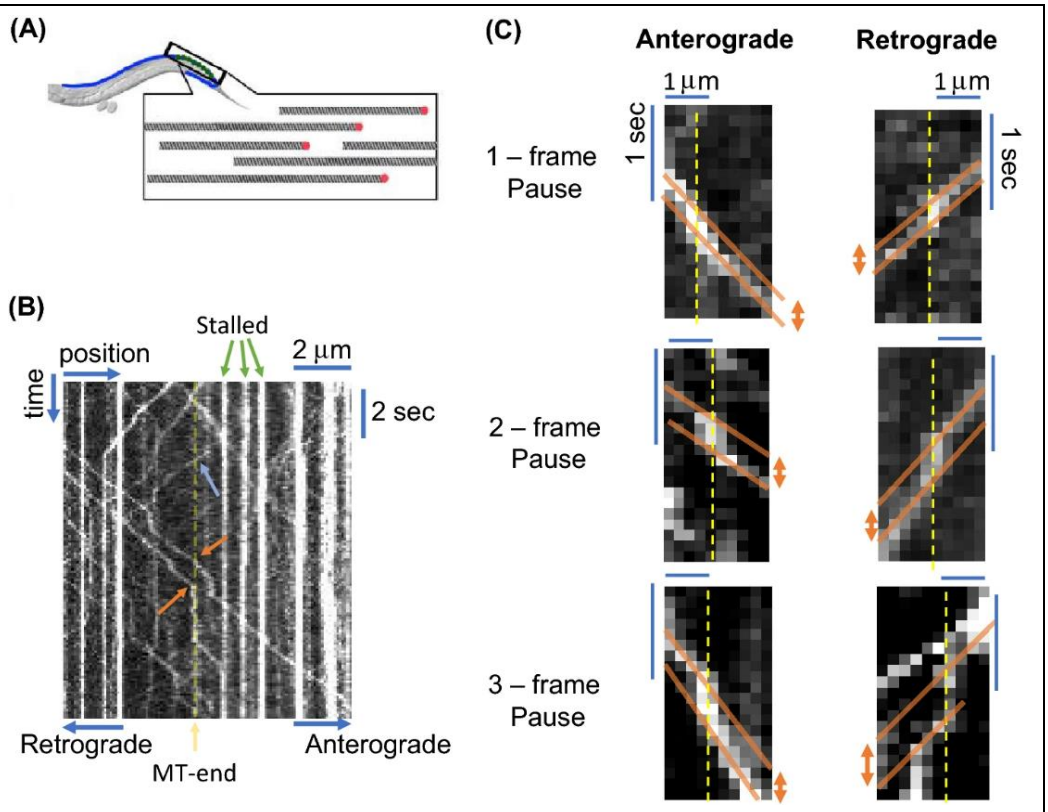

Figure 5.1: MT end kymograph analysis method. (A) Cartoon geometry of *C. elegans* axon and microtubule network. The axon has multiple tracks of microtubules aligned parallel to each other with breaks between individual microtubules. Figure reproduced with permission from Yogev et al. 2016 (B) Kymograph (time/space) representation of cargo navigating an axon. A microtubule end is designated as dashed-yellow line (determined by fraction of traverses as described in Figure 5.2. Vesicles are marked as traversing (blue arrow) or pausing (orange arrow) at the microtubule end. Vesicles engage in both anterograde and retrograde motion. (C) Examples of quantification of short-time vesicle pausing at microtubule-ends (dashed yellow lines). The pause-time at an MT end is determined as the time difference between velocity traces (orange solid lines). Both anterograde and retrograde motion are quantified the same and exhibit the same pausing behavior. Figure reproduced from Gramlich et al., 2021

Previous studies indicate that locations where SVPs pause reliably are likely MT end sites (Yogev et al., 2016). We classified likely MT end sites as locations where at least 10 SVP traversals and at least 5 SVP pauses were observed. Pause times were measured as stated above for each identified MT end site. Random sites were also selected where at least 20 SVPs were observed to traverse but made no requirement for the number of pauses. A fraction of traversal (or complementarily, a fraction of pausing) can be calculated simply by dividing the number of fractions of pauses or traversals by the total number of measured pause/traverse events. Comparing traversal fractions at MT end sites and random sites shows statistically significant differences between the faction of traversals that occur at suspected MT end sites and other locations (Figure 5.2).

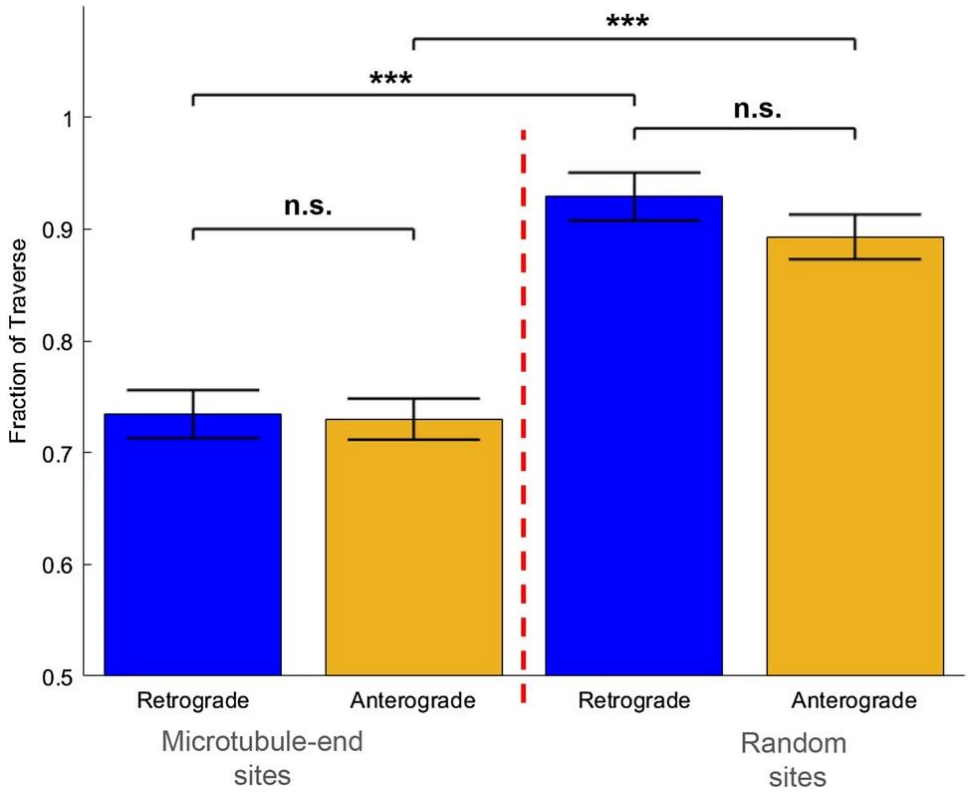

Figure 5.2: Probability Vesicles Traverse An MT end. Both retrograde (Blue Bars) and anterograde (Yellow Bars) driven vesicles traverse MT ends for the majority fraction of attempts (>0.7 for both). Retrograde and anterograde motion traverse a greater amount at randomly chosen axon locations, as compared to MT end locations. *** = $p < 0.01$; Error-bars are determined by standard-deviations in fraction of observed traversals per location. Figure reproduced from Gramlich et al., 2021

Because axonal MTs are oriented uniformly, knowing the direction of worm bodies as set during sample preparation allows discernment of SVP directionality. In each kymograph, moving left to right or moving right to left is consistently anterograde or retrograde motion, motion away from or towards the cell body. Analysis was performed without knowledge about which direction corresponded to anterograde or retrograde motion. MT-based motility is different based on direction. Anterograde motion is driven by kinesin family motor proteins while retrograde motion is driven by dynein motor proteins (Reck-Peterson et al., 2018, Hirokawa et al., 2009). Because of this difference, it is possible that anterograde and retrograde motion of SVPs can function very differently. To investigate this possibility, we compared the difference in capture fraction between MT end sites and our randomly selected sites as mentioned before. Comparisons of traversal fractions at both MT ends and random locations indicate that SVP motility is the same in both directions. This indicates that the pause/traverse mechanics at MT ends are dictated MT structure, and not by motor protein properties.

These results indicate that we can distinguish MT end sites from randomly selected spots based on the pause and traversal fraction. However, they do not indicate why the pause occurs at the MT ends or how motion continues after a pause. When the

SVP comes to the end of an MT, it must travel a distance larger than a single motor protein step size in order to reach another MT within the axon motion (Gennerich and Vale, 2009, Kapetein and Hoogenrad, 2011). There are multiple possibilities for how paused SVPs can navigate the MT end. 1) SVPs could be bound to multiple motor proteins. The observed motion of the SVP would then be the result of combined effects of the motors. 2) SVPs could reach the MT end, detach, and then diffuse to the next MT in order to continue motion. These possibilities will be examined further below.

5.1.2 Low Reversals Among Trafficked SVPs

A possible explanation for SVP pausing that could contribute to the isotropic traverse fraction behavior observed is a Tug-of-War interaction between multiple motors. Among other cargos, it is commonly observed that multiple motor proteins act on the same cargo and the net motion of the cargo is a result of the combined effects of multiple motors (Kural et al., 2005, Muller et al., 2008). It is unknown whether multiple motors combine to affect the motion of SVPs or SVs. A Tug-of-War mechanism can account for difficulties faced by MT-Trafficked endosomes because as one MT ends and the motor protein is unable to travel across the gap, other attached proteins bound to other nearby MTs can continue the motion until the motor on the terminated MT is able to re-attach at a new MT within the bundle. However, it is also possible that cargo utilizing Tug-of-War motion can be bound to motor proteins traveling in opposite directions. In this case, it would be likely to see cargo reverse direction in the axon as one motor halts, possibly because the MT ends, but also potentially due to other factors, such as the motor protein otherwise detaching.

Reversals within the kymographs appear similar to other pauses, except that when motion resumes it is a reflection of the line of incoming motion. Biologically, these reversals indicate a change in direction within the axon, shifting from anterograde motion to retrograde, or vice-versa. One possible cause of these reversals is that the observed SVP motion is the composite motion caused by several motor proteins. To investigate this, we carried out an additional analysis, counting the number of reversals that occur at each location. The locations analyzed for SVP motion at MT end points revealed low probability of reversal for both directions, with no significant difference between the two (See Figure 5.3) (Retrograde = 0.05 ± 0.086, Anterograde = 0.048 ± 0.057; P = 0.6255 from 2-tailed t-test).

The same analysis carried out in the control (Non-MT End) points indicated a similar anisotropy with a similarly low fraction of SVP reversals (Retrograde = 0.017 ± 0.02, N = 599; Anterograde = 0.008 ± 0.01, N = 737; P = 0.182 from 2-tailed t-test).

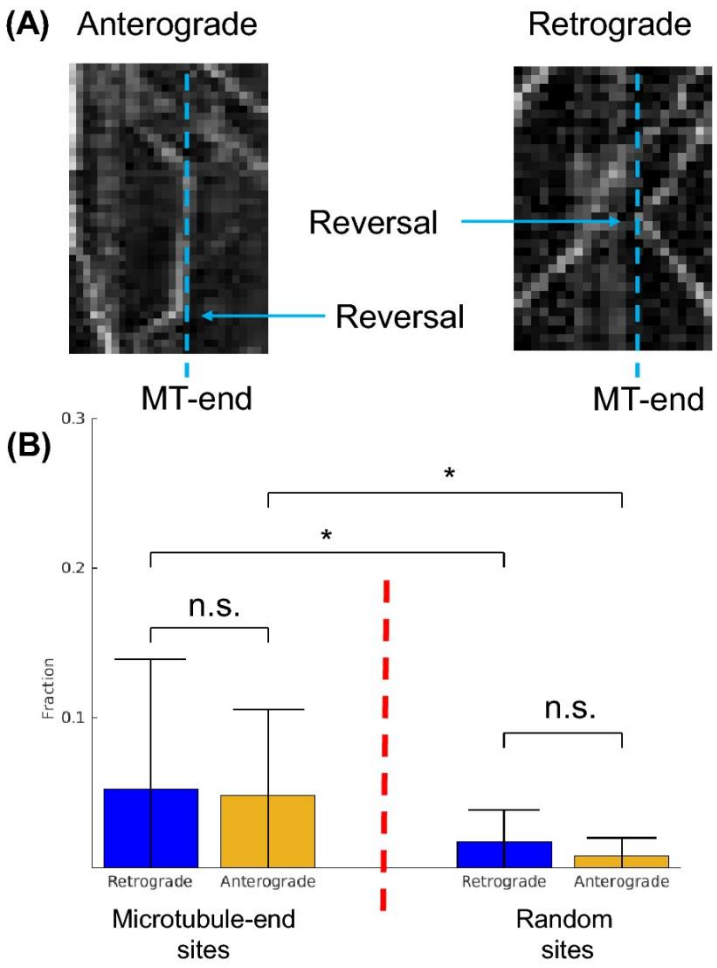

Figure 5.3: Vesicle Reversal Fraction *after* Pausing at a Microtubule-end. (A) Both anterograde and retrograde motion exhibit reversals at a microtubule-end location. Reversals are not observed to correlate with pause time. (B) The overall fraction of reversals at microtubule-ends is <0.05 for both retrograde and anterograde motion. There is no statistical difference for direction of motion at MT end. The overall fraction of reversals at random locations along the axon is <0.02 for both retrograde and anterograde motion. There is no statistical difference for direction of motion at random locations. Error-bars are determined by standard-deviations in fraction of observed traversals per location. * = p <0.05, two-tailed student t-Test. Figure reproduced from Gramlich et al., 2021

There is, however, a small but statistically significant difference observed between the reversal fraction at MT end sites and that at random sites. This difference is consistent with the model that MT ends impede SVP motion, however, because reversals are so low even in the increased case, we conclude that Tug-of-War motion plays a limited role in SVP motility.

5.1.3 Single Rate Constant Model of SVP Pauses at MT Ends

Because of the previous evidence that SVP pauses at MT ends are caused by the structure of the MT ends and the necessity for SVP-bearing motor proteins to navigate the ends before they can continue along the axon, and not caused by properties of the motors or collections of motors, we developed a hypothesis wherein the limiting step for SVPs traversing MT ends is how long it takes them to

detach from the MT that comes to an end and diffuse across the gap separating it from the next MT (or another MT in the bundle). This model incorporates MT organization as a 2-dimensional array where empty lattice sites indicate MT ends See Figure 5.4).

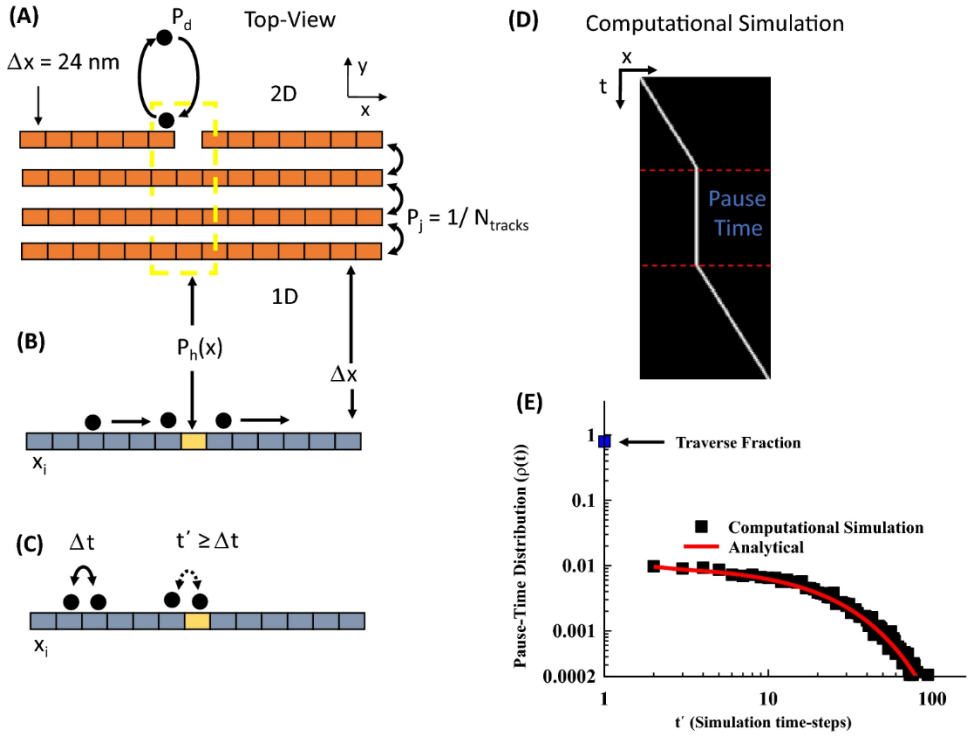

Figure 5.4: Dominant Motor-driven model. (A) We model an axonal bundle as lattice sites along a series of parallel tracks. Vesicles are modeled with a single detachment/attachment parameter (P_d). The probability a motor will jump between tracks is modeled as a uniform probability (P_j). MT ends are modeled as missing lattice sites.(B) We reproduce kymograph results by making a one-dimensional simplification of our two-dimensional model. Each one-dimensional lattice site has the same spatial resolution as the two-dimensional lattice site (Δx). Vesicle inhibition by an MT end site is now modeled as a probability (Ph), due to the loss of information about which track the vesicle is on. (C) The time a simulated SVP pauses at a location with an MT end (t') is greater than the time required to transition to the next lattice site (Δt).(D) We introduce the Pause-time parameter to quantify and measure the probability a vesicle will pause at an MT end. We show that our detachment parameter hypothesis (Red-line, Eq 1) will show a uniform decrease in pause-time with increasing time. We compare our analytical expression with a computational simulation (Black-squares, 1000 simulations). Figure reproduced from Gramlich et al., 2021

This model uses a single rate constant as a parameter to describe SVP motion. SVP motion is modeled along the lattice by propagating vesicles at a constant speed while not at an MT end site in the lattice. When the vesicle reaches an MT end site, it has equal probability on any of the tracks in the MT bundle, so the probability it interacts with an MT end is $1/N_{Tracks}$. If it does not interact with an MT end, it will continue unimpeded. If it does interact with an MT end, it pauses for a time before detaching from the current MT and reattaching to an MT that allows it to continue its motion. We model this process with a single coarse-grained parameter, the pause duration, or time the SVP remains paused at the MT end before continuing. This parameter includes the time it takes for the vesicle to detach from its current MT

track, diffuse to another MT, and re-attach. Each of these steps, as well as others essential to the motion of the motors but not relevant to the present study, occurs on a shorter time scale than the 20 ms used within the simulation, and indeed much shorter than the than the lower limit of experimental exposure times needed in fluorescence microscopy experiments, so the course grained model is capable of capturing experimentally observable behaviors.

At each time step in the simulation, there is a fixed probability that the SVP detaches, diffuses to another MT track, and re-attaches. If the SVP does successfully navigate the end during the time step, the pause time is added to the aggregate distribution, otherwise the time continues until the SVP is able to successfully navigate the MT end. The simulation does not include the possibility of reversals, which occurred in a very low number of observed SVPs.

Analytically, this proposed model of SVP behavior can be described by the following equations, derived from a probabilistic model of SVP motion previously described.

$$\rho(t = 1) = 1 - P_h \tag{1a}$$

$$\rho(t > 1) = P_h[(1 - P_d) + P_d P_h]^t P_d(1 - P_h) \tag{1b}$$

This equation captures the behavior of both traversing vesicles, which have P_h=1/N_{Tracks} probability of being on the track with the MT end, and therefore a 1-P_h probability of being on a track that does not have an MT end and therefore would traverse the MT end unimpeded. If the SVP is on an MT track with an MT end it will pause and its behavior can be described by the second equation. Here the behavior is described in terms of both the number of MT tracks in the bundle (P_h) as well as the probability of detachment, diffusion, and reattachment at each time step (P_d).

5.1.4 Retrograde Pause Time Distribution

By fitting the model to the experimental distributions of pause times at MT ends in retrograde SVPs, values of P_h and P_d can be obtained and entered into the computational model to determine how well the simulation describes the behavior. The traverse fraction in both retrograde (0.7345 ± 0.02, Figure 5.2) and anterograde (0.7299 ± 0.02, Figure 5.2) driven SVPs allows inference of P_h of approximately 0.25, which corresponds to N_{Tracks}=4, this determines the number of MT tracks to be included in the simulated MT bundle. This result is consistent with electron microscopy studies of axonal MTs (Yogev et al., 2016)

Then, fitting the analytical model to the experimental distribution allows determining a value for P_d=0.35 however, this is based on the longer experimental time steps of 100ms. Converting to the simulation time scale of 20 ms yields a P_d of 0.07 (0.35 * 20 ms/ 100 ms). Using the results of the analytical model as the parameters for the simulation was able to accurately replicate experimental results (See figure 5.5).

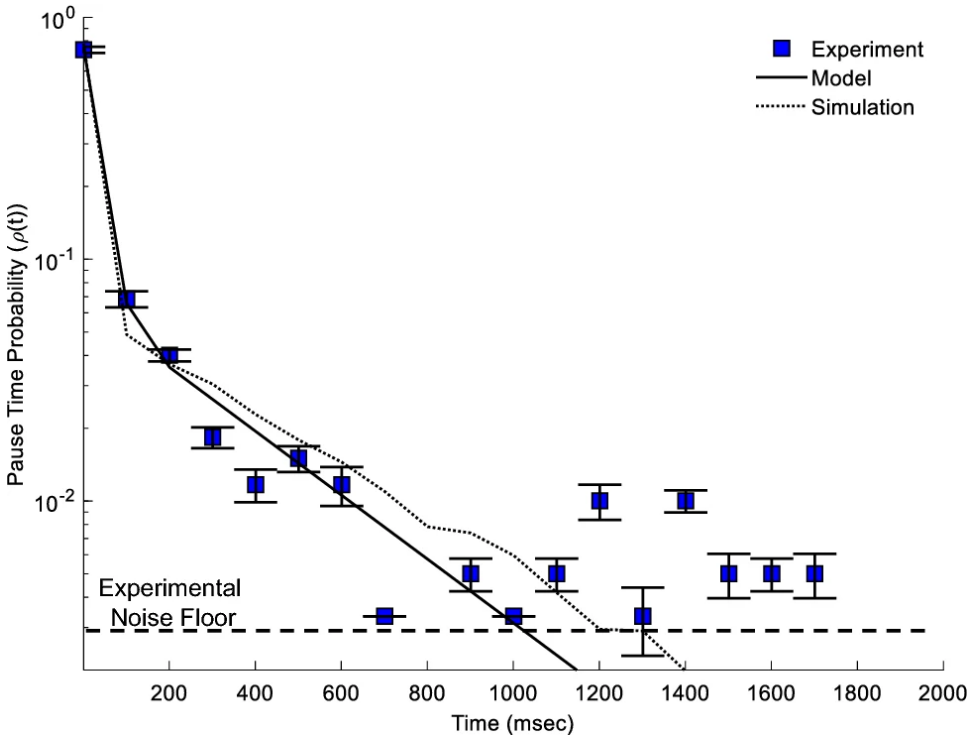

Figure 5.5: Retrograde-driven transport pause distribution as a function of time. The SVP traverse fraction (t = 0 ms) is included along with the model fit at that data point for context. Experimental data shows a decrease in pause-time probability with increasing time (Blue squares, N = 599. Both the analytical model (Eq. 1, solid line, Pd = 0.35) and the coarse-grained computational simulation (dashed line, Pd = 0.35) reproduce the observed experimental results. The lower-limit of pause-time fraction used to fit to the model was the gaussian random noise (1/Number of SVPs, "Experimental Noise Floor", dashed line). Figure reproduced from Gramlich et al., 2021

Comparisons of traversal fractions and reversal fractions did not show any differences between anterograde and retrograde motion, but it is well known that MT-based motion relies on different families of motor proteins for anterograde and retrograde traffic (Reck-Peterson et al., 2018, Hirokawa et al., 2009).

Motor proteins moving in opposite directions also meet different ends to the microtubule. Anterograde motion is toward the plus end while retrograde motion is towards the minus end. Kinesin and Dynein each take steps that move their center of mass roughly 8 nm in the direction of motion (Gennerich and Vale, 2009), and the space between consecutive microtubules is around 20 nm for small caliber axons (Kapetein and Hoogenrad, 2011). The step size smaller than the gap between MT ends means that directional cargo is limited to interactions with the end it reaches. The different ends of the microtubules are differentiated by different proteins and serve different functions (Akhmenova and Steinmetz, 2015).

Thus, some difference in traffic mechanics are likely to be observed, however there are multiple possibilities for what those differences might be as cargo navigates MT ends. First, it is possible that the different motor proteins driving motion in different directions result in completely different, motor-dependent detachment probabilities. A second option is that the process of navigating MT ends is

independent of motor proteins and thus would be equal in the different directions of motion. A third possibility is that different proteins at MT plus and minus ends mediate how SVPs pass MT ends, and thus there would be a difference between pause times in the retrograde and anterograde directions, but these pause times would not be closely linked to the pause times observed in the motor proteins driving the motion themselves, instead reflecting differences in protein behavior at opposite ends of the MTs.

5.1.5 Anterograde Pause Time Distribution

Comparison of experimental distributions of pause times does indeed show a difference between anterograde and retrograde motion. Vesicles moving in the retrograde direction have the previously stated P_d of 0.35, while following the same procedure with vesicles moving in the anterograde direction gives a P_d of 0.5. The simulation that best recreates the experimental observation uses a P_d = 0.13, consistent with a P_d = 0.65 in the experimental time scale (See figure 5.6). The small differences between the best P_d in the analytical model and the computational simulation can be attributed to the course graining of the simulation.

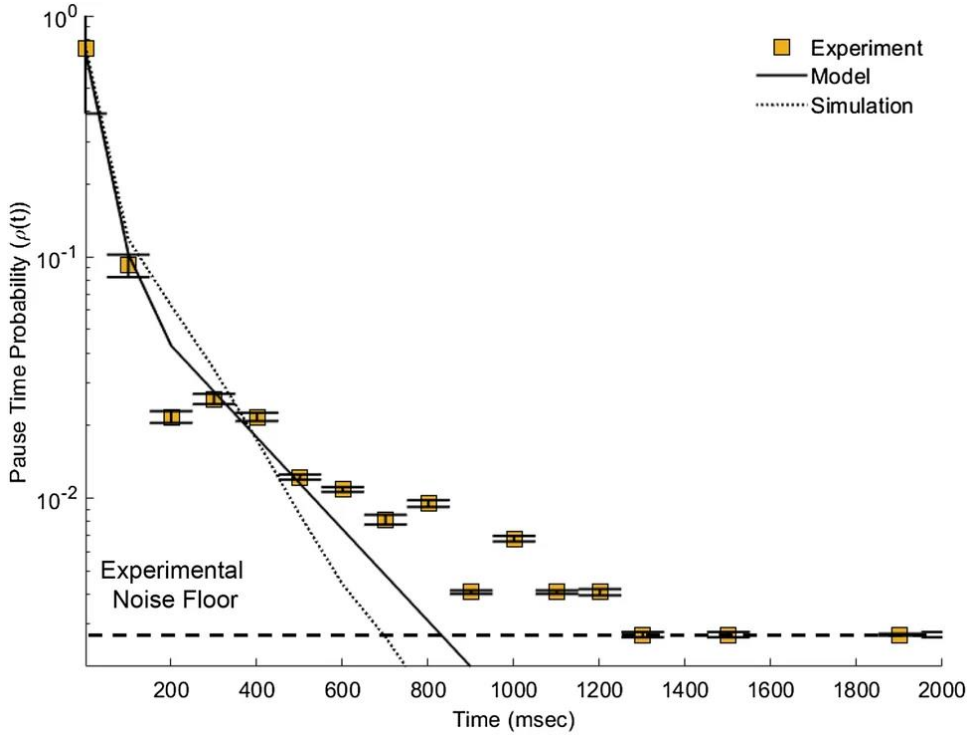

Figure 5.6: Anterograde-driven transport pause distribution as a function of time. The SVP traverse fraction (t = 0 ms) is included along with the model fit at that data point for context. Experimental data shows a decrease in pause-time probability with increasing time (Yellow squares, N = 737). Both the analytical model (Eq. 1, solid line, Pd = 0.5) and the coarse-grained computational simulation (dashed line, Pd = 0.65) reproduce the observed experimental results. The lower-limit of pause-time fraction used to fit to the model was the gaussian random noise (1/Number of SVPs, "Experimental Noise Floor", dashed line). Figure reproduced from Gramlich et al., 2021

These different P_d values, combined with the difference in time scales between these detachment probabilities and those of the motor proteins themselves support the third hypothesis listed above, that the pause times are dependent on proteins located at MT ends, which are different, and provide a difference in distributions between the two directions of travel, but do not depend purely on the different motor proteins that drive the motion.

The difference between pause time distributions of SVP traveling in the anterograde and retrograde direction before pausing at MT ends shows that in addition to the previously discovered impact that MT structure can have on MT-based cargo, there can also be directionally different mechanics as MT-based cargo navigates the MTs. SVPs play a vital role in maintaining SV populations used in synaptic transmission, and understanding the directional differences in how long it takes them to traverse an MT end is important to understanding their overall motion as this is a rate limiting step in their intracellular trafficking. This result also raises questions about the impact the MT cytoskeleton can have on SV trafficking, and thus on other parts of the SV life cycle.

5.2 Synaptic Vesicles use Actin and Microtubule Cytoskeletons for Transport

Actin, another cytoskeletal protein, supports the trafficking of recycling SVs between presynapses, a process known as intersynaptic vesicle exchange (ISVE) (Park et al., 2012; Lee et al., 2012; Rizzoli, 2014; Joensuu et al., 2016; Gramlich and Klyachko, 2017; Chenouard et al., 2020; Chen et al., 2021; Park et al., 2022). However, because the MT network is also present within axons and known to support trafficking of various other cellular cargos and SVPs, which contain similar proteins and lipids to the SVs they are eventually synthesized into it is of interest to see if MTs support ISVE as well.

In order to investigate the role MT based transport plays in ISVE we utilized FM studies of recycling SVs and MAPs within cultured rat-hippocampal neurons. Nano-scale tracking of SVs and imaging of EB3 marked MT ends show that SVs are more likely to pause near MT ends, similar to other MT base cargo like SVPs. The unique polarization of the axonal MT network allows for directional biases in motion, however these are not observed in the axonal motion of most SVs, consistent with some portion of these SVs using actin-based motors for transport. A closer look using pharmacological agents to manipulate the cytoskeleton or motor proteins shows that both MT and actin modulations cause changes in SV motion within the axon. Indicating that SVs do indeed use both actin and MT cytoskeletal networks for motion.

5.2.1 SV Pauses Correlate with MT Ends

To investigate the potential use of the MT cytoskeleton in ISVE, we used fluorescence microscopy to track SV motion in cultured hippocampal rat neurons. Transfecting the neurons with Lentibrite EB3-RFP allowed labeling of End Binding Protein 3 (EB3) a protein found at the growing plus tips of dynamic MTs (Stepanova et al., 2003). By using videos of SV motion and images of EB3

locations (see figure 5.7) we were able to investigate the effects of MT structure as SVs traverse those points.

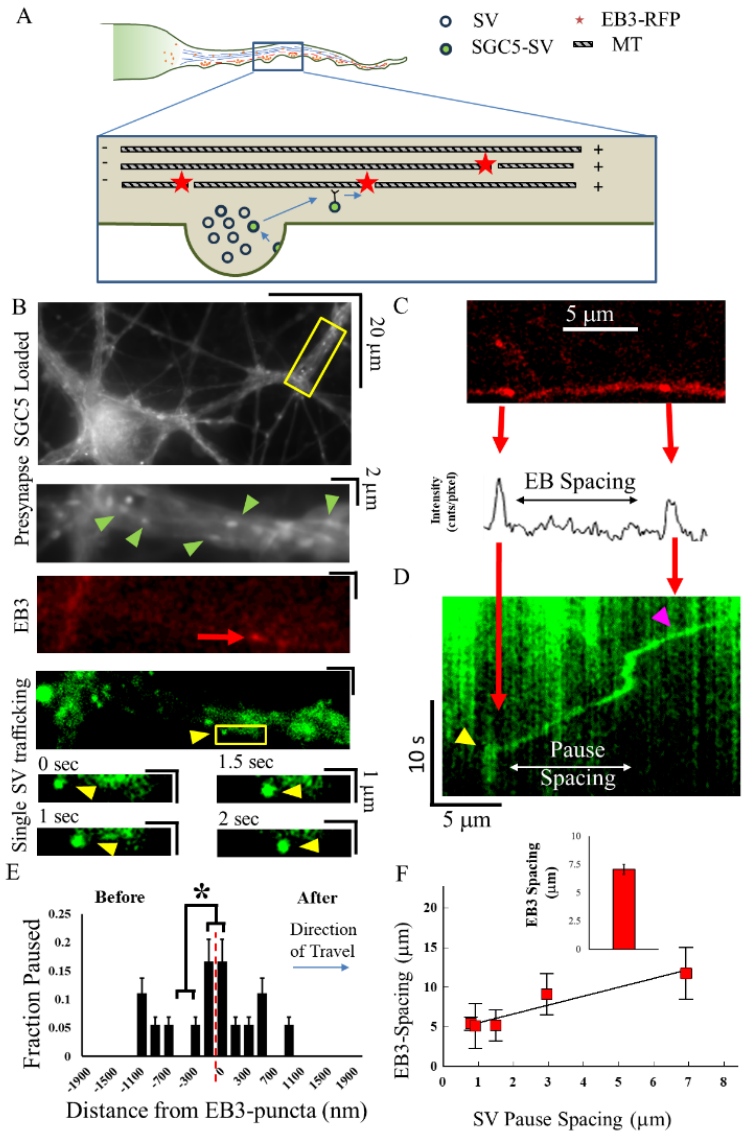

Figure 5.7: MT structure correlates with SV mechanics. (A) Cartoon of MT-supported SV motility along the axon. MT plus-end locations are labeled with EB3–RFP shown by red dots. SVs travel until reaching an MT end and pause before continuing motion. (B) Cultured cell images showing experimentally measured co-localization of labeled presynapses (green arrows), EB3–GFP puncta (red arrow), and single SGC5-labeled SVs (yellow arrows). Single SVs travel toward EB3-puncta locations (lower images). (C) EB3–RFP puncta are first imaged along axonal processes and quantified via fits to line-intensity analysis (lower panel). (D) Single SVs are then imaged, and kymograph analysis is used to identify locations of pausing (yellow arrows) or locations of traversal of EB3 puncta (magenta). (E) Co-localization of SV pausing with an EB3-punctum location is determined by quantifying the number of SV pauses as a function of distance from an EB3-punctum position (x = 0). SV pausing is separated before (−x axis) and after (+x-axis) it reaches the EB3 location. (F) SV-pause spacing correlates with local EB3 punctum spacing. The average EB3 punctum spacing (inset) is consistent with previously measured MT end spacing. Single-pause events $N_{cultures} = 2$; $N_{samples} = 3$; $N_{SVs} = 21$. * = $p < 0.1$ from comparing two-proportion tests. SV-pause spacing correlation $N_{cultures} = 2$; $N_{samples} = 6$; $N_{SVs} = 13$. Fit to line R2 = 0.97. Figure reproduced from Parkes et al., 2023

Using images of EB3 puncta taken before a video of SV motion, we were able to project the location of the EB3 point to overlap its location with the a moving SV. The analysis resulted in the observation that SVs pause preferentially at EB3 points, with 32±8% pausing within 100 nm of the EB3 spot or 50±11% within 500 nm. Notably, the percentage of SVs that pause near an EB3 point is similar to P_h=(1-Traverse Fraction) measured for SVP (Fig. 5.2) The probability of inhibition P_h, used in modeling SVP motion was the inverse of the number of parallel MTs in the axon. A similar number here also indicates a similar number of parallel MTs in the bundle, again consistent with previous observations.

This measurement is complicated by the fact that axonal MTs are uniquely stable (Desai and Mitchison, 1997; Conde and Caceres, 2009; Kapitein and Hoogenraad, 2015), thus viewing the dynamic plus ends where EB3 is present reveals a small fraction of MT ends. It is unknown whether the dynamic or stable ends would have different processes governing MT-based cargo navigation of those end points. To account for this, we compared a more global measurement of EB3 spacing within an axon and the spatial frequency of SV pauses in the same axon. Assuming that EB3 spacing is indicative of more general MT end spacing in the region, this then gives a connection between more general MT structure effects on SV motion. Measurements show a linear relationship between EB3 spacing and SV pause spacing (see figure 5.7F), with a Pearson correlation coefficient of 0.97, indicating a strong correlation between the two.

5.2.2 No Observed Directional Bias in SV motion

These results suggest that SVs are indeed trafficked on SVs, and given that MT based cargo is driven by different motor proteins, it is possible that the differences in motor protein properties affect the motion of SVs. We are able to investigate this because we know where EB3 is located on the MTs, and also its direction of motion. Even in still images, EB3 puncta have distinctive profiles indicating the direction of growth (Stepenova et al., 2003). Thus, we are able to identify directionality within the axon, where generally movies make it more difficult to pair axons and cell bodies and determine where an axon begins and thus which direction corresponds to anterograde or retrograde motion.

SV motion was analyzed via computational algorithms to produce more precise location information (Jaqaman et al., 2008; Gramlich and Klyachko, 2017) as well as to classify motion into three categories: Fast, motor driven motion; Slow, subdiffusive, paused motion; and intermediate motion that does not fit either category (See figure 5.8). Based on these computational analyses, we did not see any difference in time the SVs spent in motor driven motion, nor the speed of the SVs, the average length of the motor driven runs, or the time spent in pauses. These results indicate that something more is at work in driving motion of SVs.

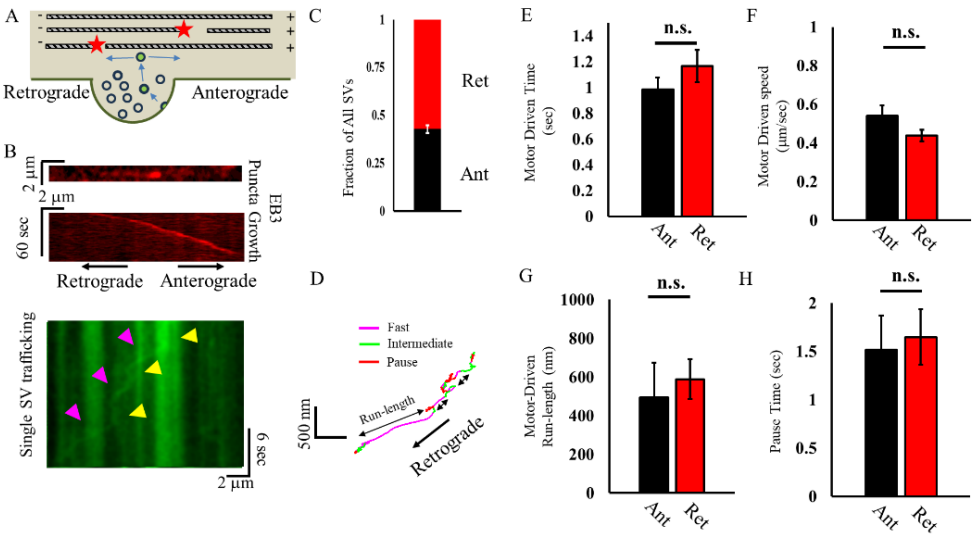

Figure 5.8: Correlation analysis distinguishes differences in anterograde and retrograde motor-driven motility. (A) Cartoon of recently recycled SVs leaving a presynapse and traveling either retrograde or anterograde. (B) Kymograph of slowly growing EB3 puncta (red) used to distinguish retrograde and anterograde motion (left). A kymograph of a single SV (green) imaged after EB3 was shown traveling in the opposite direction of the EB3 punctum growth, indicating retrograde motion. (C) Fraction of all SVs that travel in the retrograde (red) and anterograde (black) directions distinguished relative to EB3 punctum growth. (D) Bouts of motion (fast, intermediate, and pause) are differentiated using a correlation analysis approach, with a fast motion corresponding to motor-driven motility along a cytoskeleton. (E–H) Correlated motion metrics discern retrograde and anterograde motility for motor-driven speed (E), time in motor-driven motion (F), distance traveled during motor-driven motion (G), and time spent in the paused state (H). All SVs measured: $N_{cultures} = 2$; $N_{samples} = 9$; $N_{retrograde} = 55$; $N_{anterograde} = 41$. Retrograde motion: N_{fast} runs = 38; $N_{Pause\text{-}times} = 44$. Anterograde motion: N_{fast} runs = 61; $N_{Pause\text{-}times} = 72$. Statistics from a two-tailed KS test. Figure reproduced from Parkes et al., 2023

5.2.3 SVs Use Multiple Cytoskeletal Systems for Trafficking

Indeed, it is known that the actin cytoskeleton also supports SV motion (Gramlich and Klyachko, 2017; Chenouard et al., 2020), and some groups have asserted that actin driven motion is the sole method of SV motion (Chenouard et al., 2020). While our results showing MT end effects on SV trafficking suggest that MT trafficking does play a role, the size of that role is uncertain. To further investigate how and to what extent the MT and Actin cytoskeleton are supporting SV motion, more detailed analysis is required. To further this investigation we use two tools, more detailed computational analysis of SV tracks, and pharmacological agents that modify the cytoskeleton.

As previously stated, motion can be broken down based on the change in SV position between time steps. Motion can further be broken down into directions. By taking into account the motion in previous time steps, an approximate axon can be modeled, allowing the SVs to be analyzed in terms of motion along the axon and motion perpendicular to the axis of the axon. The analysis uses the path of the tracked SV in question to fit either a straight line or a circle to the axon in that location (Gramlich and Klyachko, 2017). Once this axon is defined, motion can be broken down into the displacement parallel to the axis and motion perpendicular to the axis (See figure 5.8). In other words, motion that is in the direction the SV is

traveling in and side to side motion as it wobbles on its way. Using these parameters we can further distinguish between motor driven motion, (previously described in terms of speed and duration) that exhibits higher parallel displacements and lower perpendicular displacements, and paused motion that exhibits relatively equal parallel and perpendicular displacements.

The second tool used to investigate the impact of various cytoskeletal elements on the trafficking of SVs are pharmacological agents that modulate the cytoskeleton or change the function of the suspected motors. To this end, a few main agents were used: one that effects the MT network, two that modify the actin cytoskeleton, and two that effect the activity of actin-based motor myosin V.

Nocodazole is a tubulin sequestering drug (Hoebeke et al., 1976, Samson et al., 1979). MTs are made up of smaller circular proteins called tubulins (Vasquez et al., 1997). MTs are usually dynamic, growing and shrinking within the cell. This requires proteins at the ends of MTs to actively assemble or disassemble the MT using tubulin in the surrounding environment. Nocodazole makes less of this tubulin available, so that MTs are not able to treadmill. Experiments with high levels of nocodazole show complete disassembly of MTs as the disassemble but are unable to form any new MTs. At lower concentrations, Nocodazole has been observed to stabilize MTs. With less tubulin being available and thus allowing some growth, perhaps enough to prevent complete destruction of the MTs, but not enough to allow them to grow as usual.

Samples were incubated for 10 minutes in 2 nM concentrations of Nocodazole. SV pause times showed a decrease after nocodazole treatment (Figure 5.9C,D). Nocodazole also caused a decrease in perpendicular displacement during motor driven motion (Figure 5.9G,H) and a decrease in overall displacement during pauses (Figure 5.9I,J). Taken together, these results indicate that stabilizing the MT cytoskeleton has a stabilizing effect on ISVE. There is less wobble side to side while SVs are moving, and while they are paused, they move less than SVs in other conditions. This indicates that SVs do, in fact, use MTs during ISVE.

Actin modulating agents were CK-666 and Lat-A (Gangulay et al., 2015). Lat-A depolymerizes the actin cytoskeleton, completely removing it and thus making it impossible to support ISVE. CK-666 inhibits the actin cytoskeletal component ARP2/3. ARP2/3 is a protein complex that allows the actin polymers to branch at their characteristic angles, forming sprawling structures of branched filaments. ARP2/3 has been found in particularly high concentrations near presynapses.

Treatment with Lat-A and CK-666 showed no impact on SV pause time (Figure 5.9C,D), but did lead to decreases in motor driven speed compared to control samples (Figure 5.9E,F). This is consistent with other experiments using Lat-A that saw a general decrease in SV speeds (Gramlich and Klyachko, 2017). Otherwise, there was little effect on ISVE observed during treatment with CK-666, but Lat-A treatment did lead to increased perpendicular displacement during active transport.

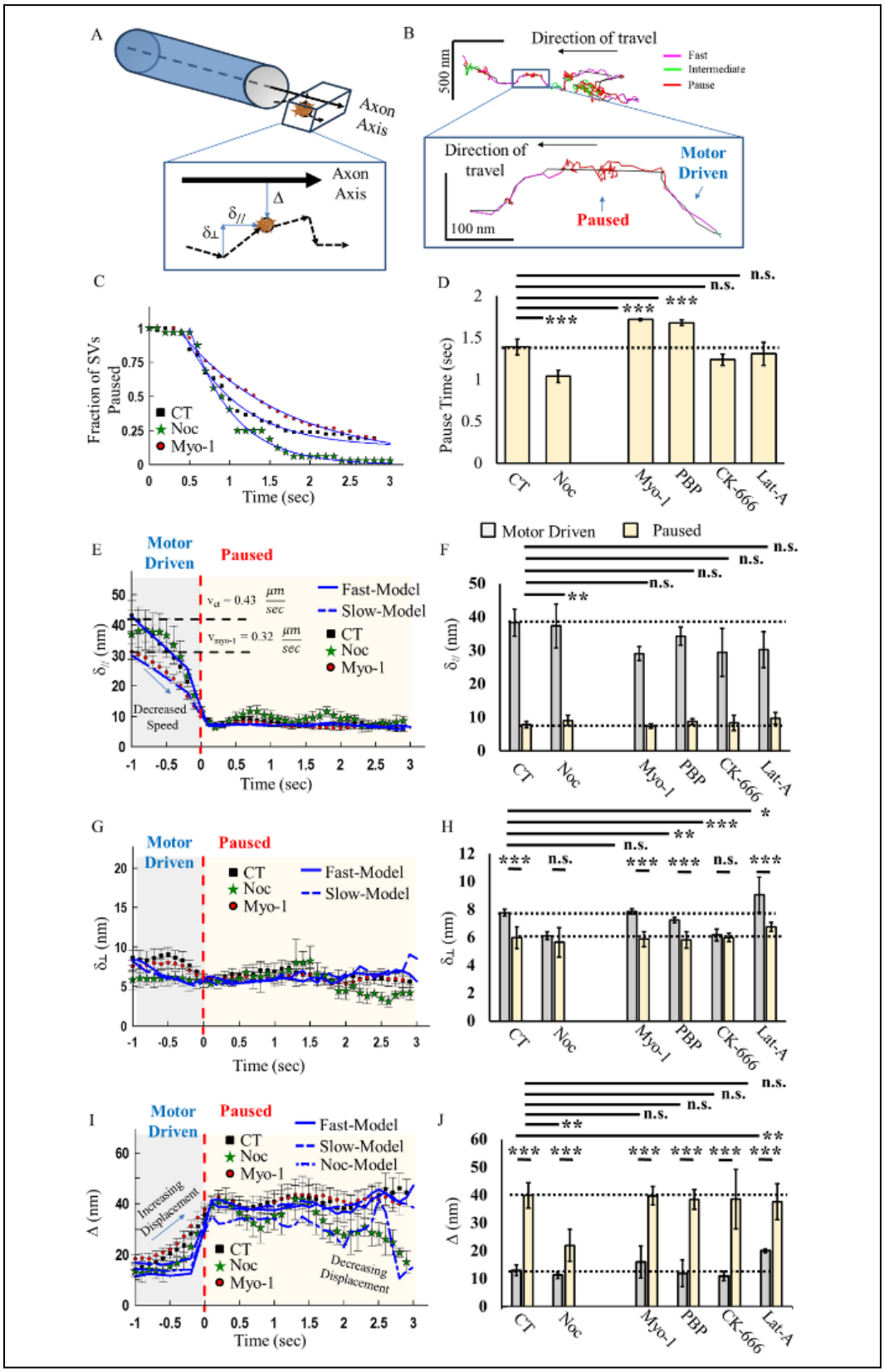
A
Axon Axis
Axon Axis
Δ
δ//
δ⊥
B
Direction of travel
500 nm
Fast
Intermediate
Pause
Direction of travel
Motor Driven
Paused
100 nm
C
Fraction of SVs Paused
CT
Noc
Myo-1
Time (sec)
D
Pause Time (sec)
n.s.
***
CT
Noc
Myo-1
PBP
CK-666
Lat-A
E
Motor Driven
Paused
Fast-Model
Slow-Model
CT
Noc
Myo-1
Decreased Speed
δ// (nm)
Time (sec)
F
Motor Driven
Paused
δ// (nm)
**
G
Motor Driven
Paused
CT
Noc
Myo-1
Fast-Model
Slow-Model
δ⊥ (nm)
Time (sec)
H
δ⊥ (nm)
*
**
***
I
Motor Driven
Paused
Fast-Model
Slow-Model
Noc-Model
CT
Noc
Myo-1
Increasing Displacement
Decreasing Displacement
Δ (nm)
Time (sec)
J
Δ (nm)

Figure 5.9: Vesicle mobility and pausing mechanics are microtubule- and actin cytoskeleton-dependent. (A) Model of axonal geometry analysis, based on SV track data, that distinguishes track motion parallel (δ//), perpendicular (δ⊥), and displacement (Δ) relative to the axon central axis. (B) Example track color coded for correlated motion (fast, intermediate, and pause) with the identified central axonal axis (black line). Inset shows a zoomed-in section of track that shows fast mobility (magenta), followed by a pause (red). SV pausing shows motion away from the central axis, followed by a return to the central axis. (C) Aggregate SV time spent in the paused state for control (CT), myosin V-inhibited (Myo-1), and 2 nM nocodazole (Noc). (D) Mean fit pause times from exponential fits to data in (C). (E) Aggregate SV parallel motion relative to the identified axon axis for control (black) and myosin V-inhibited (Myo-1). SV mobility is organized relative to the start of the pause (T = 0), with the identified fast motion (motor-driven), followed by paused motion. (F) Maximum SV parallel motion during motor-driven motion (gray) and during pausing (yellow). Statistical comparisons are carried out for parallel motion during a pausing condition. (G) Aggregate SV perpendicular motion relative to the identified axon axis. SV mobility is organized relative to the start of pause (T = 0), with the identified fast motion (motor-driven), followed by paused motion. (H) Maximum SV displacement during motor-driven motion (gray) and during pausing (yellow). (I) Aggregate SV displacement relative to the identified axon axis. SV mobility is organized relative to the start of the pause (T = 0), with the identified fast motion (motor-driven), followed by paused motion. (J) Baseline SV displacement during motor-driven motion (gray) and average SV displacement during pausing (yellow). CT: $N_{cultures} = 9$; $N_{samples} = 18$; $N_{SVs} = 58$; $N_{fast\text{-}runs/pause} = 72$. Myo-1: $N_{cultures} = 9$; $N_{samples} = 12$; $N_{SVs} = 84$; $N_{fast\text{-}runs/pause} = 132$. PBP: $N_{cultures}$ =; $N_{samples}$ =; $N_{SVs} = 166$; $N_{fast\text{-}runs/pause} = 122$. CK-666: $N_{cultures} = 3$; $N_{samples} = 10$; $N_{SVs} = 46$; $N_{fast\text{-}runs/pause} = 12$. Noc: $N_{cultures} = 3$; $N_{samples} = 9$; $N_{SVs} = 56$; $N_{fast\text{-}runs/pause} = 32$. Lat-A: $N_{cultures} = 3$; $N_{samples} = 7$; $N_{SVs} = 71$; $N_{fast\text{-}runs/pause} = 43$. * = $p < 0.05$, ** = $p < 0.01$, and *** = $p < 0.001$. Comparisons within data conditions (before/during pause) and comparisons across data conditions were obtained from the Mann–Whitney U-test. Figure reproduced from Parkes et al., 2023

MyoVin-1 (Myo-1) and Pentabromopseudilin (PBP) are the two pharmacological agents that act on the myosin motors directly to inhibit their function (Gramlich and Klyachko, 2017). Both drugs bind to a location on the motor that prevents proper function by not allowing ADP to dissociate, a necessary step before the motors can bind new ATP to hydrolyze and continue their forward motion (Bond et al., 2014). While each drug is capable of impacting other motors, there are known to effect myosin V, which is known to support some proportion of ISVE (Gramlich and Klyachko, 2017) and has been posited by some as the main proponent (Chenouard et al., 2020), so the behavior of trafficked SVs in its absence is of interest.

In the presence of myosin V inhibitors measured SV pause times increased (Figure 5.9 C,D) and parallel displacements decreased slightly (Figure 5.9 E,F) however more important distinctions will be made in the next section as the effects of these drugs near the presynapse reveals important differences.

5.3 Multi-Cytoskeletal Trafficking Supports Two-State Trafficking near Presynapses resulting in Net Flux towards Soma

SV use of MT-based motion has not been previously observed, however, given the preponderance of evidence that other, similar, cargo uses MT for trafficking it is not surprising. However, in order to reconcile past studies which assert actin as the dominant driver of ISVE, we sought deeper answers about the circumstance in which each cytoskeletal network plays a role in ISVE. Near presynapses, two different modes of transport were observed, with SVs either falling into a category

of fast-moving SVs that were unlikely to stop at a presynapse or slower moving SVs that were more likely to stop (See figure 5.10). Pharmacological modulation further revealed that the presence of myosin V motors on SVs is the controlling factor of this motion (See Figure 5.11).

The directionally polarized structure of MTs provides possible benefits to the SVs like enabling directional biases in motion. SVs are protein studded, lipid-membrane enclosed organelles within cells. The proteins on their surface must be in good working order if SVs are able to perform their essential function of fusing with the cell membrane to release neurotransmitters during synaptic communication. All proteins become misshapen and damaged over time and these changes can negatively impact functionality. In order to ensure that SVs continue to function properly, new proteins must be provided (via SVPs) while older proteins are transported back to the cell body for degradation. The two-state behavior of SVs near presynapses, coupled with the dependence of that behavior on different cytoskeletal elements provides an opportunity for subpopulations of SVs that are restricted to more local motion with frequent stops at presynapses and those that engage in longer range motion and are much less likely to stop at presynapses along the way. By constructing a computational model of this two-state motion we show that such an arrangement makes a net flux towards the soma possible at rates that are similar to those at which SV proteins enter the axon to replace old or damaged proteins (See figure 5.13).

5.3.1 Two-State SV Motility near Presynapses

Changes to the MT and Actin cytoskeletons both lead to observable changes in ISVE, however, that does not explain the nature of the differences in motion on the two networks or provide too much insight into why two networks may be useful. It is possible that the two trafficking systems function side by side to add redundancy to this important cellular process. Indeed, the hypothesis that actin alone is sufficient to support ISVE could point in that direction. However, it is also possible that the unique MT polarization in the axon allows MT based trafficking different functionality that could support synaptic function in a different way. Additionally, cytoskeletal organization in the axon is not homogeneous. While the MTs run down the entire length of the axon, actin structures are particularly enriched near the presynapses, though they are also present throughout (Gangulay et al., 2015). Thus, we developed a hypothesis wherein Actin based trafficking plays a larger role in ISVE near the presynapses, while the MT based trafficking could play a role in motion further from the presynapse. We are able to investigate this by colocalizing SV tracks in our samples with presynapses and observing the motion of synaptic vesicles as they approach and or pass these positions.

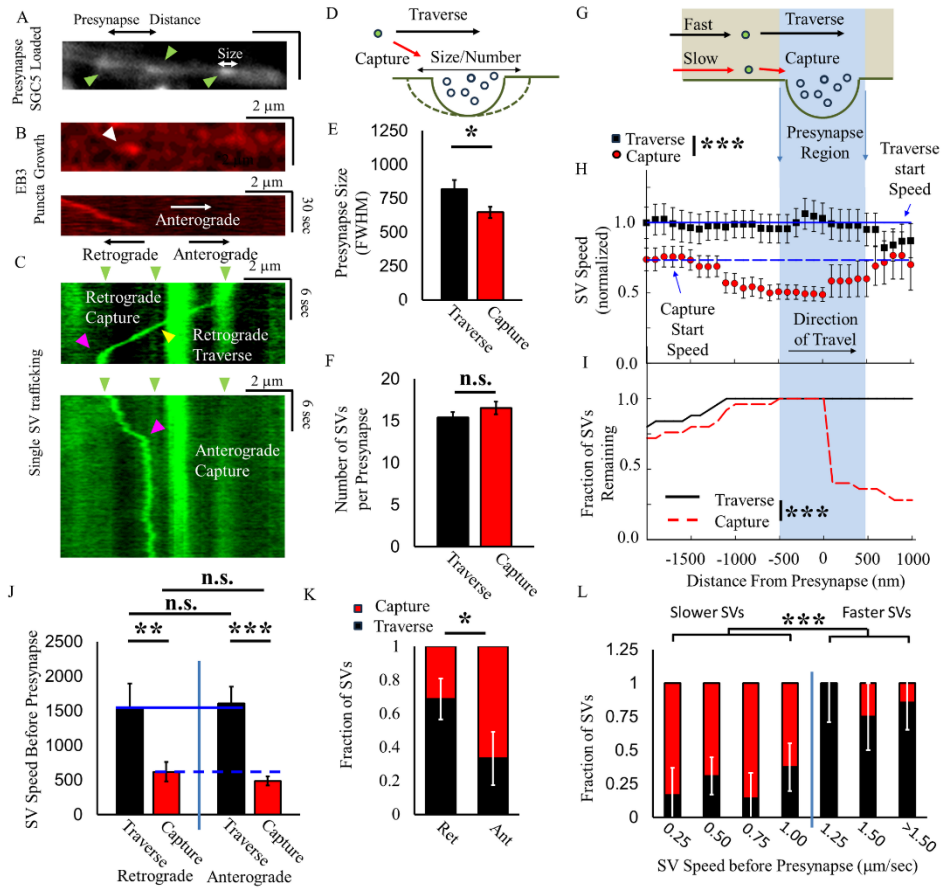

Figure 5.10: SV velocity and direction mediate presynaptic capture probability. (A) Presynapses are identified as bulk SGC5-loaded puncta (green arrows). (B) EB3–RFP (red kymograph) growth direction (white arrow) is identified relative to presynaptic puncta and corresponds to the anterograde axonal direction. (C) Single-SGC5 SVs (green kymograph) are recorded during ISVE transport near presynaptic puncta (green arrows). SGC5 is observed to either traverse (yellow arrows) or pause (magenta arrows) at presynaptic positions. Retrograde-driven SVs exhibit more traversal events than pauses at presynapses. Anterograde-driven SVs exhibit more pause events at presynapses than traverses. (D) Cartoon model hypothesizing whether SV capture/traverse by presynapses is dependent on presynapse size and SV recycling pool number. (E) SVs are separated as either traversing an identified presynapse (black) or captured by presynapses (red), and presynapse size [white arrow panel (A)] is defined as the FWHM size of the SGC5 intensity. (F) Number of SVs within presynapses, determined by the relative presynapse SGC5 intensity (A) divided by single-SGC5 intensity (C) for ISVE SVs that traverse (black) and are captured (red) by presynapses. (G) Cartoon model of hypothesized SV speed prior to presynapses is different for captured/traversed SVs. (H) Relative SV speed for SVs that are captured (red) is lower than that for SVs that traverse (black) presynapses. Aggregate SVs are compared to their starting speed for captured (blue dashed line) and traversed SVs (blue solid line). (I) Fraction of captured SVs (red dashed line) and traversed SVs (black solid line) as a function of distance from the presynapse. A small fraction of captured SVs remain within the presynapse and are then observed to leave the presynapse after capture. (J) SV speeds before reaching a presynapse are separated by direction (retrograde and anterograde). Traversing SV speed (black) is significantly larger than captured SV speed (Red) for retrograde and anterograde directions. Traversing (solid blue line) and captured SV speeds (dashed blue line) are the same for retrograde and anterograde directions. (K) The fraction of SVs that traverse presynapses (Black) is higher for retrograde motility (>70%) and lower for anterograde motility (<30%). (L) Capture/traverse fractions are separated by speed to determine the speed-dependent relationship. Slower-moving SVs (<1 µm/s) have a lower traverse fraction and higher capture fraction than faster-moving SVs (>1 µm/s).

Directional capture/traverse: $N_{cultures} = 3$; $N_{samples} = 9$; $N_{retrograde} = 19$; $N_{anterograde} = 15$. Capture/Traverse: $N_{cultures} = 4$; $N_{samples} = 5$; $N_{SVs} = 23$ * = $p < 0.1$, ** = $p < 0.01$, and *** = $p < 0.001$. Fractional capture statistics obtained by comparing two-proportion tests. Distance-dependent speed and fraction comparisons under data conditions (speeds before/at the presynaptic region) were obtained from the repeated-measures pair-wise t-test, and comparisons under data conditions were obtained from the Mann–Whitney U-test. Presynapse size, number, and direction-dependent SV speeds statistics were obtained from the two-tailed t-test. Figure reproduced from Parkes et al., 2023

While comparison of anterograde and retrograde SV motion did not show differences when compared in general (See figure 5.8), observations of anterograde and retrograde motion near presynapses did show an important difference: Retrograde SVs are more likely to be captured near a presynapse (See Figure 5.10K). This difference is slight, but statistically significant and allows for an important possibility for SV traffic on MT networks: The directional nature of MT organization in the axon allows for directional biases in ISVE. Particularly, since motion towards the soma is less likely to be stopped at a presynapse than motion toward the distal end of the axon, it allows for a larger portion of SVs to travel towards the soma. These differences may take time to manifest, and not be visible over the ~1 min of our observation, but in the bulk behavior of trafficking SVs in the long-time scales that neurons with functional SV pools must be maintained, may be able to make an important difference.

However, if direction is important, that still does not explain the importance of the multiple cytoskeletal networks involved. To see those effects, we look closely at the behavior of vesicles that are captured at the presynapse (observed as a pause in the data) or vesicles that traverse the presynapse. When compared between anterograde and retrograde SVs, it can be observed that there is no difference in the speed of vesicles in general, consistent with previous results, however, when the speed of vesicles that are captured is compared with the speed of SVs that traverse the presynapse, traversing vesicles travel at a much faster speed.

Comparing SV speeds as they approach the presynapse offers additional insights. Captured SVs start at lower speeds, even microns from the presynapse, and then slow further as they enter the presynaptic region. Some portion of these SVs pause at the presynapse for short enough times to be observed leaving the presynapse. These return to previous speeds but still do not match the speeds of SVs that traverse the presynapse. Traversing SVs start at a higher speed than captured SVs and maintain this speed throughout the presynaptic region.

When re-binned to see the capture and traverse fraction for SVs as a function of speed, SVs moving 1 μm/s or slower are captured more than half of the time, while faster SVs show traversal fractions nearer 75%. This suggests a cutoff speed where behavior shifts drastically between slow and fast SVs. Indicating that direction and speed provide key insights into predicting SV behavior near a presynapse. Slower SVs and SVs traveling away from the soma are more likely to be captured, while faster SVs and those moving towards the soma are more likely to traverse the presynapse.

5.3.1.1 Fast and Slow SVs Otherwise Appear Identical

To ensure that the differences observed in the behavior near presynapses between the fast- and slow-moving SVs an analysis was conducted into their appearance within the data. Many different objects are being trafficked near the presynapse, and if the observed fast-moving cargo was some other endosome rather than an SV undergoing ISVE that could explain the difference in motion and attempts to compare them would be flawed. To ensure we are comparing similar particles a trace along the axon was created for measured particles and a 1-D intensity plot generated (See Figure 5.11). A gaussian fit was created for this plot and fit parameters for the full width at half maximum (FWHM) and amplitude were recorded.

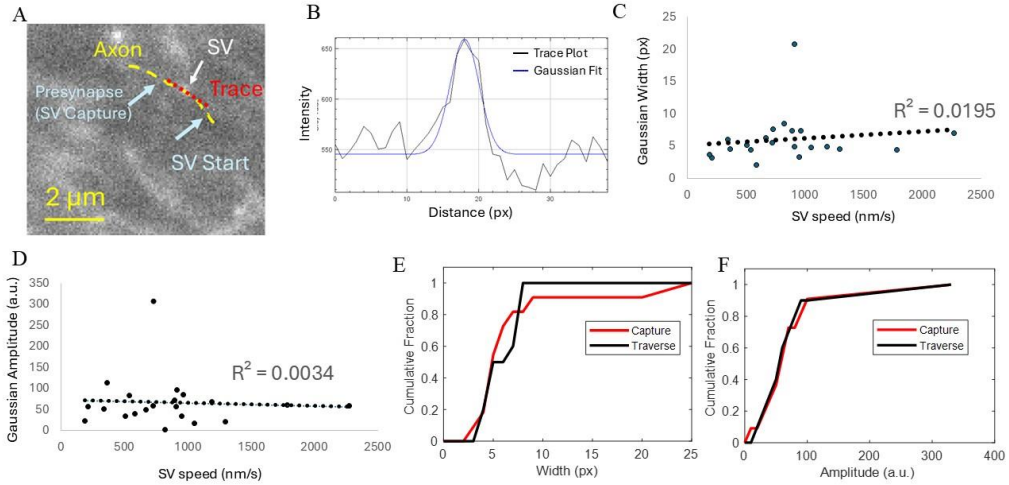

Figure 5.11: A comparison of visual parameters of captured and traversing SVs. (A) image of SV within axon near a presynapse. An overlay is shown to indicate the axon and the trace made used to generate a 1-D intensity plot for the SVS. (B) 1-D Intensity plot generated based on the trace shown in (A). Also shown is the Gaussian fit for the data. (C) shows a correlation plot between SV speed and the width calculated from the fits in (B). There is no correlation between the values. (D) Correlation plots for the amplitudes of the SVS intensity as measured in (B). Again, no correlation is seen between brightness of the observed objects and sped. (E) Cumulative distribution of measured full width at half maximum (FWHM) for the observed populations of captured and traversing SVs, no difference observed in the two populations. (F) Cumulative distributions for the measured amplitudes f the two SV populations, again, no differences are observed. Gaussian Width vs. SV Speed: N=21, Correlation coefficient R^2=0.0195; Gaussian Amplitude vs. SV Speed N=21, Correlation Coefficient R^2=0.0034; Cumulative fraction width distribution: $N_{Capture}$=11, $N_{Traverse}$=10, 2-Sample KS Test p= 0.2637; Cumulative fraction amplitude distribution: $N_{Capture}$=11, $N_{Traverse}$=10, 2-Sample KS Test p= 0.9999

While behavior near the presynapse (Capture/Traverse) changed abruptly above speeds of 1 µm/s (Figure 5.10L) there is no such trend observed in the measured characteristics of the observed particles. No trend is seen in either the width of the observed particles or the amplitude of the observed particles with respect to speed. Further, when the captured and traversing populations are compared, there are no differences observed in the distribution of widths or amplitudes. These

investigations add a degree of certainty that the observed objects exhibiting this two-state behavior are drawn from the same population (i.e. they are both SVs).

5.3.2 Differential Cytoskeletal Use Supports Two-State Motion

The next important step is to discover the underlying mechanism allowing this two-state motion. Previous observations (See Figure 5.9) indicate that MTs as well as actin filaments support ISVE, so it may be possible that these two cytoskeletal networks support the two-state motion. To investigate this, we use the aforementioned drugs that modify cytoskeletal structures or molecular motor behaviors to observe changes near presynapses in particular. Of primary interest is the molecular motor myosin V.

Inhibiting myosin V using the MyoVin-1 and PBP and measuring SV capture fraction as a function of speed showed no changes to the capture rate among faster moving SVs, but among those moving slower, the capture rate was decreased. This marks a departure from the control condition, specifically among the slower moving SVs. Suggesting that myosin V, driving actin-based motion near the presynapse, is responsible for the slower motion that exhibits more captures while the faster motion is primarily driven by MT-based motion (See Figure 5.12).

Figure 5.11C further elucidates the situation by showing that there is no change in the SV speed with position as it nears the presynapse, showing that both captured and traversing SVs move at similar rates, but captured SVs now show a sudden drop in speed as they are captured instead of a slowing down as seen in control samples. This qualitatively different behavior suggests a different system is now responsible for this motion.

While changes in the overall capture rates are fairly similar among the different treatments, differences can be seen as SVs are grouped into fast and slow groups. Among fast moving SVs, changes to the actin-based motors and actin structure showed no change. Among those SVs moving slower as they approached the synapse, differences were indeed seen. When actin was completely depolymerized using Lat-A, or when myosin V motors were inhibited, fewer of the slower SVs were captured. This result was not seen in CK-666 samples.

It is also important to investigate the effects that MT modulation has on motion near the presynapse. Introducing 1nM concentration of nocodazole caused an increase in the speed of SVs that go on to traverse presynapses, but no change in speed among SVs captured at the presynapse. As previously stated, nocodazole at these concentrations serves to stabilize the MTs, potentially allowing MT based motion driven by kinesin and dynein family motors to increase in average speed as they no longer need to navigate complicated and dynamic MT ends at the same rates. The conservation of speed seen among captured SVs in these conditions indicates that the MT cytoskeleton is not responsible for the motion of captured SVs.

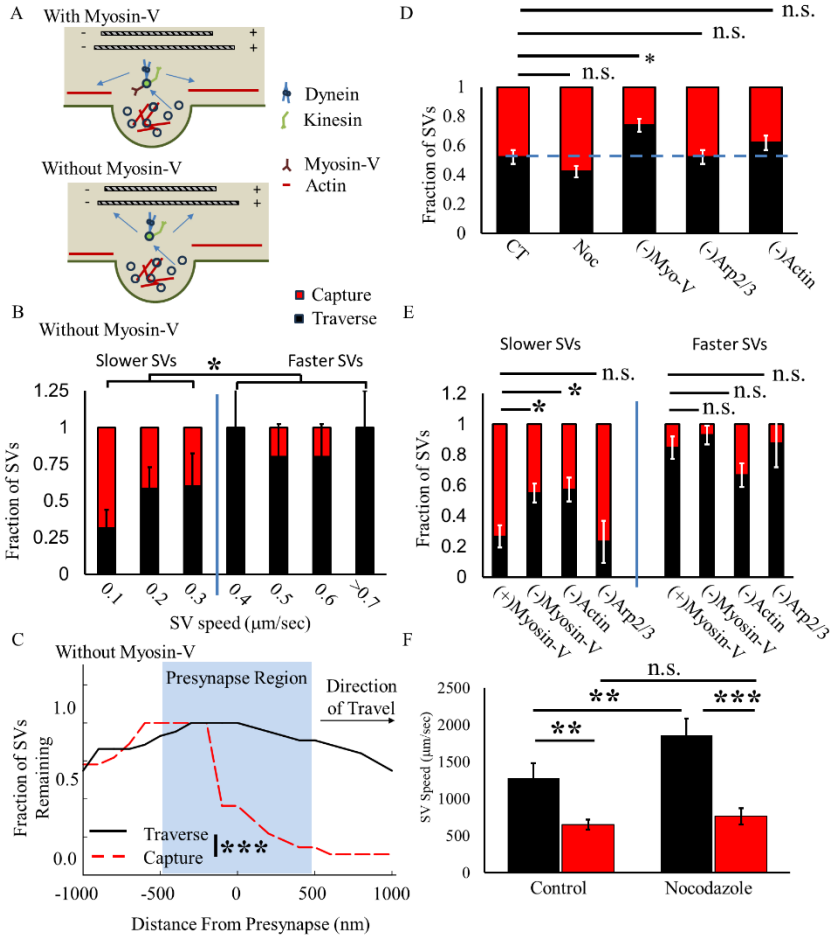

Figure 5.12: Myosin V/actin mediates slow-SV capture fraction but not fast-SV capture fraction. (A) Hypothesized model of two-state recycled SV ISVE transport. SVs with myosin V attached predominantly use actin cytoskeleton motility (top panel). SVs without myosin V attached utilize MT cytoskeleton motility (bottom panel). (B) The SV presynaptic capture fraction decreases with increasing SV speed similar to CT (Figure 4L). (C) The fraction of SVs undergoing ISVE without myosin V decreases for captured SVs but not for traversing SVs, similar to CT (Figure 4I). (D) The overall fraction of SVs that traverse presynapses increases without myosin V but does not significantly change under any other condition. (E) The traverse fraction for slower-moving SVs increases without myosin V [(-)Myosin V] or polymerized actin [(-)Actin], but traverse rates are unchanged for faster SVs. (F) Traversing SV speed (black) increases in the presence of 2 nM nocodazole, but captured SV speed (Red) is unchanged in the presence of nocodazole. CT: $N_{cultures}$ = 4; $N_{samples}$ = 5; N_{SVs} = 23. Noc: $N_{cultures}$ = 3; $N_{samples}$ = 6; N_{SVs} = 26. (-)MyosinV (combined Myo-1 and PBP conditions): $N_{cultures}$ = 15; $N_{samples}$ = 24; N_{SVs} = 68. (-)Arp2/3: $N_{cultures}$ = 1; $N_{samples}$ = 5; NSVs = 21. (-)Actin: $N_{cultures}$ = 3; $N_{samples}$ = 7; N_{SVs} = 16. * = $p < 0.1$, ** = $p < 0.01$, and *** = $p < 0.001$. Fractional capture/traverse probability was obtained by comparing two-proportion tests. Comparison within data conditions (speeds before/at the presynaptic region) was obtained from the repeated-measures pair-wise t-test. Comparisons across data conditions were obtained from the Mann–Whitney U-test. Figure reproduced from Parkes et al., 2023

Because MT based modulation leaves captured SV speeds alone, but changes measured speed among traversing SVs, while actin changes effects the behavior of the slower, more frequently captured SVs, we are able to conclude that MT based motors are primarily responsible for the motion of traversing SVs while the actin myosin system is responsible for motion of the slower SVs and capture at the

presynapse. This allows us to suggest a rather simple model where motion is either based entirely on the MT cytoskeleton, in which case SVs will travel faster, and make fewer stops at presynapses, or on the actin system, which is slower and makes more frequent stops at presynapses.

5.3.3 Two-State Model Results in Net Retrograde Flux

5.3.3.1 Rate Based Model

Based on the observed difference in motion in the retrograde and anterograde direction and the fast and slow motion exhibited near presynapses, we develop a two-state model of SV motion within the axon. Each SV within a presynapse has some probability of being released into the axon, represented by a rate constant ζ. It then has a finite probability of moving in the anterograde direction (*p*) or retrograde direction, (1-*p*) observed experimentally to be equal. Finally, the SVs can move in either the fast mode (probability Γ). SVs moving through the axon then have probabilities of being captured at a presynapse, experimentally observed to be different in the anterograde (χ_{Ant}) or retrograde (χ_{Ret}) direction. The axonal SV flux (ϕ_{Syn}) can then be modeledu using those parameters as the following equation.

$$\phi_{Syn} = \zeta * p * \Gamma * \chi_{Ret}$$

The total flux of SVs towards the soma will depend on the contribution of each presynapse along the axon. Summing the individual contributions to the retrograde flux will then yield the net retrograde flux towards the soma.

$$\Phi_{Net} = \sum_{i=1}^{N} \phi_{Syn}$$

Previously measured SV release rates (Gramlich and Klyachko, 2017) indicate a rate constant of SV release of 0.013 SV/s. This, multiplied by the number of SVs within a presynapse roughly 40-80 (Alabi and Tsien, 2012), provides the number of SVs released from the presynapse per second. This indicates that 0.5-1 SV are released per presynapse per second. In the proposed two state model, it is the fast, retrograde motion that contributes the net retrograde flux. Experimentally observed SVs were measured with equal probabilities of moving in either direction (*p*=0.5) and a 20%-30% probability of moving with a speed greater than 1.25 μm /s.

This yields a retrograde flux per presynapse of between 0.05 and 0.16 SV/s. Throughout the length of a typical hippocampal neuron there can be 300-500 presynapses. Assuming equal contributions from each presynapse, this model predicts a net retrograde flux of 4-20 SV/s reaching the soma. This is similar to measured rates of SVP entering the soma (Watson et al., 2023)

5.3.3.2 Simulation of SV motion in Two-state model

Moving forward with this model, it is of interest to see what the effects of such two-state behavior among SVs has on SVs within the axon over time. As mentioned in previous sections, SVs are formed from SVPs which must be trafficked from the

soma. One possibility is that they return to the soma to be degraded and returned to their fundamental building blocks to be reused. The two-state model of ISVE motion could aid in explaining how this is possible.

Actin filaments are randomly oriented within the axon (Gangulay et al., 2015), so although myosin V processes in only one direction along an actin filament, its motion can be in either direction within the axon because of the orientation within the axon. MTs, meanwhile, are oriented unidirectionally throughout the axon. Because of this, there is the potential for there to be directional biases in the motion. Indeed, experimental results show a directional bias in the capture/traverse rates of vesicles moving in the anterograde and retrograde directions (See Figure 5.10K) . This difference was slight, but because SVs are constantly being trafficked over the lifetime of organisms, and because of the large number of SVs within an axon, these differences can be substantial over time. It is, however, impossible to probe such differences over time with our experimental limitations, so we introduce a model we can simulate computationally to view the effects of these directional differences over time. This is accomplished using two binary parameters that distinguish SV motion. The first is speed. When each SV is "released" from a "presynapse" its speed is determined. This is a function of whether or not myosin V is present on the SV. The second is direction. SVs may travel in either direction. Because reversals were observed rarely among SVPs and SVs, there is no chance of reversal included during un-paused SV motion. When reinitiating motion following a pause (capture) at a presynapse it has an equal chance of beginning its motion in either direction. The probability of each SV being captured is dependent on its speed and direction. Capture probabilities are based off experimentally measured capture fractions.

SV tracks were then simulated according to these parameters for times up to 5 hours. In order to simulate large scale motion of SVs within the axon, the individual SV simulations were selected at random whenever an SV was released during the simulation. SVs were selected to leave each presynapses every six seconds for the first 33 seconds of the simulation, resulting in a total number of ~60,000 presynapses being released. This large number of SVs allows a representative picture to be determined. It should be noted that SVs do not interact with each other at any point in the simulation.

By observing the number of simulated SVs that reach the soma as a function of time we are able to see differences introduced by the varying fast-retrograde capture probability (See Figure5.13). For all capture probabilities, SVs initially returned to the soma at a faster rate, and then reached a slower rate that they maintained for a longer period of time. In fact, the slow rate that each axonal simulation reached was similar for each of the conditions, however this ignores where the vesicles that reach the soma actually come from. So while the total number of vesicles reaching the soma in a given time may be similar between fast-anterograde capture probabilities, we must look closer at motion of SVs within the axon to see if there is any effect provided by the differential directional capture probabilities.

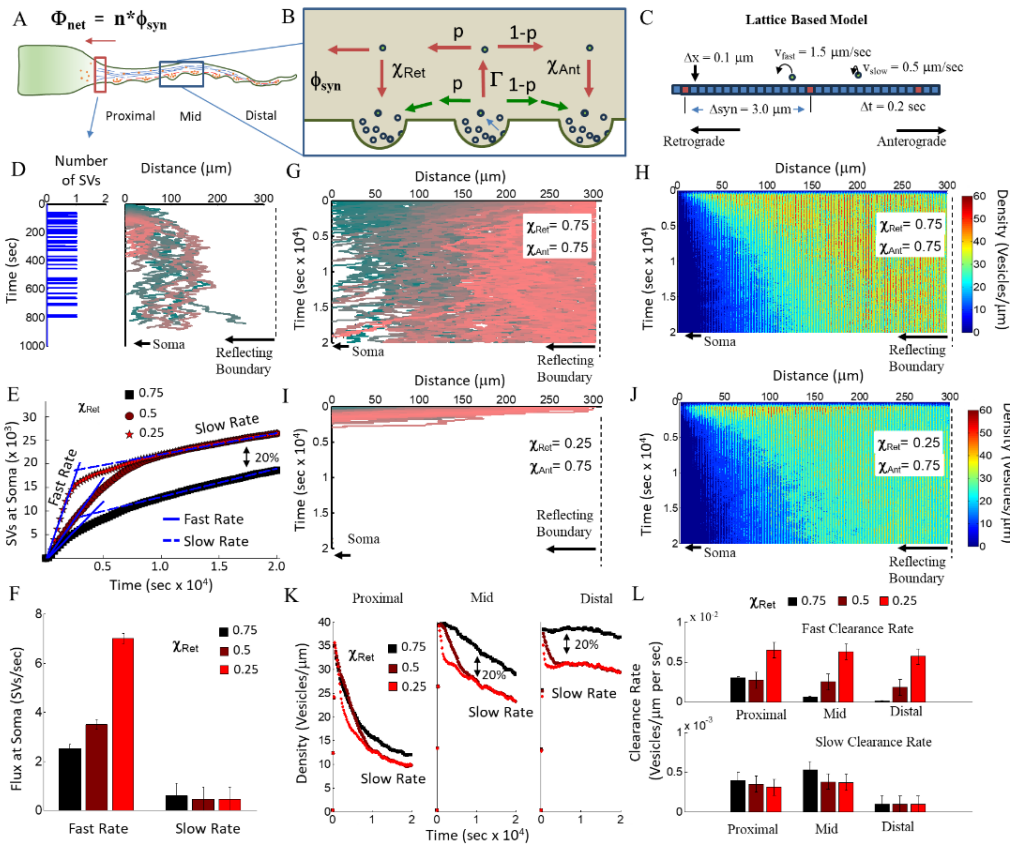

Figure 5.13: Computational model of two-state recycled SV motility and capture. (A) Net SV flux into the soma (Φ_{net}) is the total number of presynapses (n) × the mean fractional flux per presynapse (ϕ_{net}). (B) Two-state model of the fractional flux per synapse. A fraction of SVs that leave a presynapse engages in MT-mediated transport (Γ), have a probability of travel in the retrograde direction (p), and traverse a neighboring presynapse during ISVE (χ_{ret}), creating a net flux toward the soma (ϕ_{syn}). (C) Lattice-based model of axonal transport using the two-state model parameters. SVs hop along the axonal lattice at one of the two possible fixed velocities (slow and fast). Presynapses are separated by fixed distances (Δ_{syn}). Each lattice site has a fixed length (0.1 μm), and each time step in the simulation is a fixed amount (0.2 s). (D) Example of simulated SV release from a single presynapse 10 μm from the soma. The presynapse releases a single SV every 6 s (right panel). SVs are captured by other presynapses along the axon with a fixed probability and random pause time. SVs that reach the soma are counted as captured (left panel). (E) Net flux of SVs at the soma as a function of time from simulations of 300 presynapses, each releasing an SV every 6 s for a total of 200 s (60,000 SVs). Each simulation has 80% slow-moving SVs and 20% fast-moving SVs. Fast-moving SVs have a retrograde capture probability of 0.75 (black squares), 0.5 (red circles), and 0.25 (red stars). Each simulation shows an initial fast flux rate and then a slow flux rate. (F) Fit flux rates for fast and slow rates in (E). The fast flux rate increases with decreasing retrograde capture probability, representing the 20% fast-moving SVs. The slow flux rate is constant under all conditions, representing SVs with equal retrograde/anterograde capture probability (independent of speed). (G) Example of simulated tracks for a single SV released from each presynapse along the axon. All SVs have equal retrograde and anterograde capture probability (0.75). (H) Simulated spatial density of SVs per micron from a distribution of 200 SVs released from 300 presynapses. Each SV has an equal retrograde and anterograde capturer probability (0.75). (I) Example of simulated tracks for a single SV released from each presynapse along the axon. All SVs have a lower retrograde capture probability (0.25) than anterograde capture probability (0.75). (J) Simulated spatial density of SVs per micron from a distribution of 200 SVs released from 300 presynapses. 20% of SVs have a lower retrograde capture probability (0.25), while 80% of SVs have an equal retrograde and anterograde capturer probability (0.75). (K) Time-dependent change in SV density per micron along the axon for proximal (left panel), middle (middle panel), and distal (right panel) regions to the soma.

(L) Quantified clearance rate of the number of SVs per micron per second is a measure for how quickly recycled SVs can be removed from a region along the axon. SVs proximal to the soma are cleared quickly regardless of the retrograde capture probability. A differential capture probability allows for SVs distal from the soma to be cleared faster than would occur for equal capture rates. Figure reproduced from Parkes et al., 2023

Panels G through H illustrate the difference observed in simulated SV tracks in the most extreme capture probability conditions. SVs set with equal capture probabilities in the anterograde and retrograde directions are observed to travel the duration of the simulation, with relatively few making their way all the way to the soma. This is seen as well by looking at the density of SVs throughout the axon. Throughout the simulation, the area near the soma slowly loses SVs, while the area further from the soma retains a much higher concentration. This is contrasted with the case of the 0.25 fast retrograde capture probability, which shows many more SVs traveling to the soma in much less than the duration of the simulated time. It is also reflected in the SV density plot in panel J, which shows a larger portion of the axon where SVs have been effectively cleared from the axon to the soma, nearly halfway through the axon, and even in the most distal parts of the axon, the concentration of SVs has decreased to be much lower than in the equal capture probability case.

To look closer at this we can inspect the change SV density over time in three regions of the axon. The proximal end of the axon shows little difference between the conditions, with a sharp decrease in SVs over time for all conditions. Differences begin to emerge in the mid-axon region, where the equal capture probability condition shows much slower decrease in SV density over time, though it does still drop to some degree. In the distal end of the axon differences are more severe, as the equal capture fraction is hardly observed to decrease SV density throughout the simulation, while there is a decrease in SVs in the region for 0.5 and 0.25 fast-retrograde capture fractions. In each of these conditions there is still a fast clearance rate that can be measured as many SVs are released and begin their motion, and then a slow clearance rate that is measured once things appear to reach a more stable situation. Here again, slow clearance rates are consistent between conditions, and throughout the proximal 2/3 of the simulated axon, while the faster clearance rates are similar throughout the axon for each condition, with the exception of the equal capture rate.

These results show that the differential capture rate for fast-retrograde SVs does indeed provide a mechanism for clearing SVs even from the most distal portion of the axon. In fact, the resulting flux of SVs to the soma is similar to measurements of SVP numbers entering the axon (Watson et al., 2023), indicating that this could indeed model the behavior of SVs within an axon that allows maintenance of SV populations without growing too large because too many SVPs enter for SVs to be retired or too many SVs leaving the overall axonal SV pool without being replaced by newly synthesized SVs.

6 Conclusion and Discussion

6.1 Summary of Key Findings

These results build upon previous literature in providing a more detailed mechanistic look at how MT-based cargo is capable of navigating the structural obstacles, namely MT ends, to drive motion across long distances.

The studies presented in this dissertation reveal a previously unknown role of the MT cytoskeleton in regulating the trafficking and turnover of SVs within neurons. These studies demonstrate that recently recycled SVs do in fact use MT-based motion, and that this MT-based motion establishes a basis for net-retrograde flux. Further, this flux is capable of returning recycling SVs to the soma at rates similar to those at which new SV proteins make their way to the axon.

We can understand these results in terms of the questions posed in chapter 3 of this dissertation:

How do SVPs and recycling SVs interact with microtubule ends in the axon?

Experimental imaging of SVPs show that their previously observed pausing behavior at MT ends can be modeled with a single rate constant. This means that the process is well described by a situation in which the motor reaches the MT end and then must wait until diffusion to a neighboring MT allows motion to continue. New super resolution microscopy methods have allowed probing even deeper into this process and allow actual measurement of this MT-track switching (Deguchi et al., 2023)

What determines whether a synaptic vesicle is recaptured by a presynapse versus continuing its journey?

Experimental observation of *in vivo* recycling SVs show that direction and speed determine the likelihood a trafficking SV will be captured by a presynapse. Further, pharmacological studies show that the presence of myosin V motors on the SVs are responsible for the slower motion of the more frequently captured SVs while motion of the faster SVs is changed by MT modulation. Indicating a multi-cytoskeletal method of transportation that directly impacts SV capture at a presynapse.

Can the cytoskeleton coordinate not just motion but vesicle lifespan, through biased retrograde transport?

Based on the experimentally measured parameters of SV motion near presynapses and analytical and computational models of SV motion, the net-retrograde flux enabled by the two-state motion near presynapses can support SV proteostasis.

How might these dynamics contribute to synaptic resilience or vulnerability in the context of aging and disease?

Given the disruptions of axonal transport observed in neurodegenerative disorders, the role that this multi-cytoskeletal based motion plays in healthy turnover of SV proteins provides a potential new way in which these disorders may effect the brain. If SV traffic is responsible at least in part for proteostasis, then disruptions to this motion can skew the age distribution of SVs. Older SV proteins that may have been deformed with time and use are unable to serve their role in the SV cycle and synaptic transmission can be impaired. There is still much to understand about how these diseases effect the brain, but this new potential may be crucial.

6.2 Broader Context and Significance

The results presented in this dissertation show the impact that the MT cytoskeleton has on motion of SVPs and SVs. Because SVs motion correlates with the MT cytoskeleton and exhibits a directional bias, the MT cytoskeleton provides a mechanism for regulation SV protein turnover as an established net retrograde flux. This net retrograde flux compares favorably with observed rates of SVP entry into the axon.

These studies shed light on the poorly understood process of the degradation of presynaptic proteins, especially in comparison to the degradation of postsynaptic proteins which is known to support synaptic plasticity (Padamsey, et al., 2017; Goo, et al., 2017). These results begin to give insight into how SVs and their associated proteins might be returned to the soma for degradation in an orderly way.

This also begins to give hints into how more active synaptic vesicles can be targeted for degradation more precisely (Jahne et al., 2021) as more active presynapses may release SVs into the axon more frequently where they can be introduced into the population undergoing net retrograde flux.

6.3 Open Questions and Future Directions

Further work can build upon these studies by investigating synaptic vesicle motion over longer time scales. Experimental observation of the net retrograde flux or of recycling SVs entering the soma would provide extra validation for the models and results presented herein. Further, the models presented here can be built upon to include more detailed description of SV populations within the axon. SV populations can change in size over time and these changes can have effects on the possible levels of synaptic transmission to postsynaptic cells. Understanding the implications of the directional bias model in synaptic transmission may give further hints into how ISVE can support synaptic plasticity.

References

Akhmanova, A., Steinmetz, M.O., 2015. Control of microtubule organization and dynamics: two ends in the limelight. Nat Rev Mol Cell Biol 16, 711–726. https://doi.org/10.1038/nrm4084

Alberts, B. (Ed.), 2002. Molecular biology of the cell, 4th ed. ed. Garland Science, New York.

Asai, D.J., Koonce, M.P., 2001. The dynein heavy chain: structure, mechanics and evolution. Trends in Cell Biology 11, 196–202. https://doi.org/10.1016/S0962-8924(01)01970-5

Ballabio, A., Bonifacino, J.S., 2020. Lysosomes as dynamic regulators of cell and organismal homeostasis. Nat Rev Mol Cell Biol 21, 101–118. https://doi.org/10.1038/s41580-019-0185-4

Bear, M., Connors, B., Paradiso, M.A., 2020. Neuroscience: Exploring the Brain, Enhanced Edition, 4th ed. ed. Jones & Bartlett Learning, LLC, Burlington.

Benoit, M.P.M.H., Rao, L., Asenjo, A.B., Gennerich, A., Sosa, H., 2024. Cryo-EM unveils kinesin KIF1A's processivity mechanism and the impact of its pathogenic variant P305L. Nat Commun 15, 5530. https://doi.org/10.1038/s41467-024-48720-4

Berth, S.H., Lloyd, T.E., 2023. Disruption of axonal transport in neurodegeneration. Journal of Clinical Investigation 133, e168554. https://doi.org/10.1172/JCI168554

Bingham, D., Jakobs, C.E., Wernert, F., Boroni-Rueda, F., Jullien, N., Schentarra, E.-M., Friedl, K., Da Costa Moura, J., Van Bommel, D.M., Caillol, G., Ogawa, Y., Papandréou, M.-J., Leterrier, C., 2023. Presynapses contain distinct actin nanostructures. Journal of Cell Biology 222, e202208110. https://doi.org/10.1083/jcb.202208110

Bonanomi, D., Benfenati, F., Valtorta, F., 2006. Protein sorting in the synaptic vesicle life cycle. Progress in Neurobiology 80, 177–217. https://doi.org/10.1016/j.pneurobio.2006.09.002

Boncompain, G., Divoux, S., Gareil, N., De Forges, H., Lescure, A., Latreche, L., Mercanti, V., Jollivet, F., Raposo, G., Perez, F., 2012. Synchronization of secretory protein traffic in populations of cells. Nat Methods 9, 493–498. https://doi.org/10.1038/nmeth.1928

Bond, L.M., Tumbarello, D.A., Kendrick-Jones, J., Buss, F., 2013. Small-molecule inhibitors of myosin proteins. Future Med Chem 5, 41–52. https://doi.org/10.4155/fmc.12.185

Bosoi, C.R., Rose, C.F., 2009. Identifying the direct effects of ammonia on the brain. Metab Brain Dis 24, 95–102. https://doi.org/10.1007/s11011-008-9112-7

Brandt, R., Lee, G., 1994. Orientation, assembly, and stability of microtubule bundles induced by a fragment of tau protein. Cell Motil. Cytoskeleton 28, 143–154. https://doi.org/10.1002/cm.970280206

Bray, D., 2001. Cell Movements: from Molecules to Motility 2nd edn (New York: Garland).

Bridgman, P.C., 2004. Myosin-dependent transport in neurons. J. Neurobiol. 58, 164–174. https://doi.org/10.1002/neu.10320

Burke, R.E., O'Malley, K., 2013. Axon degeneration in Parkinson's disease. Experimental Neurology 246, 72–83. https://doi.org/10.1016/j.expneurol.2012.01.011

Burkhardt, J.K., Echeverri, C.J., Nilsson, T., Vallee, R.B., 1997. Overexpression of the Dynamitin (p50) Subunit of the Dynactin Complex Disrupts Dynein-dependent Maintenance of Membrane Organelle Distribution. The Journal of Cell Biology 139, 469–484. https://doi.org/10.1083/jcb.139.2.469

Cai, Q., Pan, P.-Y., Sheng, Z.-H., 2007. Syntabulin–Kinesin-1 Family Member 5B-Mediated Axonal Transport Contributes to Activity-Dependent Presynaptic Assembly. J. Neurosci. 27, 7284–7296. https://doi.org/10.1523/JNEUROSCI.0731-07.2007

Chen, S., Yoo, H., Li, C.H., Park, C., Park, G., Tan, L.Y., Jung, S., Park, H., 2021. Real-time three-dimensional tracking of single vesicles reveals abnormal motion and pools of synaptic vesicles in neurons of Huntington's disease mice. iScience 24, 103181. https://doi.org/10.1016/j.isci.2021.103181

Cheng, X.-T., Zhou, B., Lin, M.-Y., Cai, Q., Sheng, Z.-H., 2015. Axonal autophagosomes use the ride-on service for retrograde transport toward the soma. Autophagy 11, 1434–1436. https://doi.org/10.1080/15548627.2015.1062203

Chenouard, N., Xuan, F., Tsien, R.W., 2020. Synaptic vesicle traffic is supported by transient actin filaments and regulated by PKA and NO. Nat Commun 11, 5318. https://doi.org/10.1038/s41467-020-19120-1

Conde, C., Cáceres, A., 2009. Microtubule assembly, organization and dynamics in axons and dendrites. Nat Rev Neurosci 10, 319–332. https://doi.org/10.1038/nrn2631

Cooper, G.M., 2000. The cell: a molecular approach, 2nd ed. ed. ASM Press, Washington, D.C. Sunderland, Mass.

Cotman, C.W., McGaugh, J.L., 1980. Synaptic Transmission, in: Behavioral Neuroscience. Elsevier, pp. 151–208. https://doi.org/10.1016/B978-0-12-191650-3.50010-6

Coy, D.L., Hancock, W.O., Wagenbach, M., Howard, J., 1999. Kinesin's tail domain is an inhibitory regulator of the motor domain. Nat Cell Biol 1, 288–292. https://doi.org/10.1038/13001

Darcy, K.J., Staras, K., Collinson, L.M., Goda, Y., 2006. Constitutive sharing of recycling synaptic vesicles between presynaptic boutons. Nat Neurosci 9, 315–321. https://doi.org/10.1038/nn1640

De Pace, R., Britt, D.J., Mercurio, J., Foster, A.M., Djavaherian, L., Hoffmann, V., Abebe, D., Bonifacino, J.S., 2020. Synaptic Vesicle Precursors and Lysosomes Are Transported by Different Mechanisms in the Axon of Mammalian Neurons. Cell Rep 31, 107775. https://doi.org/10.1016/j.celrep.2020.107775

Decet, M., Verstreken, P., 2021. Presynaptic Autophagy and the Connection With Neurotransmission. Front Cell Dev Biol 9, 790721. https://doi.org/10.3389/fcell.2021.790721

Deguchi, T., Iwanski, M.K., Schentarra, E.-M., Heidebrecht, C., Schmidt, L., Heck, J., Weihs, T., Schnorrenberg, S., Hoess, P., Liu, S., Chevyreva, V., Noh, K.-M., Kapitein, L.C., Ries, J., 2023. Direct observation of motor protein stepping in living cells using MINFLUX. Science 379, 1010–1015. https://doi.org/10.1126/science.ade2676

Delcroix, J.-D., Valletta, J.S., Wu, C., Hunt, S.J., Kowal, A.S., Mobley, W.C., 2003. NGF Signaling in Sensory Neurons. Neuron 39, 69–84. https://doi.org/10.1016/S0896-6273(03)00397-0

Desai, A., Mitchison, T.J., 1997. MICROTUBULE POLYMERIZATION DYNAMICS. Annu. Rev. Cell Dev. Biol. 13, 83–117. https://doi.org/10.1146/annurev.cellbio.13.1.83

Ding, M., Shen, K., 2008. The role of the ubiquitin proteasome system in synapse remodeling and neurodegenerative diseases. Bioessays 30, 1075–1083. https://doi.org/10.1002/bies.20843

Emperador-Melero, J., Kaeser, P.S., 2020. Assembly of the presynaptic active zone. Current Opinion in Neurobiology 63, 95–103. https://doi.org/10.1016/j.conb.2020.03.008

Fan, J., Griffiths, A.D., Lockhart, A., Cross, R.A., Amos, L.A., 1996. Microtubule Minus Ends can be Labelled with a Phage Display Antibody Specific to Alpha-Tubulin. Journal of Molecular Biology 259, 325–330. https://doi.org/10.1006/jmbi.1996.0322

Farías, G.G., Britt, D.J., Bonifacino, J.S., 2016. Imaging the Polarized Sorting of Proteins from the Golgi Complex in Live Neurons, in: Brown, W.J. (Ed.), The Golgi Complex, Methods in Molecular Biology. Springer New York, New York, NY, pp. 13–30. https://doi.org/10.1007/978-1-4939-6463-5_2

Fletcher, D.A., Theriot, J.A., 2004. An introduction to cell motility for the physical scientist. Phys. Biol. 1, T1–T10. https://doi.org/10.1088/1478-3967/1/1/T01

Forgac, M., 2007. Vacuolar ATPases: rotary proton pumps in physiology and pathophysiology. Nat Rev Mol Cell Biol 8, 917–929. https://doi.org/10.1038/nrm2272

Fornasiero, E.F., Mandad, S., Wildhagen, H., Alevra, M., Rammner, B., Keihani, S., Opazo, F., Urban, I., Ischebeck, T., Sakib, M.S., Fard, M.K., Kirli, K., Centeno, T.P., Vidal, R.O., Rahman, R.-U., Benito, E., Fischer, A., Dennerlein, S., Rehling, P., Feussner, I., Bonn, S., Simons, M., Urlaub, H., Rizzoli, S.O., 2018. Precisely measured protein lifetimes in the mouse brain reveal differences across tissues and subcellular fractions. Nat Commun 9, 4230. https://doi.org/10.1038/s41467-018-06519-0

Forte, L.A., Gramlich, M.W., Klyachko, V.A., 2017. Activity-Dependence of Synaptic Vesicle Dynamics. J Neurosci 37, 10597–10610. https://doi.org/10.1523/JNEUROSCI.0383-17.2017

Ganguly, A., Tang, Y., Wang, L., Ladt, K., Loi, J., Dargent, B., Leterrier, C., Roy, S., 2015. A dynamic formin-dependent deep F-actin network in axons. Journal of Cell Biology 210, 401–417. https://doi.org/10.1083/jcb.201506110

Gennerich, A., Vale, R.D., 2009. Walking the walk: how kinesin and dynein coordinate their steps. Curr Opin Cell Biol 21, 59–67. https://doi.org/10.1016/j.ceb.2008.12.002

Goldberg, A.L., 2003. Protein degradation and protection against misfolded or damaged proteins. Nature 426, 895–899. https://doi.org/10.1038/nature02263

Gong, T.-W.L., Winnicki, R.S., Kohrman, D.C., Lomax, M.I., 1999. A novel mouse kinesin of the UNC-104/KIF1 subfamily encoded by the Kif1b gene. Gene 239, 117–127. https://doi.org/10.1016/S0378-1119(99)00370-4

Goo, M.S., Sancho, L., Slepak, N., Boassa, D., Deerinck, T.J., Ellisman, M.H., Bloodgood, B.L., Patrick, G.N., 2017. Activity-dependent trafficking of lysosomes in dendrites and dendritic spines. Journal of Cell Biology 216, 2499–2513. https://doi.org/10.1083/jcb.201704068

Goodman, B.S., Derr, N.D., Reck-Peterson, S.L., 2012. Engineered, harnessed, and hijacked: synthetic uses for cytoskeletal systems. Trends in Cell Biology 22, 644–652. https://doi.org/10.1016/j.tcb.2012.09.005

Gramlich, M.W., Balseiro-Gómez, S., Tabei, S.M.A., Parkes, M., Yogev, S., 2021. Distinguishing synaptic vesicle precursor navigation of microtubule ends with a single rate constant model. Sci Rep 11, 3444. https://doi.org/10.1038/s41598-021-82836-7

Gramlich, M.W., Klyachko, V.A., 2017. Actin/Myosin-V- and Activity-Dependent Inter-synaptic Vesicle Exchange in Central Neurons. Cell Reports 18, 2096–2104. https://doi.org/10.1016/j.celrep.2017.02.010

Guedes-Dias, P., Holzbaur, E.L.F., 2019. Axonal transport: Driving synaptic function. Science 366, eaaw9997. https://doi.org/10.1126/science.aaw9997

Hall, D.H., Hedgecock, E.M., 1991. Kinesin-related gene unc-104 is required for axonal transport of synaptic vesicles in C. elegans. Cell 65, 837–847. https://doi.org/10.1016/0092-8674(91)90391-B

Hancock, W.O., 2016. The Kinesin-1 Chemomechanical Cycle: Stepping Toward a Consensus. Biophysical Journal 110, 1216–1225. https://doi.org/10.1016/j.bpj.2016.02.025

Hancock, W.O., 2014. Bidirectional cargo transport: moving beyond tug of war. Nat Rev Mol Cell Biol 15, 615–628. https://doi.org/10.1038/nrm3853

Hendricks, A.G., Perlson, E., Ross, J.L., Schroeder, H.W., Tokito, M., Holzbaur, E.L.F., 2010. Motor Coordination via a Tug-of-War Mechanism Drives Bidirectional Vesicle Transport. Current Biology 20, 697–702. https://doi.org/10.1016/j.cub.2010.02.058

Herzog, E., Nadrigny, F., Silm, K., Biesemann, C., Helling, I., Bersot, T., Steffens, H., Schwartzmann, R., Nägerl, U.V., El Mestikawy, S., Rhee, J., Kirchhoff, F., Brose, N., 2011. *In Vivo* Imaging of Intersynaptic Vesicle Exchange Using VGLUT1^{Venus} Knock-In Mice. J. Neurosci. 31, 15544–15559. https://doi.org/10.1523/JNEUROSCI.2073-11.2011

Hirokawa, N., Noda, Y., Tanaka, Y., Niwa, S., 2009. Kinesin superfamily motor proteins and intracellular transport. Nat Rev Mol Cell Biol 10, 682–696. https://doi.org/10.1038/nrm2774

Hoebeke, J., Van Nijen, G., De Brabander, M., 1976. Interaction of oncodazole (R 17934), a new anti-tumoral drug, with rat brain tubulin. Biochemical and Biophysical Research Communications 69, 319–324. https://doi.org/10.1016/0006-291X(76)90524-6

Huang, T.G., Suhan, J., Hackney, D.D., 1994. Drosophila kinesin motor domain extending to amino acid position 392 is dimeric when expressed in Escherichia coli. Journal of Biological Chemistry 269, 16502–16507. https://doi.org/10.1016/S0021-9258(17)34034-6

Hurley, J.H., 2008. ESCRT complexes and the biogenesis of multivesicular bodies. Curr Opin Cell Biol 20, 4–11. https://doi.org/10.1016/j.ceb.2007.12.002

Jähne, S., Mikulasch, F., Heuer, H.G.H., Truckenbrodt, S., Agüi-Gonzalez, P., Grewe, K., Vogts, A., Rizzoli, S.O., Priesemann, V., 2021. Presynaptic activity and protein turnover are correlated at the single-synapse level. Cell Reports 34, 108841. https://doi.org/10.1016/j.celrep.2021.108841

Jaqaman, K., Loerke, D., Mettlen, M., Kuwata, H., Grinstein, S., Schmid, S.L., Danuser, G., 2008. Robust single-particle tracking in live-cell time-lapse sequences. Nat Methods 5, 695–702. https://doi.org/10.1038/nmeth.1237

Jeune-Smith, Y., Hess, H., 2010. Engineering the length distribution of microtubules polymerized in vitro. Soft Matter 6, 1778. https://doi.org/10.1039/b919488f

Joensuu, M., Padmanabhan, P., Durisic, N., Bademosi, A.T.D., Cooper-Williams, E., Morrow, I.C., Harper, C.B., Jung, W., Parton, R.G., Goodhill, G.J., Papadopulos, A., Meunier, F.A., 2016. Subdiffractional tracking of internalized molecules reveals heterogeneous motion states of synaptic vesicles. J Cell Biol 215, 277–292. https://doi.org/10.1083/jcb.201604001

Kamin, D., Lauterbach, M.A., Westphal, V., Keller, J., Schönle, A., Hell, S.W., Rizzoli, S.O., 2010. High- and low-mobility stages in the synaptic vesicle cycle. Biophys J 99, 675–684. https://doi.org/10.1016/j.bpj.2010.04.054

Kapitein, L.C., Hoogenraad, C.C., 2011. Which way to go? Cytoskeletal organization and polarized transport in neurons. Molecular and Cellular Neuroscience 46, 9–20. https://doi.org/10.1016/j.mcn.2010.08.015

Kapitein, L.C., Hoogenraad, C.C., 2015. Building the Neuronal Microtubule Cytoskeleton. Neuron 87, 492–506. https://doi.org/10.1016/j.neuron.2015.05.046

Kawahata, I., Fukunaga, K., 2020. Degradation of Tyrosine Hydroxylase by the Ubiquitin-Proteasome System in the Pathogenesis of Parkinson's Disease and Dopa-Responsive Dystonia. Int J Mol Sci 21, 3779. https://doi.org/10.3390/ijms21113779

Kodera, N., Yamamoto, D., Ishikawa, R., Ando, T., 2010. Video imaging of walking myosin V by high-speed atomic force microscopy. Nature 468, 72–76. https://doi.org/10.1038/nature09450

Komarova, Y., De Groot, C.O., Grigoriev, I., Gouveia, S.M., Munteanu, E.L., Schober, J.M., Honnappa, S., Buey, R.M., Hoogenraad, C.C., Dogterom, M., Borisy, G.G., Steinmetz, M.O., Akhmanova, A., 2009. Mammalian end binding proteins control persistent microtubule growth. J Cell Biol 184, 691–706. https://doi.org/10.1083/jcb.200807179

Korn, E.D., Carlier, M.-F., Pantaloni, D., 1987. Actin Polymerization and ATP Hydrolysis. Science 238, 638–644. https://doi.org/10.1126/science.3672117

Kural, C., Kim, H., Syed, S., Goshima, G., Gelfand, V.I., Selvin, P.R., 2005. Kinesin and Dynein Move a Peroxisome in Vivo: A Tug-of-War or Coordinated Movement? Science 308, 1469–1472. https://doi.org/10.1126/science.1108408

Labbadia, J., Morimoto, R.I., 2015. The biology of proteostasis in aging and disease. Annu Rev Biochem 84, 435–464. https://doi.org/10.1146/annurev-biochem-060614-033955

Lee, J.S., Ho, W.-K., Lee, S.-H., 2012. Actin-dependent rapid recruitment of reluctant synaptic vesicles into a fast-releasing vesicle pool. Proc. Natl. Acad. Sci. U.S.A. 109. https://doi.org/10.1073/pnas.1114072109

Martineau, M., Guzman, R.E., Fahlke, C., Klingauf, J., 2017. VGLUT1 functions as a glutamate/proton exchanger with chloride channel activity in hippocampal glutamatergic synapses. Nat Commun 8, 2279. https://doi.org/10.1038/s41467-017-02367-6

Maschi, D., Klyachko, V.A., 2017. Spatiotemporal Regulation of Synaptic Vesicle Fusion Sites in Central Synapses. Neuron 94, 65-73.e3. https://doi.org/10.1016/j.neuron.2017.03.006

Mason, A., Nicoll, A., Stratford, K., 1991. Synaptic transmission between individual pyramidal neurons of the rat visual cortex in vitro. J Neurosci 11, 72–84. https://doi.org/10.1523/JNEUROSCI.11-01-00072.1991

Müller, M.J.I., Klumpp, S., Lipowsky, R., 2008. Tug-of-war as a cooperative mechanism for bidirectional cargo transport by molecular motors. Proc. Natl. Acad. Sci. U.S.A. 105, 4609–4614. https://doi.org/10.1073/pnas.0706825105

Mullins, R.D., Heuser, J.A., Pollard, T.D., 1998. The interaction of Arp2/3 complex with actin: Nucleation, high affinity pointed end capping, and formation of branching networks of filaments. Proc. Natl. Acad. Sci. U.S.A. 95, 6181–6186. https://doi.org/10.1073/pnas.95.11.6181

Muzio, M.R., Fakoya, A.O., Cascella, M., 2025. Histology, Axon, in: StatPearls. StatPearls Publishing, Treasure Island (FL).

Nakata, T., Terada, S., Hirokawa, N., 1998. Visualization of the dynamics of synaptic vesicle and plasma membrane proteins in living axons. J Cell Biol 140, 659–674. https://doi.org/10.1083/jcb.140.3.659

Niwa, S., Tanaka, Y., Hirokawa, N., 2008. KIF1Bbeta- and KIF1A-mediated axonal transport of presynaptic regulator Rab3 occurs in a GTP-dependent manner through DENN/MADD. Nat Cell Biol 10, 1269–1279. https://doi.org/10.1038/ncb1785

Nogales, E., Grayer Wolf, S., Khan, I.A., Ludueña, R.F., Downing, K.H., 1995. Structure of tubulin at 6.5 Å and location of the taxol-binding site. Nature 375, 424–427. https://doi.org/10.1038/375424a0

Okada, Y., Yamazaki, H., Sekine-Aizawa, Y., Hirokawa, N., 1995. The neuron-specific kinesin superfamily protein KIF1A is a unique monomeric motor for anterograde axonal transport of synaptic vesicle precursors. Cell 81, 769–780. https://doi.org/10.1016/0092-8674(95)90538-3

Okerlund, N.D., Schneider, K., Leal-Ortiz, S., Montenegro-Venegas, C., Kim, S.A., Garner, L.C., Waites, C.L., Gundelfinger, E.D., Reimer, R.J., Garner, C.C., 2017. Bassoon Controls Presynaptic Autophagy through Atg5. Neuron 93, 897-913.e7. https://doi.org/10.1016/j.neuron.2017.01.026

Olmi, S., Angulo-Garcia, D., Imparato, A., Torcini, A., 2017. Exact firing time statistics of neurons driven by discrete inhibitory noise. Sci Rep 7, 1577. https://doi.org/10.1038/s41598-017-01658-8

Padamsey, Z., McGuinness, L., Bardo, S.J., Reinhart, M., Tong, R., Hedegaard, A., Hart, M.L., Emptage, N.J., 2017. Activity-Dependent Exocytosis of Lysosomes Regulates the Structural Plasticity of Dendritic Spines. Neuron 93, 132–146. https://doi.org/10.1016/j.neuron.2016.11.013

Pampaloni, F., Lattanzi, G., Jonáš, A., Surrey, T., Frey, E., Florin, E.-L., 2006. Thermal fluctuations of grafted microtubules provide evidence of a length-dependent persistence length. Proc. Natl. Acad. Sci. U.S.A. 103, 10248–10253. https://doi.org/10.1073/pnas.0603931103

Park, C., Jung, S., Park, H., 2022. Single vesicle tracking for studying synaptic vesicle dynamics in small central synapses. Current Opinion in Neurobiology 76, 102596. https://doi.org/10.1016/j.conb.2022.102596

Park, H., Li, Y., Tsien, R.W., 2012. Influence of Synaptic Vesicle Position on Release Probability and Exocytotic Fusion Mode. Science 335, 1362–1366. https://doi.org/10.1126/science.1216937

Piper, R.C., Luzio, J.P., 2007. Ubiquitin-dependent sorting of integral membrane proteins for degradation in lysosomes. Curr Opin Cell Biol 19, 459–465. https://doi.org/10.1016/j.ceb.2007.07.002

Pohl, C., Dikic, I., 2019. Cellular quality control by the ubiquitin-proteasome system and autophagy. Science 366, 818–822. https://doi.org/10.1126/science.aax3769

Ravikumar, B., Acevedo-Arozena, A., Imarisio, S., Berger, Z., Vacher, C., O'Kane, C.J., Brown, S.D.M., Rubinsztein, D.C., 2005. Dynein mutations impair autophagic clearance of aggregate-prone proteins. Nat Genet 37, 771–776. https://doi.org/10.1038/ng1591

Ray, S., Meyhöfer, E., Milligan, R.A., Howard, J., 1993. Kinesin follows the microtubule's protofilament axis. The Journal of cell biology 121, 1083–1093. https://doi.org/10.1083/jcb.121.5.1083

Reck-Peterson, S.L., Redwine, W.B., Vale, R.D., Carter, A.P., 2018. The cytoplasmic dynein transport machinery and its many cargoes. Nat Rev Mol Cell Biol 19, 382–398. https://doi.org/10.1038/s41580-018-0004-3

Reck-Peterson, S.L., Yildiz, A., Carter, A.P., Gennerich, A., Zhang, N., Vale, R.D., 2006. Single-Molecule Analysis of Dynein Processivity and Stepping Behavior. Cell 126, 335–348. https://doi.org/10.1016/j.cell.2006.05.046

Rizzoli, S.O., 2014. Synaptic vesicle recycling: steps and principles. The EMBO Journal 33, 788–822. https://doi.org/10.1002/embj.201386357

Ropireddy, D., Scorcioni, R., Lasher, B., Buzsáki, G., Ascoli, G.A., 2011. Axonal morphometry of hippocampal pyramidal neurons semi-automatically reconstructed after in vivo labeling in different CA3 locations. Brain Struct Funct 216, 1–15. https://doi.org/10.1007/s00429-010-0291-8

Rosé, S.D., Lejen, T., Casaletti, L., Larson, R.E., Pene, T.D., Trifaró, J., 2003. Myosins II and V in chromaffin cells: myosin V is a chromaffin vesicle molecular motor involved in secretion. Journal of Neurochemistry 85, 287–298. https://doi.org/10.1046/j.1471-4159.2003.01649.x

Sakaba, T., 2008. Two Ca2+-Dependent Steps Controlling Synaptic Vesicle Fusion and Replenishment at the Cerebellar Basket Cell Terminal. Neuron 57, 406–419. https://doi.org/10.1016/j.neuron.2007.11.029

Sakamoto, H., Ariyoshi, T., Kimpara, N., Sugao, K., Taiko, I., Takikawa, K., Asanuma, D., Namiki, S., Hirose, K., 2018. Synaptic weight set by Munc13-1 supramolecular assemblies. Nat Neurosci 21, 41–49. https://doi.org/10.1038/s41593-017-0041-9

Sakamoto, T., Amitani, I., Yokota, E., Ando, T., 2000. Direct Observation of Processive Movement by Individual Myosin V Molecules. Biochemical and Biophysical Research Communications 272, 586–590. https://doi.org/10.1006/bbrc.2000.2819

Sakamoto, T., Wang, F., Schmitz, S., Xu, Y., Xu, Q., Molloy, J.E., Veigel, C., Sellers, J.R., 2003. Neck Length and Processivity of Myosin V. Journal of Biological Chemistry 278, 29201–29207. https://doi.org/10.1074/jbc.M303662200

Samson, F., Donoso, J.A., Heller-Bettinger, I., Watson, D., Himes, R.H., 1979. Nocodazole action on tubulin assembly, axonal ultrastructure and fast axoplasmic transport. J Pharmacol Exp Ther 208, 411–417.

Seog, D.-H., Lee, D.-H., Lee, S.-K., 2004. Molecular motor proteins of the kinesin superfamily proteins (KIFs): structure, cargo and disease. J Korean Med Sci 19, 1–7. https://doi.org/10.3346/jkms.2004.19.1.1

Sheehan, P., Zhu, M., Beskow, A., Vollmer, C., Waites, C.L., 2016. Activity-Dependent Degradation of Synaptic Vesicle Proteins Requires Rab35 and the ESCRT Pathway. J Neurosci 36, 8668–8686. https://doi.org/10.1523/JNEUROSCI.0725-16.2016

Soykan, T., Maritzen, T., Haucke, V., 2016. Modes and mechanisms of synaptic vesicle recycling. Current Opinion in Neurobiology 39, 17–23. https://doi.org/10.1016/j.conb.2016.03.005

Staras, K., Branco, T., Burden, J.J., Pozo, K., Darcy, K., Marra, V., Ratnayaka, A., Goda, Y., 2010. A Vesicle Superpool Spans Multiple Presynaptic Terminals in Hippocampal Neurons. Neuron 66, 37–44. https://doi.org/10.1016/j.neuron.2010.03.020

Stepanova, T., Slemmer, J., Hoogenraad, C.C., Lansbergen, G., Dortland, B., De Zeeuw, C.I., Grosveld, F., van Cappellen, G., Akhmanova, A., Galjart, N., 2003. Visualization of microtubule growth in cultured neurons via the use of EB3-GFP (end-binding protein 3-green fluorescent protein). J Neurosci 23, 2655–2664. https://doi.org/10.1523/JNEUROSCI.23-07-02655.2003

Südhof, T.C., 2012. The Presynaptic Active Zone. Neuron 75, 11–25. https://doi.org/10.1016/j.neuron.2012.06.012

Sudhof, T.C., 2004. The synaptic vesicle cycle. Annu Rev Neurosci 27, 509–547. https://doi.org/10.1146/annurev.neuro.26.041002.131412

Takamori, S., Holt, M., Stenius, K., Lemke, E.A., Grønborg, M., Riedel, D., Urlaub, H., Schenck, S., Brügger, B., Ringler, P., Müller, S.A., Rammner, B., Gräter, F., Hub, J.S., De Groot, B.L., Mieskes, G., Moriyama, Y., Klingauf, J., Grubmüller, H., Heuser, J., Wieland, F., Jahn, R., 2006. Molecular anatomy of a trafficking organelle. Cell 127, 831–846. https://doi.org/10.1016/j.cell.2006.10.030

Teramae, J., Tsubo, Y., Fukai, T., 2012. Optimal spike-based communication in excitable networks with strong-sparse and weak-dense links. Sci Rep 2, 485. https://doi.org/10.1038/srep00485

tom Dieck, S., Sanmartí-Vila, L., Langnaese, K., Richter, K., Kindler, S., Soyke, A., Wex, H., Smalla, K.H., Kämpf, U., Fränzer, J.T., Stumm, M., Garner, C.C., Gundelfinger, E.D., 1998. Bassoon, a novel zinc-finger CAG/glutamine-repeat protein selectively localized at the active zone of presynaptic nerve terminals. J Cell Biol 142, 499–509. https://doi.org/10.1083/jcb.142.2.499

Truckenbrodt, S., Viplav, A., Jähne, S., Vogts, A., Denker, A., Wildhagen, H., Fornasiero, E.F., Rizzoli, S.O., 2018. Newly produced synaptic vesicle proteins are preferentially used in synaptic transmission. EMBO J 37, e98044. https://doi.org/10.15252/embj.201798044

Turegano-Lopez, M., Santuy, A., DeFelipe, J., Merchan-Perez, A., 2020. Size, Shape, and Distribution of Multivesicular Bodies in the Juvenile Rat Somatosensory Cortex: A 3D Electron Microscopy Study. Cereb Cortex 30, 1887–1901. https://doi.org/10.1093/cercor/bhz211

Ulferts, S., Prajapati, B., Grosse, R., Vartiainen, M.K., 2021. Emerging Properties and Functions of Actin and Actin Filaments Inside the Nucleus. Cold Spring Harb Perspect Biol 13, a040121. https://doi.org/10.1101/cshperspect.a040121

Vale, R.D., 2003. The molecular motor toolbox for intracellular transport. Cell 112, 467–480. https://doi.org/10.1016/s0092-8674(03)00111-9

Vallee, R.B., Williams, J.C., Varma, D., Barnhart, L.E., 2004. Dynein: An ancient motor protein involved in multiple modes of transport. J Neurobiol 58, 189–200. https://doi.org/10.1002/neu.10314

Vasquez, R.J., Howell, B., Yvon, A.M., Wadsworth, P., Cassimeris, L., 1997. Nanomolar concentrations of nocodazole alter microtubule dynamic instability in vivo and in vitro. MBoC 8, 973–985. https://doi.org/10.1091/mbc.8.6.973

Verstreken, P., Koh, T.-W., Schulze, K.L., Zhai, R.G., Hiesinger, P.R., Zhou, Y., Mehta, S.Q., Cao, Y., Roos, J., Bellen, H.J., 2003. Synaptojanin is recruited by endophilin to promote synaptic vesicle uncoating. Neuron 40, 733–748. https://doi.org/10.1016/s0896-6273(03)00644-5

Watson, E.T., Pauers, M.M., Seibert, M.J., Vevea, J.D., Chapman, E.R., 2023. Synaptic vesicle proteins are selectively delivered to axons in mammalian neurons. eLife 12, e82568. https://doi.org/10.7554/eLife.82568

Wegner, A., 1976. Head to tail polymerization of actin. Journal of Molecular Biology 108, 139–150. https://doi.org/10.1016/S0022-2836(76)80100-3

Westphal, V., Rizzoli, S.O., Lauterbach, M.A., Kamin, D., Jahn, R., Hell, S.W., 2008. Video-rate far-field optical nanoscopy dissects synaptic vesicle movement. Science 320, 246–249. https://doi.org/10.1126/science.1154228

Yano, H., Chao, M.V., 2004. Mechanisms of neurotrophin receptor vesicular transport. J. Neurobiol. 58, 244–257. https://doi.org/10.1002/neu.10321

Yerbury, J.J., Ooi, L., Dillin, A., Saunders, D.N., Hatters, D.M., Beart, P.M., Cashman, N.R., Wilson, M.R., Ecroyd, H., 2016. Walking the tightrope: proteostasis and neurodegenerative disease. J Neurochem 137, 489–505. https://doi.org/10.1111/jnc.13575

Yildiz, A., Forkey, J.N., McKinney, S.A., Ha, T., Goldman, Y.E., Selvin, P.R., 2003. Myosin V Walks Hand-Over-Hand: Single Fluorophore Imaging with 1.5-nm Localization. Science 300, 2061–2065. https://doi.org/10.1126/science.1084398

Yogev, S., Cooper, R., Fetter, R., Horowitz, M., Shen, K., 2016. Microtubule Organization Determines Axonal Transport Dynamics. Neuron 92, 449–460. https://doi.org/10.1016/j.neuron.2016.09.036

Zhao, C., Takita, J., Tanaka, Y., Setou, M., Nakagawa, T., Takeda, S., Yang, H.W., Terada, S., Nakata, T., Takei, Y., Saito, M., Tsuji, S., Hayashi, Y., Hirokawa, N., 2001. Charcot-Marie-Tooth disease type 2A caused by mutation in a microtubule motor KIF1Bbeta. Cell 105, 587–597. https://doi.org/10.1016/s0092-8674(01)00363-4

Zhao, L., Zhao, J., Zhong, K., Tong, A., Jia, D., 2022. Targeted protein degradation: mechanisms, strategies and application. Signal Transduct Target Ther 7, 113. https://doi.org/10.1038/s41392-022-00966-4

Appendix

Appendix 1: Media Preparation

A1.1 Fetal Calf Serum

Volume	Name
175 mL	Minimum Essential Medium (MEM)
20 mL	Fetal Bovine Serum
4 mL	1 M glucose in MEM (sterifiltered)
1 mL	Penicillin/Streptomycin
1 mL	N2 Supplement

Prepare this media in 250 mL sterifilter container, in cell culture hood. Make sure everything is ethanol clean first. Use vacuum tube to filter media through membrane. Label, parafilm cap, and place in 4C fridge in cell culture room

A1.2 Neuronal Growth Medium

Volume	Name
175 mL	Minimum Essential Medium (MEM)
20 mL	Horse Serum
4 mL	1 M glucose in MEM (sterifiltered)
1 mL	Penicillin/Streptomycin
2 mL	N2 Supplement
2 mL	Sodium Pyruvate
4.375 mL	HEPES

Prepare this media in 250 mL sterifilter container, in cell culture hood. Make sure everything is ethanol clean first. Use vacuum tube to filter media through membrane. Label, parafilm cap, and place in 4C fridge in cell culture room

A1.3 Enhanced Neurobasal Medium

Volume	Name
154 mL	Neurobasal Media
4 mL	B27 Supplement
500 uL	Glutamax-1
2 mL	Penicillin/Streptomycin

Prepare this media in 250 mL sterifilter container, in cell culture hood. Make sure everything is ethanol clean first. Use vacuum tube to filter media through membrane. Label, parafilm cap, and place in 4C fridge in cell culture room

A1.4 Digestion Medium

Volume	Name
5 mL	EBSS
100 uL	Papain Enzyme

Prepare before rat dissection begins, and make sure it is warm! Use syringe filter to sterilize solution before using.

A1.5 Plate Substrate Coating media

Material	Quantity (ml)	Stock concentration	Quantity (mg)	Final concentration (mg/ml)	mass per plate (ug)
Acetic acid	14	17 mM			
Rat tail collagen	6	5 mg/mL	30	1.401869159	0.24953271
poly-D-lysine	1.1	0.1 mg/mL	0.11	0.005140187	0.000914953
laminin	0.3	1 mg/mL	0.3	0.014018692	0.002495327
total volume	21.4				
volume per plate	0.178				
Number of plates	120				

Prepare plate substrate coating during plate coating protocol. Prepare enough to make 180 uL per plate to be coated. Stock concentrations of materials (particularly the rat tail collagen) must be accounted for each time new materials are made and careful care taken to ensure that final concentrations of laminin and poly-D-lysine and final mass per plate of rat tail collagen are maintained close to these values.

Appendix 2: Cell Culturing Protocols

A2.1 Plate Preparation

A2.1.1 Plate Etching

You must wear goggles, lab coat, and large rubber gloves when working with acids

1. Place coverslips into a large beaker and cover with nitric acid (clean).
    a. Cover beaker with parafilm.
    b. Sonicate for 1 hour, swirling intermittently.
    c. *When done, dilute acid into 2.5 gal water. Pour diluted solution into sink and let water run for several minutes.*
2. Wash 3 times with ddH_20
3. Replace ddH_20 with Hydrochloric Acid (HCl) USE CAUTION!!!
    a. Cover beaker with parafilm
    b. Sonicate for 1 hour, swirling intermittently.
    c. *When done, dilute acid into 2.5 gal water. Pour diluted solution into sink and let water run for several minutes.*
4. Wash 10 times with ddH_20
5. Rinse 2 times with 100% Ethanol.
6. Store in a beaker in 4C refrigerator in 100% Ethanol.

A2.1.2 Plate Coating

Make a large quantity (12+ 12-well plate containers), which is good for up to two months

1. Take a set of 12-well plate containers (~12 containers) and put in cell culture hood
2. Take biologically clean coverslips (plate etching protocol above) and put one into each well
    a. Place only one per well. When you take them out of the storage bath multiple slips stick together. Take two forceps and pull them apart
    b. Place each coverslip against the wall of the well so that both sides can dry evenly
3. Let dry 1 hour (up to overnight)
4. Put plates flat on bottom by shaking the well
5. Prepare plate substrate coating
6. Add 180 µL of Substrate Coating to center of each plate
    a. Use a plastic pipette tip
    b. Touch tip to surface to ensure even coat
    c. NOTE: Once coating has been applied, ensure plates are not exposed to UV light except as directed in step 14 below. Cover with aluminum foil if BSL-2 cabinet needs to be closed.
7. Incubate 1 hour
    a. Leave lids slightly ajar to allow for better drying
8. Aspirate excess using autoclaved glass pipette (the ones without cotton) and hood vacuum.
9. Let dry 1 hour
10. Wash with Biologically clean ddH20
    a. Note: add water to the side of the well to avoid washing away the coating on the plates
11. Aspirate excess water
12. Let Dry at least 1 hour
13. Repeat (10)-(12) 3 times
    a. Let dry overnight after final wash
14. Expose dry plates to UV light in culture hood for 10-12 min
    a. Remove lids and place upside down next to plates in culture hood
    b. Close sash and turn on UV light
15. Place prepared dried well plates in plastic ziplock bags (2 per bag) and store in culture room. In a dark place.

A2.2 Dissection Day

Prepare all dishes, media, and materials before starting the rat dissections!

A2.2.1 Preparations

Prepare Digestion media and place in water bath

Prepare dishes with cold EBSS (~4 dishes)

Prepare an ice bucket (spray with Ethanol)

Put all media needed to be warm for dissection in 37C bath

Prepare all tools for dissection and place in culture hood

Place Microscope inside of BSL2 hood

Be sure to wear proper PPE:

Face Mask

Hair Bonnet

Clothes Cover

Gloves

A2.2.2 Euthanasia

Rat euthanized according to approved CO_2 asphyxiation protocol. Dam is then decapitated and pups removed through incision in abdomen and placed onto ice.

When finished with rat, clean up immediately, and quickly, before going to the next steps (Bottom of -20C freezer in front of room).

Euthanasia protocols should always be developed and implemented carefully with assistance and oversight from trained vivarium and veterinary staff and the Institutional Animal Care and Use Committee (IACUC) and carried out by trained individuals.

A2.2.3 Dissection

1. Take ice bucket, with pups obtained from mother and stored on ice, and put in cell culture hood
2. One-by-one decapitate the mice and remove the brains
    a. With scissors, cut off heads at the base of the skull
    b. With curved forceps, grasp the skull, by puncturing the nose
    c. Carefully cut away the skin layer from base of skull and peel off
    d. Carefully cut the skull parallel, from base to ocular region.
    e. Cut two lines transverse to previous cut, on either end.
    f. If possible carefully cut away one of the skull flaps
    g. Through the cavity the brain can easily be seen.
    h. Carefully tease out the brain using the spatula tool.
    i. Try not to damage or tear the brain

1. ii. Scoop around and underneath the brain for cleanest removal

2. iii. The brain is not tethered to anything and should easily fall out
    j. Place into dish with cold EBSS
3. With all mice decapitated separate the two cortical lobes of each brain and place in a
3. new dish with EBSS
    a. Place brain with hypothalamus facing up and use spatula and sharp tweezers to
4. separate lobes
    b. With lobes separated, use curved spatula end to scoop up each lobe.
5. Stabilize with sharp tweezers
    c. Transfer to new dish
4. The next steps require use of the microscope to view the necessary details, raise the sash high enough to put your head inside (be sure all PPE is in place to maintain sample cleanliness)
5. Place a new dish with dissection media on the scope
6. Transfer a single lobe to the dish on the scope
7. Remove the meninges from the lobe (blood layer that surrounds brain)
    a. Start on sliced side of the hemisphere
6. Using two forceps (must be in good condition) pull apart from the sides along the edges
7. Flip over lobe, hold meninges near the olfactory bulb, and pull the meninges over the opposite (rounded) end.
    b. Gently tear away the meninges from the remaining tether at the hippocampus

8. The hippocampus should now be visible as a slightly darker banana shaped area (outline in image below)

Figure A1: View of interior of rat brain lobe, with hippocampus marked in right image

1. Remove the Dentate gyrus from the hippocampus
2. Carefully cut out the hippocampus

3. Avoid any extra tissue around the hippocampus. This will include other neurons besides CA3-CA1 cells. Below is an image of two hippocampi freshly extracted (left) with excess tissue still to be removed. And another (right) after excess tissue has been cleared away.

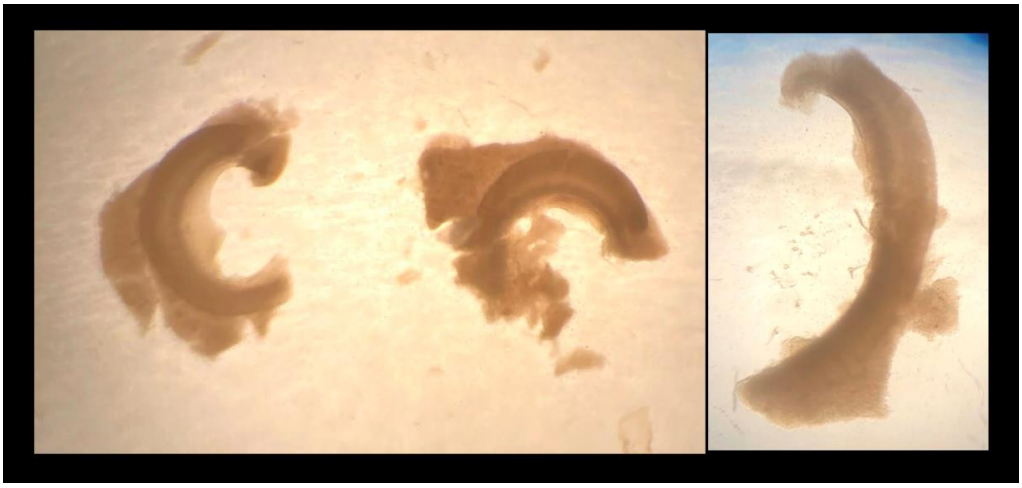

Figure A2: Magnified images of extracted hippocampi

4. Transfer hippocampi to another fresh dish of cold dissection solution
5. Clean off excess material from hippocampus by holding down either end with one forceps (use the duller one for this part), and carefully trim the excess material with the sharper forceps.
    c. Carefully cut each hippocampus into 6-8 pieces with sharp forceps
6. At this point the digestion media should be warm. Take out and sterile filter media into a 15 mL conical tube.
7. Using a pre-sterilized glass pipette, transfer hippocampi to a 15 mL conical tube with digestion media, and incubate for 30 min. in cell culture incubator.
    d. Every 10 min gently agitate the solution by tapping conical
8. Wash digested hippocampi with NEU (Neutralizes Digestion Media)
    a. Make three solutions of NEU in falcon tubes
        i. 2 with 2 mL and 1 with 1 mL
8. Transfer hippocampi to first falcon tube with NEU (transfer as little digestion media as possible) using glass pipette
    b. Tap solution to wash hippocampi and then wait for them to settle to bottom
    c. Transfer hippocampi to second falcon tube with 2 mL NEU
    d. Tap solution again, and then wait for them to settle
    e. Finally, transfer to falcon tube with 1mL NEU
9. Shear hippocampi

    a. Method 1: Using sharpened glass pipettes, pipette hippocampi up and down until no large pieces can be seen
10. Clean cells with a cell strainer
    a. Put a 70 μm cell strainer (Falcon 2350) on a 50 mL conical tube
    b. pour in cell suspension
11. Prepare Astrocyte colonies for next preparation:

A2.2.4 Neuron Plating

1. Count the cell density
    a. Take the cell counter slide and clean thoroughly!
    b. Put small amount (~50 μL) of media on either side of the counter pillars
    c. Put coverslip on top
    d. Place 20 μL of sheared/strained cell into cell counter via capillary effect
    e. Count number of cells in 12-grid window
    f. Multiply # of cells by 104 and that is the density (number per μL).
2. Plate desired cell density (10K cells/mL provided best results for most experiments)

A2.2.5 Astrocyte Culturing

1. Spin down remainder of strained cells in centrifuge (@ 3-4 speed for 4 min)
2. Dump out supernatant
3. Add 5 mL of FCS and re-suspend
4. Put into falcon blue capped flask container

A2.2.6 Cell Culture Log

After astrocytes are placed in cell culturing flasks, a cell log can be created for each flask. The cell culture log can be used to keep track of all necessary media changes as well as the date of creation for each media. This allows a single location for all information that is needed throughout the cell culturing process. If at any point cell health deteriorates it is easy to identify when changes were made (e.g. the you used a new batch of FCS on the 11 DIV media change and noticed cell health deteriorate after that, so you may wat to remake FCS for the next batch of astrocytes)

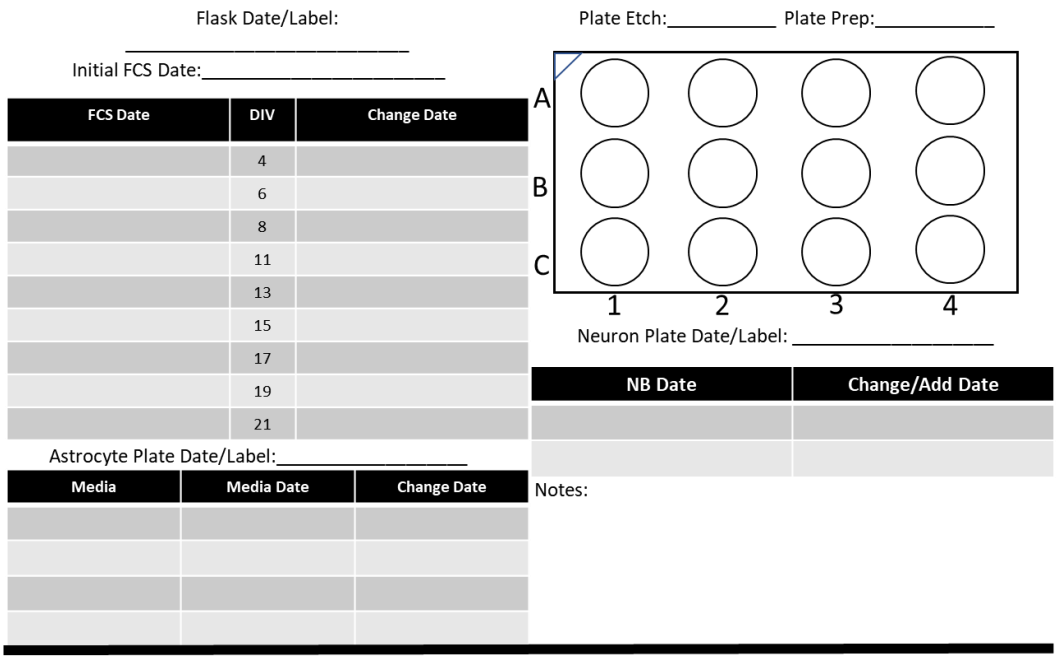

The cell culture log can be updated once astrocytes are plated (see below) and when neurons are plated. This can then be pasted into a lab notebook when the cells are used for imaging, allowing all relevant information to be preserved alongside other information about the experiments performed and kept in a safe place to be referenced during analysis.

A2.3 Astrocyte Plating

Take cultured Astocytes in flask from incubator and put in BSL-2 Cabinet

1. Aspirate away media
2. Add 5 mL of Trypsin media
    a. Mix up and down in pipette tube
3. Incubate 3 min in Cell Culture incubator
4. Check that cells are floating using microscope in culture room
5. If not completely floating, tap container lightly on microscope and check again
    a. Add 5 mL of FBS to Astrocytes
6. Pipette up and down to mix
7. Transfer mix to 15 mL conical tube
8. Centrifuge on high for ~3-4 min
9. Aspirate away supernatant
10. Add 12 mL of FCS (1 mL per well to be plated)
    a. Pipette up and down to re-suspend pellet
11. Add mix to 50 mL conical
    a. Vortex briefly ~10 sec
12. Add 1 mL of mixture to each well in 12-well plate

13. Label plated container and place in Cell Culture incubator

Appendix 3: Experimental Protocols

1. Make Imaging Media (Beginning of week, good for 2 experiments)
    1.1. Fill Beaker with 1L ddH20
    1.2. Add the following, stirring with stir bar until dissolved:

Material	Quantity
NaCl	7.31 g
KCl	0.19 g
HEPES	2.38 g

    1.3. Adjust pH to 7.25 with NaOH pellets
        1.3.1. Calibrate pH meter before each use
        1.3.2. Measure pH of solution (Should be around 5.5)
        1.3.3. Add NaOH until you reach desired pH
            1.3.3.1. Note: Wait for pellets to dissolve between measurements, you can usually add 1 pellet the first time and then proceed with fourths or eighths of pellets until you reach the final pH.
    1.4. Transfer to storage container, seal top (parafilm or screw on cap) store in 20C fridge
2. Prepare Individual Media (Day of experiments)
    2.1. Take 500 mL of imaging solution and add to 1L beaker
    2.2. Add to solution and allow to mix:

Name	Final Concentration	In 500 mL
Glucose	15 mM	1.39 g
CNQX	5 μM	50 μL

    2.3. Separate into 2 buffers:
        2.3.1. 100 mL into graduated cylinder (High Ca2+)
        2.3.2. 400 mL stays in beaker (Wash)
        2.3.3. Add 100 μL 2 M CaCl2 stock solution to Wash
        2.3.4. Add 100 μL 2 M CaCl2 stock solution to High Ca2+
        2.3.5. Add 100 μL 1 M MgCl2 stock solution to wash
        2.3.6. Add 100 μL 1 M MgCl2 stock solution to High Ca2+
        2.3.7. Mix solutions
            2.3.7.1. Use stir bar to continue mixing beaker
            2.3.7.2. Cover top of graduated cylinder with parafilm and turn upside down a few times to mix
    2.4. Separate additional media for dye
        2.4.1. 10 mL from High Ca2+ for SV dye

2.4.1.1. Add to small foil covered beaker
2.4.1.2. Add 10 μL SGC5 stock solution
2.4.1.3. Cover with parafilm, turn to mix, place in microscope box
2.4.2. 10 mL for Mitoview/CK-666
2.4.2.1. Add to 15 mL conical tube
2.4.2.2. Add desired quantities of dyes/drugs
2.4.2.3. Vortex to mix, place in microscope box

3. Prepare Microscope for experiments
3.1.Media – You should now have warming up:
3.1.1. Any dyes you will use
3.1.2. 2x 15 mL conical tubes of wash used as needed to help wash away dye while profusion system runs
3.1.3. Small petri dish filled with wash used for transferring samples
3.1.4. Immersion oil for microscope lens
3.2.Add Media to Profusion system
3.2.1. Fill first channel up to top with wash
3.2.2. Fill second channel up to top with High Ca2+
3.3.Turn on Equipment
3.3.1. Flip switch on light source nearest the microscope
3.3.2. Turn on Microscope
3.3.3. Turn on Camera
3.3.4. Turn on Pulse generator
3.3.5. Turn on profusion system controller
3.3.6. Turn on Profusion system warmer
3.3.7. Turn on Master-9
3.3.8. Finish turning on light source by flipping switch on the door side (once you can hear fan turning on)
3.4.Log into computer
3.4.1. Check storage space available
3.4.1.1. Estimate required storage space and make sure you have it
3.4.1.1.1. Tracking movies take 700 frames and take up around 5.7 GB
3.4.1.1.2. Synapse identification movies take 500 frames and 4.1 GB
3.4.1.2. Create a file folder for the days experiment
3.4.1.2.1. Name with the date, example, April 12th 2021 -> 04122021
3.4.2. Open necessary programs
3.4.2.1. HC Image Live
3.4.2.2. Nikon microscope software

3.4.2.3. Master-9 control panel
3.4.2.4. Note: HC Image Live must be opened first to allow proper communication between the computer and the camera
3.4.3. Ensure that programs properly control equipment
3.4.3.1. Turn on “live capture” on HC image live, you should see static if you aren’t looking at anything and the auto-contrast is on
3.4.3.2. Make sure Nikon software can turn lights on and off on the microscope
3.4.3.3. Click through preset paradigms on Master-9 to make sure that they are correctly set (There have been a few instances of these having been erased)

4. Final preparations
4.1.1. Make sure profusion system is working
4.1.1.1. Turn on each channel manually to run ~10 mL through each
4.1.1.2. Set drainage channel into temporary waste beaker
4.1.1.3. Run Channel 2 first, then Channel 1
4.1.1.3.1. This is because channel 1 will run first after loading dye, so you want it to be the last thing in the tubing before you start
4.1.2. Check sample quality under Leica microscope
4.1.2.1. Make note of poor-quality samples that you want to avoid or high-quality samples you want to be sure to image

5. Run a sample
5.1.Transfer sample to microscope
5.1.1. Move transfer dish into sterile hood (spray with ethanol first)
5.1.1.1. Dish should contain:
5.1.1.1.1. Petri dish
5.1.1.1.2. Straight tweezers
5.1.1.1.3. Bent tweezers
5.1.2. Retrieve samples from incubator
5.1.2.1. Minimize time spent outside of incubator to preserve health of later samples
5.1.3. Transfer sample from well to dish
5.1.3.1. Use bent tip tweezers to lift plate up
5.1.3.2. Use straight tweezers to grab plate and add to petri dish

5.1.3.3. Be sure to only grab top plate, if there are more than one in the well
5.1.3.4. Mark that you removed sample on top plate
5.1.4. Return remaining samples to incubator
5.1.5. Move transfer dish to microscope box
5.1.6. Load sample into sample holder
5.1.6.1. Use tweezers to move plate from petri dish to sample holder
5.1.6.2. Place rubber O-ring around the sample
5.1.6.3. Use plastic pippette to fill O-ring with wash
5.1.6.4. Place top plate of sample holder and begin to screw on
5.1.6.4.1. Screw carefully, they don't need to be very tight. SAMPLES BREAK EASILY
5.1.6.4.2. Screw in moving to alternate corners to evenly apply pressure
5.1.6.5. Fill sample holder the rest of the way up with wash solution
5.1.7. Add immersion oil to top of objective lens
5.1.7.1. Remove lid and pull up dropper
5.1.7.2. Hover over lens until a single drop of oil drips onto the lens
5.1.8. Wipe bottom of sample plate with kimwipe
5.1.8.1. Helps keep your lens clear of errant cells
5.1.8.2. If wipe absorbs too much fluid it could indicate leak in sample holder, plate could be cracked or sample holder may not be tightened enough
5.1.9. Place sample holder into base plate
5.1.9.1. Fit is tight, so usually you need to do one side (right) and then snap in the other side after
5.1.10. Insert profusion system needle to hole on back left side
5.1.11. Add temperature probe to hole near front
5.1.11.1. Be sure it rests within the fluid for accurate measurement
5.1.12. Place metal prongs to keep sample holder secure
5.1.13. Ensure that vacuum tubing is fully inserted
5.2.Find spot to image
5.2.1. Bring objective up until the image from the microscope is clear

5.2.1.1. If you have already run a sample and pushed escape, then pushing escape will bring it back to where it was

5.2.1.2. Otherwise you'll have to use the wheel on the side to move it up, potentially for a while, until it comes into focus

5.2.2. Move laterally until you find a "good spot"

5.2.2.1. Be careful or moving too much, if you get near the edge of the sample holder it can push the sample holder up and out of focus.

5.2.2.2. Look for spots where you can see several clear processes, hopefully without too many cell bodies in the frame as well

5.2.2.3. Once you have an idea of where you'd like to be, press the "PFS" button on the zoom wheel

5.2.2.3.1. If it successfully activates the PFS indicator on the front of the microscope will have a solid green light glowing

5.2.3. Take a prestain image

5.2.3.1.

5.3.Load Single Dye

5.3.1. With a plastic pippette, remove wash that is currently in the sample holder

5.3.2. Pick up around 1 mL of dye and drop it into the well to replace the wash

5.3.3. Select paradigm 6 on the master-9 control panel

5.3.4. Press the green button next to "8" to trigger the paradigm

5.3.5. When profusion system starts (Green light turns on on Master-9 and Profusion control system) open valve for vacuum system

5.3.6. When all lights are off, close vacuum valve

5.4.Take Single Movie

5.4.1. Make sure image is in focus

5.4.1.1. Turn on live imaging on HC image live

5.4.1.2. Turn on blue florescent light

5.4.1.3. Adjust contrast and focus

5.4.1.3.1. You should see many white dots against a very black background

5.4.1.3.2. Adjust focus until the dots are clear, for at least some portion of the image

5.4.1.3.3. Do this quickly so that the sample doesn't photobleach

5.4.2. Turn off Fluorescent light
5.4.3. Set camera for external triggering
5.4.4. Select paradigm 7 on Master-9
5.4.5. Turn on fluorescent light
5.4.6. Press “5” to trigger
5.4.7. When image collection is finished, press “Stop” and “Abort” to save the image

5.5.Load Bulk Dye

5.5.1. With a plastic pipette, remove wash that is currently in the sample holder
5.5.2. Pick up around 1 mL of dye and drop it into the well to replace the wash
5.5.3. Select paradigm 8 on the master-9 control panel
5.5.4. Press the green button next to “8” to trigger the paradigm
5.5.5. When profusion system starts (Green light turns on on Master-9 and Profusion control system) open valve for vacuum system
5.5.6. When all lights are off, close vacuum valve

5.6.Take Bulk Movie

5.6.1. Make sure image is in focus
5.6.1.1. Turn on live imaging on HC image live
5.6.1.2. Turn on blue florescent light
5.6.1.3. Adjust contrast and focus
5.6.1.3.1. You should see many white dots against a very black background
5.6.1.3.2. Adjust focus until the dots are clear, for at least some portion of the image
5.6.1.3.3. Do this quickly so that the sample doesn’t photobleach
5.6.2. Turn off Fluorescent light
5.6.3. Set camera for external triggering
5.6.4. Select paradigm 9 on Master-9
5.6.5. Turn on fluorescent light
5.6.6. Press “5” to trigger
5.6.7. When image collection is finished, press “Stop” and “Abort” to save the image

5.7.Remove sample

5.7.1. Press “Escape” on microscope
5.7.2. Remove fluid from well using pipette
5.7.3. Pry sample holder out of base plate
5.7.3.1. Use screwdriver to lift under the notched side of the sample holder

5.7.4. Unscrew sample plate
5.7.5. Move O-ring out of the way
5.7.6. Pop glass coverslip out of bottom plate and into sharps container near microscope

5.8. Repeat all of 5 until you run out of samples or media for doing experiments

6. Clean up
   6.1. Flush Profusion system
   6.2. Rinse glassware
   6.3. Power off equipment
   6.4. Clean lens
   6.5. Final checks

A3.1 Master-9 Paradigms

Referenced in the experiment protocol above mention running master 9 paradigms to control the camera and profusion systems. The relevant paradigms are described below.

A3.1.1 Single Vesicle Loading

Paradigm 6 is designed to load SGC5 dye for optimal imaging of single SVs. It begins with a paired pulse of electrical stimulation delivered to the sample by the function generator. The system then waits 60s for dye loaded SVs to endocytose. Following the delay, the profusion system is triggered for the Wash media to flow into the sample chamber. Wash flows for 3 minutes, followed by 1 min of the High Ca2+ media before sample is imaged.

A3.1.2 Single Vesicle Imaging

Paradigm 7 sends the proper signals to the camera for imaging. When triggered, it sends 700 pulses to the external control point on the camera, one every 100ms, initiating collection of the 700 frame movie at 10 frames per second.

A3.1.3 Bulk Vesicle Loading

Bulk Vesicle Loading controlled by paradigm 8 on the master 9 proceeds similar to single vesicle loading except for parameters which are modified to ensure more dye loading, enabling imaging bulk SV behavior in presynapses rather than individual SV motion. This includes sending 200 action potential simulating stimulations instead of 2 and waiting longer (3 min) for dye uptake before beginning the wash step.

A3.1.4 Bulk Vesicle Imaging

The paradigm for bulk vesicle imaging is similar to the paradigm for single vesicle imaging, with the change from 500 total frames from 700 total frames (still at 10 frames per second). Additionally, starting at 10s, action potential stimulation begins (500 AP at 50 Hz) to induce bulk SV exocytosis. The number of action potentials

and the frequency can be tuned to obtain optimal exocytosis for presynapse identification (Described below)

Electrical stimulation can be supplemented or replaced by chemical stimulation (e.g. addition of ammonium hydroxide) to better elicit a response from the neurons and better record presynaptic activity.

Appendix 4: Analysis Protocols

A4.1 SV Track analysis

A4.1.1 uTrack

Batch running of single vesicle movies is possible using the scriptDetectGeneral_b.m and runTrack_Mason.m scripts.

Modify information within the scriptDetectGeneral.m script to correctly run the uTrack program on each desired video.

Likewise, modifications are needed for each desired video in the runTrack script.

Once the desired parameters are set in these two files. Run the runTrack script which will, in turn, run the scriptDetectGeneral script to first run the detection step for each video and then complete the tracking setup and output the track data into the files set in the runTrack script.

Tracks data can then be sorted through and relevant tracks analyzed based on position or other track parameters, such as total length.

A4.2 Presynapse Identification

Presynapse locations are identified from videos collected under the bulk loading protocol described in appendix 3. First, locations of potential presynapses are identified by finding local intensity maxima in a frame of the video before stimulation starts. Then, the intensity in a region surrounding these points is analyzed over time. Functioning presynapses decrease in intensity as recycling SVs loaded with dye during the bulk loading exocytose and the associated dye is able to diffuse into the extracellular medium.

A4.2.1 Local Maxima Identification

1. Load a frame of the video from before stimulation into imageJ
2. Process->Filter->Gaussian Blur
    a. A radius of around 4 works well for most images
    b. This step smooths the image slightly to better find representative maxima to further analyze
3. Process->Find Maxima
    a. Prominence must be tuned by image
    b. The higher the prominence the fewer points you get, you generally want around 500 points to analyze

    c. Check the points in the image to make sure you are getting points that look like potential presynapses
4. Analyze->Measure
    a. Generates a table with the X,Y values you need for the next step
5. In the Results window that opens after step 4, File->Save As…
    a. Enter a file name corresponding to the sample

A4.2.2 Presynapse Identification

1. Import X,Y points from previous step into matlab
2. open MaskFormationFit.m script
3. Change X,Y variable names to fit variable names within script
    a. X->Xvalues
    b. Y->Yvalues
4. Ensure path and image names are correct for your sample
5. Define ROI (20 works for most samples)
6. Run the script
    a. Proceed through each point looking for the dropoff at the appointed time corresponding to presynaptic exocytosis
    b. Press the button to save any relevant points
    c. Continue until all identified maxima have been screened
7. Save identified presynapses

A4.3 Kymograph Construction and Analysis

To obtain the kymograph:

1. Used the freehand line tool in imageJ to trace over the path of the kymograph (This usually takes several tries to get the line to overlay the line with the SV motion well enough to see it throughout the kymograph)
2. Used standard ImageJ functions to make the kymograph: Image->Slice->Reslice

To match up kymograph motion with presynapse location:

1. Find the presynapse location in the bulk movie, and corresponding location in the single movie
2. Note the time in the single movie that the SV arrived at the presynapse
3. Mark recorded the x position (in the kymograph) where the SV was at that time

To obtain SV speeds from the kymograph:

1. Draw a straight line along a portion of the kymograph

2. Record the end points of that line into an excel spreadsheet and use them to calculate speed
3. Record the x positions in the kymograph between which the SV had that speed
4. Use the marked presynapse location and the locations recorded in (3) to measure position relative to the presynapse
5. In secondary location in the excel file that had distances from the presynapse in 100nm increments, from -6000nm (before the presynapse) to 6000nm (after the presynapse)
6. For each SV/Presynapse pair, use the location ranges in (4) to fill in the table in (5) with the relevant speeds for each distance from the presynapse